Eka Priadi

BEHAVIOUR OF TIANG TONGKAT FOUNDATION OVER PONTIANAK SOFT ORGANIC SOIL USING 3D - FINITE ELEMENT ANALYSIS

Dissertation

Freiberg, 2008

BEHAVIOUR OF TIANG TONGKAT FOUNDATION OVER PONTIANAK SOFT ORGANIC SOIL USING 3D - FINITE ELEMENT ANALYSIS

By the Faculty of
Geowissenschaften, Geotechnik und Bergbau

of the
Technischen Universität Bergakademie Freiberg

approved

THESIS

to attain the academic degree of

DOKTOR-INGENIEUR

DR.-ING

Submitted

By Magister Teknik in Geotechnical Engineering, Eka Priadi

Born on the 24th March 1963 in Sambas, Indonesia

Assessor
Prof. Dr. Herbert Klapperich, Freiberg
Prof. Dr. Rafig Azzam, Aachen
Dr. Ir. Marsudi, MT, Pontianak-Indonesia

Date of the award: 18-12-2007

ACKNOWLEDGEMENTS

The author wishes to express his gratitude to Prof. Dr. Herbert Klapperich, the chairperson of his dissertation committee, for his very kind encouragement, guidance, friendship and inspiration given throughout the graduate work. The author is also grateful to the other dissertation committee members, Prof. Dr. Rafig Azzam and Dr. Ir. Marsudi, MT, for their very precious time for reading this dissertation.

The author is very grateful to Dr.-Ing. habil Nandor Tamaskovics for his kind encouragement, competent guidance, care and criticism of the manuscripts. Thanks to all of the author's colleagues and staff at Soil Mechanics laboratory, Institut für Geotechnik for their help, co-operation and useful discussions and especially to Dipl. –Ing. Ernst-Dieter Hornig, Dipl. –Ing.(FH) Roy John and Frau Helga Vanselow.

The financial support of the Technological and Professional Skills Development Sector Project ADB Loan No. 1792-INO during the author's studies at the Technische Universität Bergakademie Freiberg-Germany is gratefully acknowledged. The support by the IUZ International Center Alexander von Humboldt is also gratefully acknowledged. The author honored to thank Dr. Chairil Effendy, the Rector of Tanjungpura University for his last minute support.

Thanks to the author's friends Indogers in Freiberg who made his years enjoyable: Yunita, Nuke, Joe, Budi, Miya, Lusi, Alin, Sugito, Arief, Yessiva, Sandi and Widia. And special thanks to Michele Tambunan for improving my English.

The author is very grateful to his parents, special thanks to the author's mother and mother-in-law, Uray Rattibah and Martiana who always pray for the success and happiness of their son. The author also wishes to thank Sastrowardoyo and Susanto families for their continued support and encouragement.

Finally, the author is overwhelmed in thanking his wife, Heti Susanto and his Children, Dede Achmad Basofi and Dewi Novita Rabbiyani, for their understanding, patience, and sacrifice throughout the period of his study.

ABSTRACT

In an island nation, such as Indonesia, economic and trade development is concentrated along each island's coastlands where in many areas peat or organic soils are often found. Indonesia has not only the largest but also some of the deepest deposits of tropical peat swamps in the world. The majority of Indonesian peat land is distributed across several islands including Sumatera, Kalimantan, Papua and some parts of Sulawesi and Maluku. Peat deposits are distributed mostly along the coast of West Kalimantan particularly in and around the provincial capital of Pontianak as well as the three other major provincial urban centres of Mempawah, Ketapang and Sambas.

There are many problems with constructing over peat soil as the existence of this type of soil always generates geotechnical engineering problems for regional development. The geotechnical properties of inorganic soil greatly differ from peat which is known for its low bearing capacity, excessive water content, high compressibility, excessive and long term settlement characteristics including primary, secondary and tertiary compressions. Three variations of the traditional floating foundations using wood piles are still commonly used today for light construction on peat land. These are the tiang tongkat (stick pillar) foundation, the wood raft foundation and the mini pile with cap.

For light construction on peat land, several variations of Indonesian traditional floating wood foundations, commonly called tiang tongkat foundations, are still being used today. An investigation of these foundations is vital as Indonesia has one of the greatest coverages of tropical peat swamps in the world. The experimental program of this study is directed toward establishing an understanding of the capacity of the tiang tongkat foundation and its load-transfer behaviour over Pontianak soft organic soil. The physical and mechanical properties tests were carried out at both the Soil Mechanic Laboratories of Tanjungpura University Pontianak-Indonesia and IFGT TU Bergakademie Freiberg-Germany.

Tested for their properties were commercially available Kaolin and natural soils from eight fields in Pontianak city. Samples were taken from 28 boreholes which varied in depth from 1 to 42 m in the following 8 fields: Perdana, A. Yani II, Terminal – Siantan, Ramayana, Yos Sudarso, Danau Sentarum, BNI-46 Tanjungpura and Astra – A. Yani. More than 180 specimens were tested for their mechanical properties.

A tiang tongkat foundation of any dimension is constructed over different soils of fields. The foundation was modelled as three-dimensional linear elastic and the Pontianak soft organic soil was modelled as undrained Soft-Soil-Creep Model. All of the 324 models were made to be used for simulation by means of the Plaxis 3-Dimensional Foundation Program. The purpose of this analysis is to predict the load-settlement behaviour and the capacity of traditional foundations.

This research paper will investigate the behaviour and capacity of several types of tiang tongkat foundations used in the provincial capital of Pontianak, West Kalimantan, Indonesia over peat or organic soils in order to approximate capacity in a practical manner. The comparison between field tests and numerical analysis and analytical solutions are also demonstrated.

TABLE OF CONTENTS

LIST OF FIGURES

LIST OF TABLES

LIST OF NOTATIONS

A	cross section area
A	pile skin area
A	swelling index
Ab	horizontal beam area
Ap	cross-sectional area of pile at point (bearing end)
Ap	pile skin area
a	primary compressibility
a	$e^{(3\pi/4-\phi/2)\tan\phi}$
B	pore pressure coefficient
B	width of footing
B	width of square floor
$B1$, $B2$	width of horizontal beam
b	secondary compressibility
C, C_B	material constant
Cc	compression index
CD	drained consolidated
CU	undrained consolidated
csl	critical state lin
C_r, C_s	swelling index
$C\alpha$	$C\alpha = C_B\,(1 + e_0)$
c, c_{soil}	cohesion of soil
c_i	cohesion of the interface
c_{ref}	cohesion of soil at particular reference level
c_U	undrained cohesion of soil
c_D	drained cohesion of soil
$\bar{c}$	effective cohesion of soil
c'	effective cohesion of soil
c'_{NC}	effective cohesion at normally consolidated state
c'_{OC}	effective cohesion at overconsolidated state
D	depth
D	pile width
d_c, d_q, d_γ	depth factors
E	elasticity modulus
E_{ref}	Young modulus at particular reference level
E_{ur}	elasticity modulus at unloading-reloading line
e	creep
e	Euler's number
e	void ratio
e_c	strain up to the end of consolidation
e_0	initial void ratio
F	ultimate axial capacity
F	inclination capacity

FE	finite element
FEM	finite element method
F_f	shear strength along the pile
f_s	unit skin friction resistance
GWL	ground water level
Gs	specific gravity
G	shear modulus
G´	effective shear modulus
g	plastic potential
g^c	creep potential
H	soil layer thickness
i_c, i_q, i_γ	inclination factors
K´	effective bulk modulus
K_0	earth pressure coefficient at rest
K_p	passive earth pressure coefficient
K_{ps}	compressibility
$K_{p\gamma}$	$3\tan^2\left[45+\left(\frac{\phi+33}{2}\right)\right]$
K_{ur}	bulk modulus at unloading-reloading line
K_0^{NC}	earth pressure coefficient at rest on normally consolidated
$k_x = k_y = k_z$	permeability at x, y and z directions
L	length of embedment of pile
LI	liquidity index
LIR	load increment ratio
LL	liquid limit
L/d	slenderness ratio
*L*t	total length of pile
M	shape factor for Cam clay ellipse, slope of critical state line
NC	normally consolidated
N_c, N_q, N_γ	bearing capacity factors
ncl	normal compression line
n_p	overconsolidated ratio
OC	organic content
OC	overconsolidated
OCR	overconsolidated ratio
PI	plasticity index
PL	plastic limit
P1	mini pile model on FEM
P2-1, P2-2	tiang tongkat with a pair horizontal beam model on FEM
P3-1, P3-2	tiang tongkat with two pairs of horizontal beams model on FEM
P4	pile combined with square floor model on FEM
p_i	perimeter of pile in contact with soil at any point
p´	effective mean stress
p'_f	value of *p´* at failure
p'_0	reference size of yield locus
p^{eq}	mean stress equivalent
p_p^{eq}	pre-consolidation stress equivalent

p_{p0}^{eq}	pre-consolidation stress equivalent before loading consolidation state
Q_p	point resistance (end-bearing)
Q_s	side-friction resistance
Q_u	ultimate bearing capacity of a single pile
q	deviator stress
q_f	value of q at failure
q_u	ultimate bearing capacity
$\bar{q}$	effective overburden pressure
$\bar{q}$	surcharge load
R_{inter}	interface strength
Sr	degree of saturation
s	pile spacing
s	settlement
s_c, s_q, s_γ	shape factors
s_{si}	shaft resistance per unit area at any point along pile
T	transpose
T1	full scale of mini pile model
T2	full scale of mini pile with a pair horizontal beam model
T3	full scale of mini pile with two pairs of horizontal beams model
t, t_k	time
t_c	time to the end of primary consolidation
t'	effective creep time
V	volume
V_0	initial volume
Wn	water content
yl	yield locus
α	angle of resultant measured from vertical axis
α	$\partial p^{eq} / \partial p'$
β	$K_0 \tan \phi' + c'/\sigma_z'$
Γ	location of critical state line in compression plane
γ	unit weight of soil
γ_{sat}	saturated unit weight of soil
γ_{unsat}	unsaturated unit weight of soil
ΔL	pile length increment
$\Delta p'$	increment effective mean stress
Δt	time increment
$\Delta \varepsilon$	strain increment
$\Delta \varepsilon_v$	increment volumetric strain
$\Delta \sigma$	stress increment
δ	small increment of …
ε	creep, normal strain
ε	normal strain
ε_a	vertical strain
ε_h	lateral strain
ε_C	strain up to the end of consolidation

ε_{cv}	critical void strain
$\varepsilon(t)$	time dependent strain
ε_v	normal volumetric strain
ε^H	creep in the logarithmic strain
ε_C^H	strain up to the end of consolidation in the logarithmic strain
ε_c^c	creep strain up to the end of consolidation
ε_v^c	volumetric creep strain
ε_c^e	elastic strain up to the end of consolidation
ε_p^e	elastic volumetric strain
ε_q^e	elastic shear strain
ε_p^p	plastic volumetric strain
ε_1, ε_2, ε_3	principal strains
$\dot{\varepsilon}$	strain rates
$\dot{\varepsilon}^c$	creep strain rates
$\dot{\varepsilon}^e$	elastic strain rates
$\dot{\varepsilon}_v^c$	volumetric creep strain rates
$\dot{\varepsilon}_1^c$, $\dot{\varepsilon}_2^c$, $\dot{\varepsilon}_3^c$	principal creep strains rates
η	stress ratio $= \frac{q}{p'}$
κ	slope of unloading-reloading line in υ : ln p' plane
κ^*	modified swelling index
λ	slope of normal compression line in υ : ln p' plane
λ^*	modified compression index
λ/b	rate factor for secondary compression
μ^*	modified creep index
N	specific volume of isotropically normally consolidated soil at p' = 1.0 kN/m^2
ν	Poisson ratio
ν_{ur}	Poisson ratio at unloading-reloading line
ν^u	undrained Poisson ratio
ν'	effective Poisson ratio
σ_p	pre-consolidation pressure
σ_{pc}	pre-consolidation pressure at the end of consolidation state
σ_{p0}	pre-consolidation pressure before loading consolidation state
σ_1, σ_2, σ_3	principal stresses
σ'	effective normal stress
σ'_h	effective horizontal stress
σ'_n	effective normal stress
σ'_0	initial effective stress
σ'_v	vertical effective stress
σ'_z	effective overburden pressure at z depth

$\sigma'_1, \sigma'_2, \sigma'_3$	effective principal stresses
$\dot{\sigma}'$	effective stress rates
τ	constant period
τ	shear stress
τ_c	time to the end of primary consolidation
τ_f	side friction resistance
$\lvert\tau\rvert$	absolute shear stress
υ	specific volume
ϕ, ϕ_{soil}	internal friction angle of soil
ϕ_{cv}	critical void friction angle
ϕ_I	friction angle of the interface
ϕ_{ps}	$\left(1.1 - 0.1\frac{B}{L}\right)\phi_{triaxial}$
ϕ_u	undrained internal friction angle of soil
ϕ'	effective internal friction angle of soil
ϕ'_{NC}	effective internal friction angle of soil on normally consolidated state
ϕ'_{OC}	effective internal friction angle of soil on overconsolidated state
2D	two dimensional
3D	three dimensional

CHAPTER I

INTRODUCTION

1.1. Introduction to Traditional Wood Foundations on Indonesian Peat Land

In an island nation, such as Indonesia, economic and trade development is concentrated along each island's coastlands where in many areas peat or organic soils are often found. For light construction on peat land, several variations of Indonesian traditional floating wood foundations, commonly called tiang tongkat (stick pillar) foundations, are still being used today. An investigation of these foundations is vital as Indonesia has one of the greatest coverages of tropical peat swamps in the world.

This research paper will investigate the behaviour and capacity of several types of tiang tongkat foundations used in the provincial capital of Pontianak, West Kalimantan, Indonesia over peat or organic soils in order to approximate capacity in a practical manner.

1.2. Background

Indonesia has not only the largest but also some of the deepest deposits of tropical peat swamps in the world. According to Rieley et al., 1997, 12% of all peat lands occur in the humid tropics (tropical peats), most of which are found in Indonesia (17 Mha to 27 Mha). Overall, Indonesian peat lands consist of an organic layer that vary from 2 to 8 m depth, occasional found about 10 m depth with a 65% organic content consisting of partly woody material. Peat layers are concentrated on lowland near coastal areas where water levels are near or above ground surface.

The majority of Indonesian peat land is distributed across several islands including Sumatera, Kalimantan, Papua and some parts of Sulawesi and Maluku. According to the Centre for Soil and Agroclimate Research, CSAR, 2002, the largest amount peat land is located on Sumatera Island being found mostly along its eastern coast from the island's most northern tip of Nangroe Aceh Darussalam down through the provinces of North Sumatra, Riau, Jambi and South Sumatra which covers a total area of about 6.591 Mha. The second largest total area of Indonesian peat land of 4.448 Mha is found on Kalimantan Island with

1.987 Mha and 1.700 Mha distributed in the provinces of Central Kalimantan and West Kalimantan respectively. While the third largest area of peat land coverage of about 2.011 Mha is widely distributed along the southern coast of Papua Island, where the deposits in some places can reach depths of more than 100 m. Considerably smaller areas of peat land are found on other islands such as Sulawesi and Maluku.

The peat of Kalimantan is characterized by a low nutrient status and a low pH. Generally, this soil has a 155% moisture content, less than 2% ash content and about 2.8 pH (Lambert and Vanderdeelen, 1991). Soepandji et.al. (1996, 1998), studied the peat soil from several regions including areas in and around the cities of Pontianak and Banjarmasin on Kalimantan Island as well as three other places in Riau and Jambi provinces on Sumatera Island. He reported that the peat in Pontianak has a 1.2% ash content, about 4.8 pH and 632% water content, which means it has a low ash content and is moderately acidic. The properties of peat from Kalimantan and Sumatera Islands are shown in Table 1-1.

Peat deposits are distributed mostly along the coast of West Kalimantan particularly in and around the provincial capital of Pontianak as well as the three other major provincial urban centres of Mempawah, Ketapang and Sambas (Fig. 1-1).

Table 1-1. Properties of Peat Soil on Kalimantan and Sumatera Islands

Properties	Kalimantan		Sumatera		
	Pontianak	Gambut City Banjarmasin	Duri	Desa Tampan	Musi
Ash Content (%)	1.2	3.29	21.96	25.2	50.7
Water Content (%)	632	198	235.4	338	235.4
Specific Gravity	1.42	1.47	1.6	1.55	1.82
Liquid Limit	260	182	440	236	274
Plastic Limit	196	148	377	309	194
Shrinkage Limit	-	28	-	59	-
pH	4.8	6.47	3.9	3.61	3.3
Bulk Density (Mg/m^3)	-	-	1.084	0.95	1.123
Compression Index (Cc)	-	-	2.55 - 3.2	2.11	1.57
Recompression Index, (Cr)	-	-	0.067 - 0.13	0.107	0.05
ASTM D4427-92 (1997) classification	Low ash, moderately acidic, peat	Low ash, slghtly acidic, peat	Organic soil	Organic soil	Organic soil

(After, Soepandji et.al, 1996, 1998)

There are many problems with constructing over peat soil as the existence of this type of soil always generates geotechnical engineering problems for regional development. The geotechnical properties of inorganic soil greatly differ from peat which is known for its low bearing capacity, excessive water content, high compressibility, excessive and long term

settlement characteristics including primary, secondary and tertiary compressions. Usually, the damage to construction is caused by the limited availability of data to engineers on soil behaviour. In addition, the most recent research in this field is limited to only a few investigations in Indonesia. Hence, more thorough investigations on peat and organic soils should be conducted immediately to assist engineers in overcoming problems in construction.

Fig. 1-1. Peat Land Deposits in West Kalimantan Province (After, Jarrett, 1997)

1.3. Geological Setting

It is suggested that the island of Kalimantan (Borneo) is the product of Mesozoic accretion of ophiolitic oceanic crustal material, marginal basin fill, island arc material and micro continental fragments onto the continental core of Sundaland by both the Australian collision and Indian Ocean subduction (Hutchison, 1989, Metcalfe, 1996, Wilson and Moss, 1999). A major series of granitoid plutons and associated volcanics form the Schwaner Mountains in southern Kalimantan. They intrude Carboniferous-Permian metasediments of the Pinoh Group. The igneous rocks yield radiometric ages ranging throughout the Cretaceous (Williams, et al, 1988).

The coasts of Kalimantan are for the most part rimmed round by low alluvial lands, which are marshy, sandy and sometimes swampy in character. In places, the sands are fringed by long lines of Casuarina trees; in others, and more especially in the neighbourhood

of some of the river mouths, there are deep banks of black mud covered with mangroves; in others the coast presents to the sea bold headlands, cliffs, mostly of a reddish hue, sparsely clad with greenery, or rolling hills covered by a growth of rank grass.

Wijaya, 2006, investigated the peat deposits in Padang Tikar district, Pontianak regency, West Kalimantan Province. Geologically, peat deposits lay on the low plain area composed by alluvial deposits rocks of the Halocene-age. Peat deposits occurred in the alluvial deposits and paleogeograpically, formed in the form of lenses that were not influenced by river sediments. Peat deposits have been formed between hills of igneneus rock and coastal levees.

Pontianak is the provincial capital of West Kalimantan (Fig. 1-1) as well as being its most populous urban centre and is located at the mouth of the Kapuas River in the Kapuas delta on the west coast. The low land elevation is about 1 to 3 m above sea level. On this delta, some alluvial formations can be found at the mouths of the surrounding rivers. This is mainly composed of very soft soil of variable thickness, generally about 30 meters. This layer is very unstable and has a low bearing capacity. The ebb-tide occurs periodically in this area with average difference in height of 1 to 2 m.

1.4. Alternative Foundations over Soft Soil

The purpose of a foundation is to transfer the weight of a structure to the soil in a manner that will not cause excessive distress to the soil or the structure. Excavation, replacement, preloading and piles are the construction methods that have been used when dealing with soft soil. Sometimes, one of these is combined with vertical drains. Recently, the most commonly used method to stabilise soft soil is ground modification. However, all of these foundations are expensive and always impractical when the foundation is constructed on a deep layer of extremely soft soil. Peat or organic soil, having a low bearing capacity and high compressibility, is considered to be among the worst foundation materials. Serious issues must be faced in the engineering practice of the construction of buildings, dikes, highways and structures over these soils (Greenfield and Shen, 1992).

The choice of construction methods in areas underlain by peat deposits is a matter of finding optimal solutions between the economic and technical factors, available construction time, and the target performance standards. Avoidance of the construction of fills over peat layers and replacement of surface peat layers by granular fill materials have been the first

choice of designers. Replacement is feasible typically for layers up to 5 to 6 m in depth (Magnan, 1994).

Peat and organic soils exhibit a high degree of spatial variability, generally much higher than exhibited by in organic soils, and their properties can change drastically in response to stress application. However, earthen structures of great longitudinal extent (embankments, dikes, levees, etc) often have to be placed directly on peat because of the high cost and impracticality of using piling or replacing deep peat deposits. Because of the known high degree of non-linearity of peat behaviour as described above and the large degree of peat heterogeneity as well as peat's rather different microstructure, there is an on-going discussion as to whether the theories and procedures developed primarily for mineral soils can be directly applied to peat and, if not, what modifications of such theories and procedures can be made or if entirely new approaches are needed (Edil and den Haan, 1994).

1.5. Traditional Floating Foundations in West Kalimantan

Three variations of the traditional floating foundations using wood piles are still commonly used today for light construction on peat land. These are the tiang tongkat (stick pillar) foundation, the wood raft foundation and the mini pile with cap.

Generally, with the tiang tongkat foundation which is used only for the light construction of buildings, e.g. houses, warehouses and shopping centres over peat or organic soils, mini wood piles ranging in sizes of about 10 to 18 cm in diameter and 400 to 1800 cm in length are widely used in West Kalimantan as foundations to support construction. Because it is not embedded into the impermeable layer, this pile is combined with horizontal beams near the ground surface to increase bearing capacity. Usually, a square wood pile is selected to be combined with horizontal beams.

For highway and road construction over peat or organic soils, there are two other variations of the tiang tongkat. The first is similar to a raft foundation where a mini pile is laid down horizontally over the ground surface. The second uses a mini pile, which is driven into the ground vertically and the top of the pile is fitted with a mini board cap. The following sections will describe these three types of traditional floating foundations in West Kalimantan in more detail.

1.5.1. Tiang Tongkat (Stick Pillar) Foundation

The tiang tongkat (stick pillar) foundation is the oldest traditional foundation which is still widely used in West Kalimantan today. This foundation is made by using a square wood pile (kayu besi) ranging from 10 to 20 cm in width and 100 to 380 cm in length which has been sharpened at one end and which is combined with one or two pairs of horizontal mini wood beams. The horizontal beam length varies from 50 to 100 cm. The beams are attached to the pile at about 50 to 100 cm from the top and the pile is then driven into the ground to a selected depth as shown in Fig. 1-2.

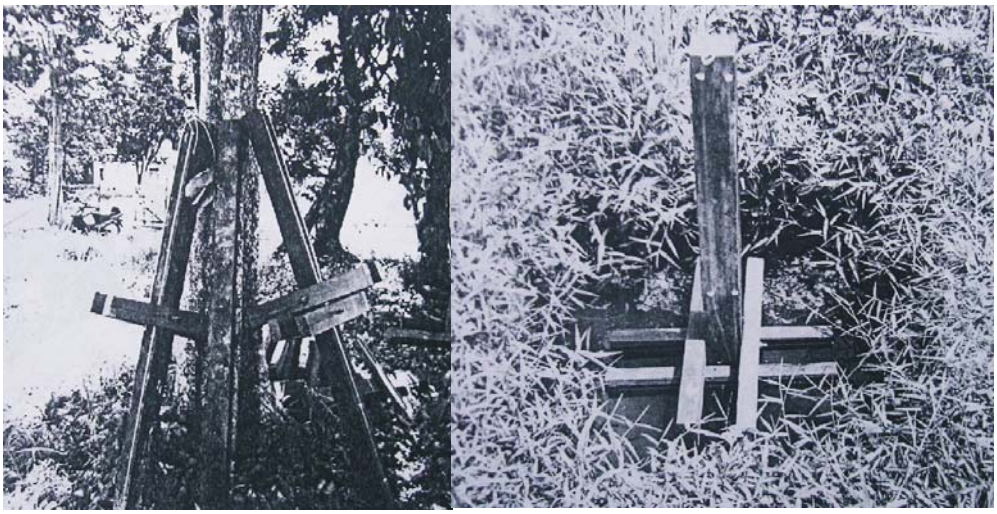

Fig. 1-2. Tiang Tongkat (Stick Pillar) Foundation (After, Sentanu, Noviarti and Suhendra, 2002)

1.5.2. Wooden Raft Foundation

Wooden raft foundations are usually used for highway and road construction over peat or organic deposits. Mini wood piles with diameters of 12 to 16 cm are laid down horizontally over the ground surface. There are two ways of laying wooden raft foundations either alternately (Fig. 1-3 (left)) or closely (Fig 1-3 (right)). After complete installation, the top of this foundation will be filled with a selected material.

Fig. 1-3. Wooden Raft Foundation: piles laid down alternately (left), piles laid down closely (right)

1.5.3. Wooden Mini Pile with Cap

Besides the wooden raft foundation, the mini pile with mini board cap is often used in highway construction. First, a mini pile of approximately 10 to 18 cm in diameter and 400 to 1800 cm in length is driven into the ground surface. Then a square mini board cap of 20 to 30 cm in width is nailed to the top of the pile. Afterwards, a selected material is laid on top of this foundation and then levelled. Finally, a geosynthetic material is laid over the selected material. Fig. 1-4 shows the foundation of mini pile with cap.

Fig. 1-4. Mini Pile with Mini Board Cap

The combination of pile with geosynthetic is quite similar with geotextile encased column (GEC) which was being used and developed widely in Germany, Sweden and Netherlands (Reithel et al, 2004 and 2005). Fig. 1-5, shows the foundation systems with GEC constructed near Büchen-Hamburg railway station. The basic principle of GEC techniques is to relieve the load on the soft soils without altering the soil structure substantially. This is achieved by installing column-or pile-type structures in a grid pattern into a bearing layer, on top of which often a load transfer mat consisting of geotextile or geogrid reinforcements is constructed. The stress relieve of the soft soils results from a redistribution of the loads in the embankment through arching, which (if present) is stabilized by the geotextile/geogrid reinforcement (membrane effect) additionally. As a result the compressibility of the improved or composite ground can be reduced and the bearing capacity and shear strength increased (Kempfert and Raithel, 2005).

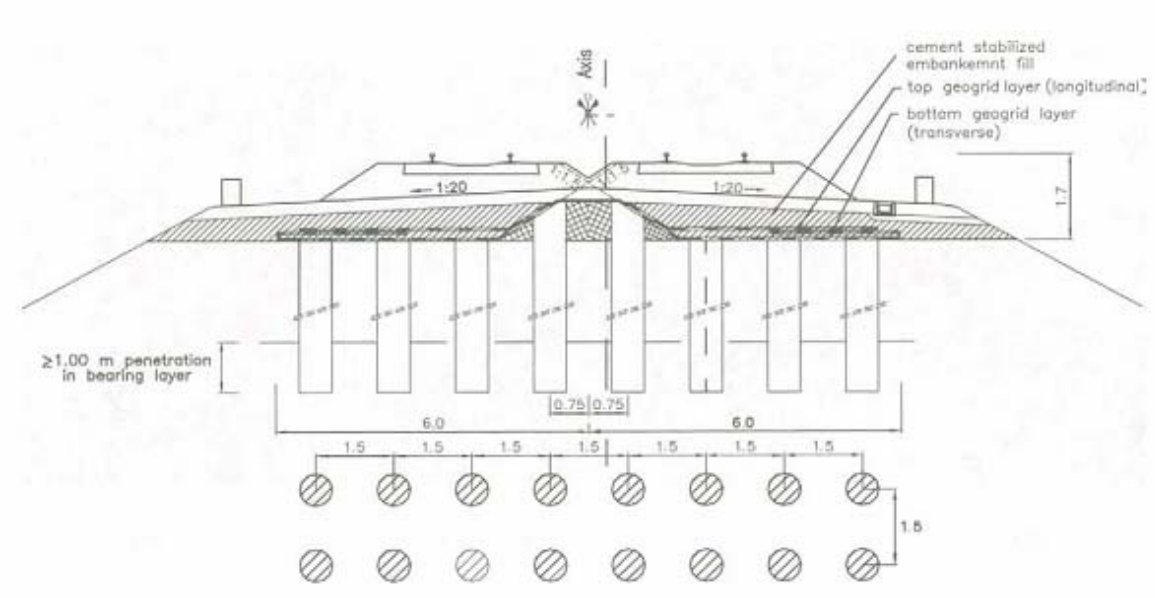

Fig. 1-5. Foundation systems with geotextile encased columns in Büchen-Hamburg (After Kempfert and Raithel, 2005)

1.6. Research Objectives

The main objective of this research is to investigate the capacity of several types of tiang tongkat foundations including the influence of their dimensions against capacity. This research is limited to this particular foundation constructed over peat and organic soils. The specific objectives of this research can be listed as follows:

a) To investigate the capacity of several types of tiang tongkat foundation over peat or organic soils analysized by means of the FE Plaxis 3-Dimensional Foundation Program;
b) To study the behaviour of tiang tongkat foundations which are subjected to vertical and inclination loads;
c) To investigate the area effects of horizontal beam pairs over pile skin against ultimate bearing capacity;
d) To develop appropriate graphs; which can be used as a practical aid in approximating the bearing capacity of the tiang tongkat foundation.

CHAPTER II

LITERATURE REVIEW

2.1. Basic Definitions of Peat and Organic Soils

Peat and organic soils are encountered in low-lying areas like coastal areas where the water table is near or above the ground surface. They are present mostly in surface soils but in some cases accumulate in deep deposits. Peat and organic soils are well known for their high compressibility and long-term settlement. In many cases, the majority of settlement results from creep at constant vertical effective stress. Soil is classified as peaty soil when its organic content ranges from 10 to 30% and its pH is generally less than 7.0 (Tan et. al, 2001).

The living vegetation covering the terrain of organic and peat soil is composed of mosses, sometimes lichens, sedges and/or grasses, with or without tree and shrub growth. Usually combinations of these plant forms are found. Plants produce organic compounds by using the energy of sunlight to combine carbon dioxide from the atmosphere with water from the soil. Soil organic matter is created by the cycling of these organic compounds in plants, animals, and micro organisms into the soil (USDA Natural Resource Conservation Service, 1996). Underneath this cover, there is a mixture of fragmented organic material derived from past vegetation but post-chemically changed and fossilized. This is often observed in various stages of decomposition with an end product known as humus (Edil, 2003) which is a dark brown, porous, spongy material that has a pleasant, earthy smell. In most soils, the organic matter accounts for less than about 5% of the volume. When this subsurface material is highly compressible (MacFarlane, 1958) compared with most mineral soils, it is commonly known as peat.

Peat, however, is distinguished from other organic soil materials by its lower ash content (less than 25% ash by dry weight) and from other phytogenic material of higher rank (i.e. lignite coal) by its lower calorific value on a water-saturated basis. Thus all peat is organic soil but not all organic soil is necessarily peat. High annual rainfall and poor drainage are essential conditions to the formation of peat. Peat typically forms inland from mangrove swamps under waterlogged conditions where the water is typically acidic. The rate of peat accumulation varies from place to place and peat accumulation continues as long as bog plants can live and die at the surface (Leong and Chin, 1997).

The 1988 meeting of the International Peat Committee TC-15 of the International Society for Soil Mechanics and Foundation (ISSMFE) in Tallin determined that the cut off organic content for “peat” varied from 25% to 75% among the member countries. The term peat as used today includes a vast range of peats, peaty organic soils, organic soils and soils with organic content (Landva et. al, 1983).

The most common definitions of peat are based on ash (or organic) content. Peat as defined by the American Society for Testing and Materials (ASTM) D4427-00 is a naturally occurring, highly organic substance derived primarily from plant materials. According to the ASTM Standard D 2487-00, organic clay/silt is a clay/silt with sufficient organic content to influence soil properties. For classification, an organic clay/silt is a soil that would be classified as a clay/silt except that its liquid limit value after oven drying is less than 75% of its liquid limit value before.

2.2. Bearing Capacity of Shallow Foundations

Bearing capacity is the ability of soil to support the load from any structure without undergoing a shear failure with accompanying large settlements. Equations used in this work for calculating bearing capacity are derived from three theories by Terzaghi, Meyerhof and Hansen respectively as these equations have found general use in geotechnical practices. Results were obtained by limit equilibrium analyses using the failure mechanism.

2.2.1. Terzaghi’s Bearing Capacity Theory

Figure 2-1 shows the basic elements in the development of Terzaghi’s theory. The four assumptions of Terzaghi are: first, a strip footing of infinite extent and unit width, second, a rough instead of a smooth base surface, third, effects of the soil weight by superimposing an equivalent surcharge load $q = \gamma D$, and fourth, the shear resistance of the soil above the base of the footing is neglected.

With the addition of shaped factors in the cohesion and base terms, Terzaghi obtained expressions for the ultimate bearing capacity for general shear conditions as follows:

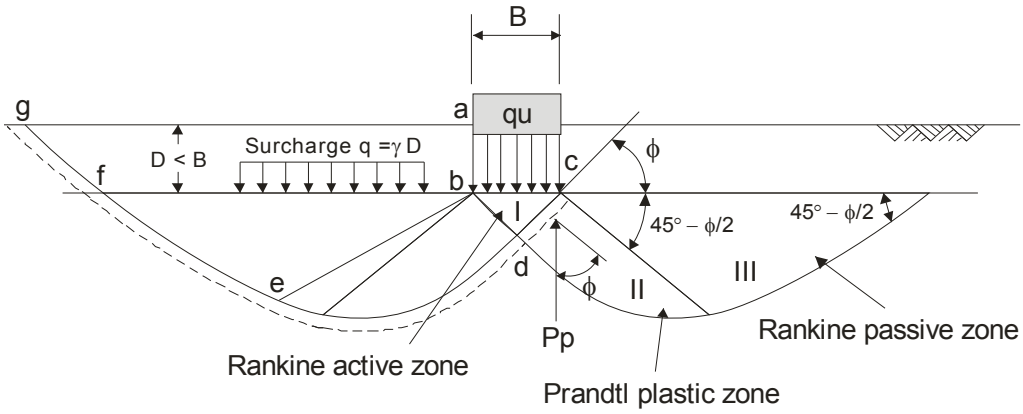

Fig. 2-1. Terzaghi's Bearing Capacity Theory (After Cernica, 1995)

Long footings: $q_u = cN_c + \gamma DN_q + \frac{1}{2}\gamma BN_\gamma$ (2-1)

Square footings: $q_u = 1.3\,cN_c + \gamma DN_q + 0.4\,\gamma BN_\gamma$ (2-2)

Circular footings: $q_u = 1.3\,cN_c + \gamma DN_q + 0.3\,\gamma BN_\gamma$ (2-3)

where

c	=	cohesion of soil
γ	=	unit weight of soil
D	=	depth
B	=	width of footing
N_c, N_q, N_γ	=	bearing capacity factors
ϕ	=	internal friction angle of soil

$$N_c = \cot\phi\left[\frac{a^2}{2\cos^2\left(45+\phi/2\right)} - 1\right] \quad (2\text{-}4)$$

$$N_q = \frac{a^2}{2\cos^2\left(45+\phi/2\right)} \quad (2\text{-}5)$$

$$N_\gamma = \frac{1}{2}\tan\phi\left(\frac{K_{p\gamma}}{\cos^2\phi} - 1\right) \quad (2\text{-}6)$$

$$a = e^{(3\pi/4 - \phi/2)\tan\phi} \tag{2-7}$$

$$K_{p\gamma} = 3\tan^2\left[45 + \left(\frac{\phi + 33}{2}\right)\right] \quad \text{(After S. Husain)} \tag{2-8}$$

2.2.2. Meyerhof's Bearing Capacity Theory

Similar to Terzaghi's theory, Meyerhof proposed shape factors, *s*, depth factors, *d*, and inclination factors, *i*, for his theory. His expressions are presented via Eq. (2-9) and (2-10) and the expressions for the shape, depth, and inclination factors are shown in Table 2-1.

Vertical load: $q_u = cN_c\, s_c\, d_c + \bar{q}\, N_q\, s_q\, d_q + 0.5\,\gamma B N_\gamma\, s_\gamma\, d_\gamma$ (2-9)

Inclination load: $q_u = cN_c\, s_c\, d_c\, i_c + \bar{q}\, N_q\, s_q\, d_q\, i_q + 0.5\,\gamma B N_\gamma\, s_\gamma\, d_\gamma\, i_\gamma$ (2-10)

where s_c, s_q, s_γ = shape factors

d_c, d_q, d_γ = depth factors

i_c, i_q, i_γ = inclination factors

$\bar{q}$ = γD = surcharge load

$$N_q = e^{\pi\tan\phi}\tan^2(45 + \phi/2) \tag{2-11}$$

$$N_c = (N_q - 1)\cot\phi \tag{2-12}$$

$$N_\gamma = (N_q - 1)\tan(1.4\,\phi) \tag{2-13}$$

Table 2-1. Meyerhof's Factors

	Shape	Depth	Inclination
Any ϕ →	$s_c = 1 + 0.2 K_p \frac{B}{L}$	$d_c = 1 + 0.2\sqrt{K_p}\frac{D}{B}$	$i_c = i_q = \left(1 - \frac{\alpha}{90^\circ}\right)^2$
For $\phi = 0°$ →	$s_q = s_\gamma = 1.0$	$d_q = d_\gamma = 1.0$	$i_\gamma = 1$
For $\phi \geq 10°$ →	$s_q = s_\gamma = 1 + 0.1 K_p \frac{B}{L}$	$d_q = d_\gamma = 1 + 0.1\sqrt{K_p}\frac{D}{B}$	$i_\gamma = \left(1 - \frac{\alpha}{\phi}\right)^2$

$K_p = \tan^2(45 + \frac{\phi}{2})$

α = angle of resultant measured from vertical axis

When triaxial ϕ is used for plane strain, adjust ϕ to obtain $\phi_{ps} = \left(1.1 - 0.1\frac{B}{L}\right)\phi_{triaxial}$

(After, Cernica, 1995)

2.2.3. Hansen's Bearing Capacity Theory

Hansen's theory is an extension of Meyerhof's proposed equations. The N_c and N_q coefficients are identical. The N_γ coefficient recommended by Hansen is almost the same as Meyerhof's for ϕ values for up to about 35°. Hansen's equation for the case of a horizontal ground surface is given in Eq. (2-14) and shape, depth, and inclination factors of his equation are shown in Table 2-2.

Table 2-2. Hansen's Factors

Shape	→	$s_q = 1 + \sin\phi\left(\frac{B}{L}\right)$; $s_\gamma = 1 - 0.4\left(\frac{B}{L}\right)$
Depth	→	$d_q = 1 + 2\tan\phi(1-\sin\phi)^2\left(\frac{D}{B}\right)$ for D ≤ B
		$d_q = 1 + 2\tan\phi(1-\sin\phi)^2 \arctan\left(\frac{D}{B}\right)$ for D > B
		$d_\gamma = 1.0$
Inclination	→	$i_q = \left[1 - \left(\frac{0.5H}{V + Ac\cot\phi}\right)\right]^5$; $i_\gamma = \left[1 - \left(\frac{0.7H}{V + Ac\cot\phi}\right)\right]^5$

(After, Cernica, 1995)

$$q_u = -c \cot \phi + (\bar{q} + c \cot \phi) N_q s_q d_q i_q + 0.5 \bar{\gamma} B N_\gamma s_\gamma d_\gamma i_\gamma \quad (2\text{-}14)$$

where $\bar{q}$ is the effective overburden pressure at base level.

2.3. Bearing Capacity of Pile Foundation

A deep pile foundation can have its bearing capacity classified when it is subjected to an axial compressive load, although some lateral forces are usually inevitable. The wood pile is the oldest as well as still one of the most common pile foundations used in Indonesia. The wood piles are made from tree trunks with the branches and bark removed.

The bearing capacity of a single pile is divided into two sources, i.e. end-bearing and side friction (Figure 2-2). The ultimate bearing capacity of pile can be written as:

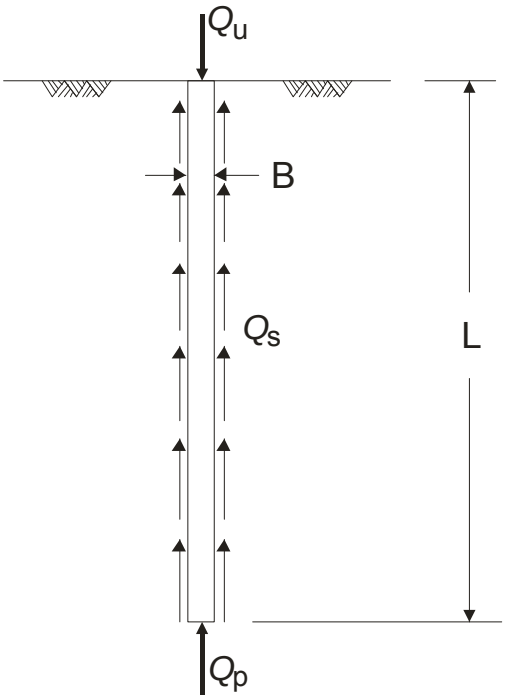

Fig. 2-2. Bearing Capacity of Single Pile (After Cernica, 1995)

$$Q_u = Q_p + Q_s \tag{2-15}$$

$$Q_u = A_p\,(\bar{c}\,N_c + \gamma L N_q + \tfrac{1}{2}\,\gamma B N_\gamma) + \Sigma\,\Delta L\,p_i\,s_{si} \tag{2-16}$$

where Q_u = ultimate bearing capacity of a single pile

Q_p = point resistance (end-bearing)

Q_s = side-friction resistance

s_{si} = shaft resistance per unit area at any point along pile

B = general dimension for pile width

A_p = cross-sectional area of pile at point (bearing end)

p_i = perimeter of pile in contact with soil at any point

L = total length of embedment of pile

γ = unit weight of soil

$\bar{c}$ = effective cohesion of soil

N_c, N_q, N_γ = bearing capacity factors

The ultimate bearing capacity of a single pile in clay could be estimated by Eq. (2-16). The term of N_γ is relatively small in comparison with the other two terms and therefore may be neglected. Hence the total resistance from end-bearing could be expressed by Eq. (2-17):

$$Q_p = A_p\,(\bar{c}\,N_c + \gamma L N_q) \tag{2-17}$$

The total resistance from friction Q_S may be estimated from Eq. (2-18),

$$Q_S = \Sigma\,(\Delta L)\,p\,f_s \tag{2-18}$$

where f_S is the unit skin friction resistance in clay. According to Meyerhof, 1953, the values for f_S could be approximated as given by Eqs. (2-19) and (2-20) for driven piles,

$$f_s = 1.5\,c_u \tan\phi \tag{2-19}$$

$$f_s = c_u \tan \phi \qquad (2\text{-}20)$$

where c_u = average cohesion, undrained condition

ϕ = angle of internal friction of the clay

Based on the Eq. (2-15), an expression for estimating the ultimate bearing capacity of a pile installed in a clayey stratum could be given by:

$$Q_u = A_p (\bar{c}\, N_c + \gamma L N_q) + A_s f_s \qquad (2\text{-}21)$$

2.4. Piled Raft Foundation

Recently, many projects combine piles and rafts when a foundation is constructed on soft soil to support the load from any structure. This combination contributes to an overall reduction of excessive settlement as the bearing capacities of both the piles and the raft will be more fully distributed simultaneously. Piled raft foundations have been studied by researchers around the world. Butterfield and Banerjee, (1971), Poulos and Davis (1980), Kuwabara (1989), Bilotta et al. (1991) and Russo (1998), have performed extensive numerical studies to analyze piled raft foundations.

Russo (1998) compared the results of piled raft foundation analyses performed by Butterfield and Banerjee (1971) and Kuwabara (1989). Figure 2-3 shows the comparison between settlement and ratio of spacing over diameter for various values of the pile spacing, *s*, slenderness ratio, *L*/*d*, and compressibility, K_{ps}. The values of applied load supported by the piles as obtained by Kuwabara are higher than those calculated by Butterfield and Banerjee. Russo (1998), who computed the loads of piled raft foundations using the Non-linear Analysis of Piled Rafts (NAPRA) program. The results were compared with Kuwabaras' analysis as shown in Figure 2-4 which shows the comparison between the load of a piled raft foundation and the slenderness ratio, *L*/*d*. The general trend of the results is very similar, even if the present method seems to slightly overestimate the percentage of the total load taken by the piles at large values of the slenderness ratio, while the opposite occurs for the lowest values.

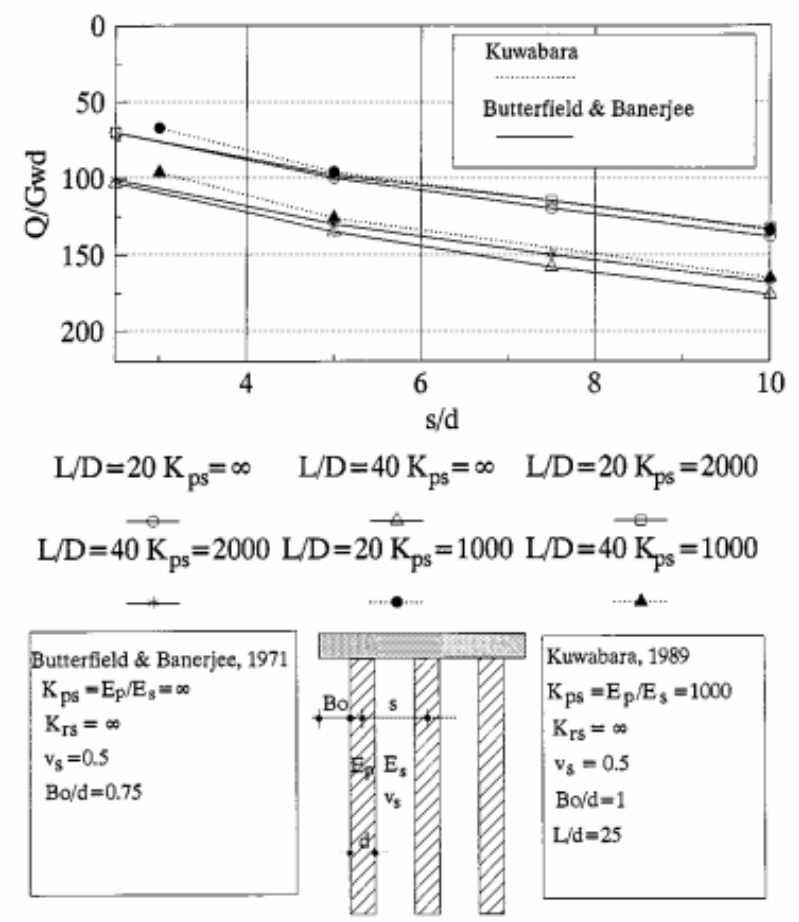

Figure 2-3 Settlement Calculated by Kuwabara and by Butterfield and Banerjee (After, Russo, 1998)

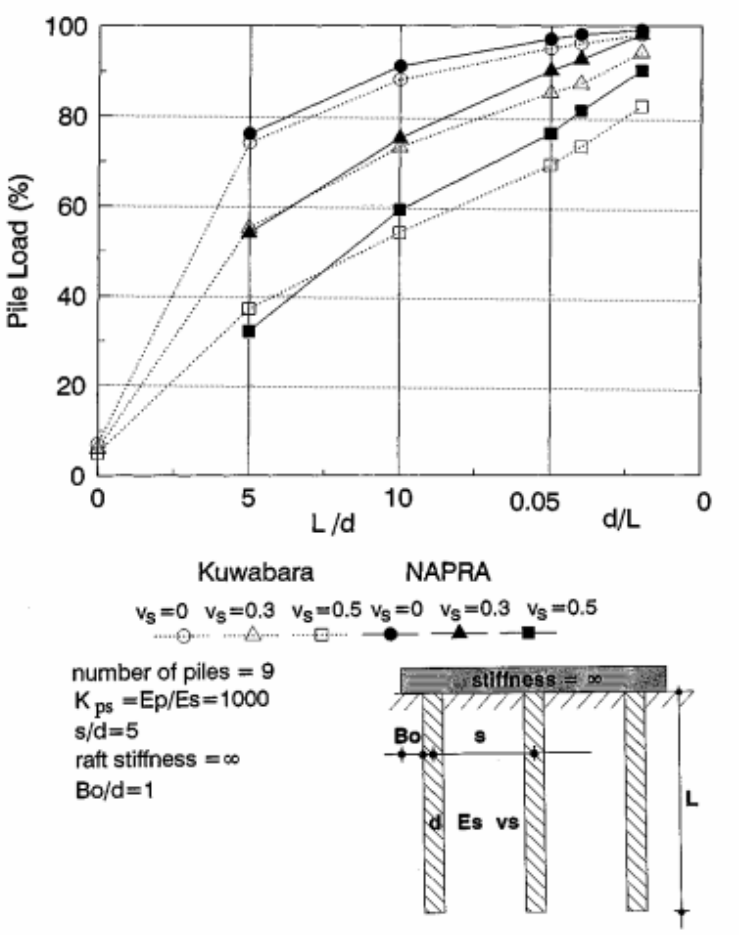

Figure 2-4 Comparison of Pile Load and Slenderness Ratio, *L*/*d*.
(After, Russo, 1998)

2.5. Field Pile Test

Generally, there are two primary objectives in conducting field pile tests, namely: to establish load-settlement relationships and to determine the capacity of the pile. The test procedure consists of applying a static load to the pile in increments up to a designated level of load and recording the vertical deflection of the pile. The load is applied to the pile incrementally until the maximum load of twice the pile design load is reached.

The interpretation of the load capacity depends on the method of loading. Two loading methods are popular. In one method, called the constant rate of penetration (CRP) test, the load is applied at a constant rate of penetration of 0.75 mm/min in fine-grained soils and 1.5 mm/min in coarse-grained soils. In the other method, called the quick maintained load (QML),

increments of load, of about 15% of the design load, are applied at intervals of about 2.5 min. At the end of each load increment, the load and settlement are recorded (Budhu, 2000).

2.6. Critical State Soil Mechanics

Sustained shearing of a soil sample eventually leads to a state in which further shearing can occur without any changes in stress or volume. When the soil is distorting at a constant state, this condition is referred to as the critical state and is depicted as a critical state line. The first model which identified this state is called the Cam-clay model which was proposed by Roscoe and Schofield (1963). Later, a modified Cam-clay model was developed by Roscoe and Burland (1968) which is more widely used to predict assumed forms of the critical state line, yield surface and consolidation.

2.6.1. Critical State Line and Undrained Shear Strength

The Mohr-Coulomb failure criterion says that the failure of a soil mass will occur if the resolved shear stress τ on any plane in that soil mass reaches a critical value. It can be written as

$$\tau = \pm (c' + \sigma' \tan \phi') \qquad (2\text{-}22)$$

where c' = effective cohesion
σ' = effective normal stress
ϕ' = effective friction angle

Mohr-Coulomb failure can also be defined in terms of principal stresses. From Fig. 2-5 the limiting relationship between the major and minor principal effective stresses σ'_1 and σ'_3 is,

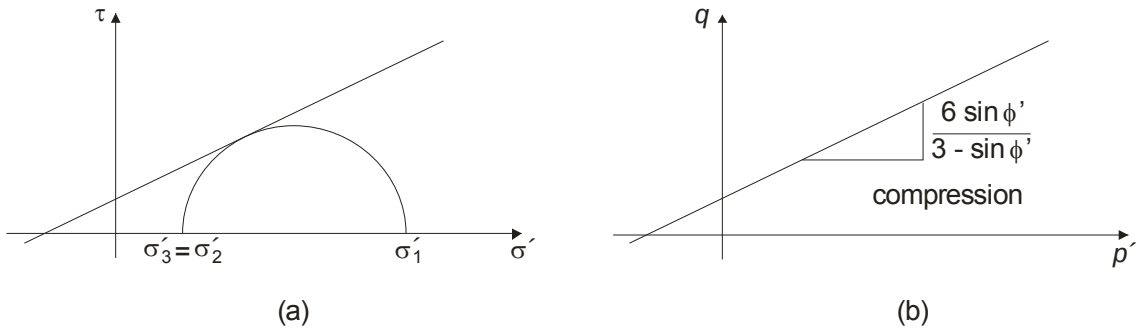

Fig. 2-5. Mohr-Coulomb Failure Criterion (After, Wood, 1990)

$$\frac{\sigma_1' + c' \cot \phi'}{\sigma_3' + c' \cot \phi'} = \frac{1 + \sin \phi'}{1 - \sin \phi'} \tag{2-23}$$

The stress conditions illustrated in Fig. 2-5(a) with $\sigma'_2 = \sigma'_3$ correspond to the triaxial compression in which the cell pressure provides the minor (and equal intermediate) principal stress. Equation (2-23) can be rewritten in terms of triaxial stress variables p' : q, where

$$p' = \frac{\sigma_1' + 2\,\sigma_3'}{3} \tag{2-24}$$

$$q = \sigma_1' - \sigma_3' \tag{2-25}$$

which becomes Fig. 2-5(b).

$$\frac{q}{p' + c' \cot \phi'} = \frac{6 \sin \phi'}{3 - \sin \phi'} \tag{2-26}$$

The gradient of the critical state line is expressed in Eq. (2-27),

$$M = \frac{6 \sin \phi'}{3 - \sin \phi'} \tag{2-27}$$

or

$$\sin\phi' = \frac{3M}{6+M} \tag{2-28}$$

A soil with specific volume υ will end on the critical state line at a mean effective stress p'_f when tested in undrained triaxial compression with the following equation:

$$p'_f = \exp\left(\frac{\Gamma - \upsilon}{\lambda}\right) \tag{2-29}$$

This implies an ultimate value of deviator stress

$$q'_f = M\, p'_f = M \exp\left(\frac{\Gamma - \upsilon}{\lambda}\right) \tag{2-30}$$

and hence an undrained shear strength

$$c_u = \frac{M\, p'_f}{2} = \frac{M}{2}\exp\left(\frac{\Gamma - \upsilon}{\lambda}\right) \tag{2-31}$$

2.6.2. Elastic-plastic Model

The recoverable changes in volume accompany any changes in mean effective stress p' is expressed in Eq. (2-32),

$$\delta\varepsilon_p^e = \kappa\frac{\delta\, p'}{\upsilon p'} \tag{2-32}$$

where κ = slope of the unloading-reloading line = $-\dfrac{\delta\upsilon}{d(\ln p')}$

υ = specific volume = 1 + e

e = void ratio

The recoverable shear strains accompanying any changes in deviator stress q is expressed in Eq. (2-33) as follows,

$$\delta\varepsilon_q^e = \frac{\delta q}{3G'} \tag{2-33}$$

with constant shear modulus G'.

The simplest shape for the yield locus in the p' : q stress plane is an ellipse (an ellipsoid in principal stress space) which is shown in Fig. 2-6. For this isotropic model, the ellipse is centred on the p' axis (see yl in Fig. 2-6).

All combinations of q and p' that lie within the yield surface will cause the soil to respond elastically. If a combination of q and p' lies on the yield surface, the soil yields similar to that of a steel bar. Any tendency of a stress combination to move outside the current yield surface is accompanied by an expansion of the current yield surface such that during plastic loading the stress point (q, p') lies on the expanded yield surface and not outside. Effective stress paths outside of the yield surface cause the soil to behave elastoplastically. If the soil is unloaded from any stress state below failure, the soil will respond like an elastic material (Wood, 1990).

The equation for elliptical yield locus which is shown in Figure (2-6) is:

$$\frac{p'}{p'_o} = \frac{M^2}{M^2 + \eta^2} \tag{2-34}$$

Where $\eta = \frac{q}{p'}$ and M are the slope of the critical state line.

The above Eq. (2-34) can be simply expressed in Fig. 2-6 as follows:

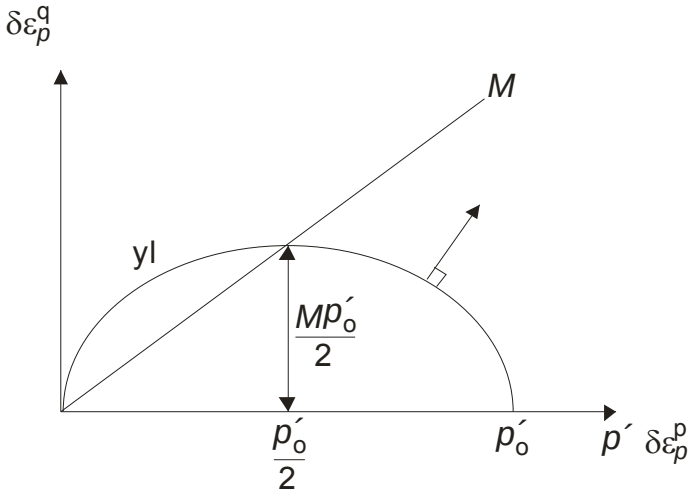

Fig. 2-6. Elliptical Yield Locus for the Cam-clay Model in the p' : q plane (After, Wood, 1990)

$$(p')^2 - (p')(p'_o) + \frac{q^2}{M^2} = 0 \tag{2-35}$$

The vector of the plastic strain increment; $\delta\varepsilon_p^p : \delta\,\varepsilon_q^p$ is in the direction of the outward normal to the yield locus as seen in Fig. 2-6 so that:

$$\frac{\delta\varepsilon_p^p}{\delta\varepsilon_q^p} = \frac{\partial g/\partial p'}{\partial g/\partial q} \tag{2-36}$$

$$= \frac{M^2(2p' - p'_o)}{2q} = \frac{M^2 - \eta^2}{2\eta} \tag{2-37}$$

Fig. 2-7 shows a swelling line in the compression plane υ : ln p' which has its tip at p' = p'_o on the isotropic normal compression line (ncl). The slopes λ and κ of the normal compression and swelling lines in υ – ln p' space are related to the compression index C_c, and swelling index, C_s, measured in Oedometer tests through the following equations.

$$\lambda = \frac{C_C}{\ln 10} \tag{2-38}$$

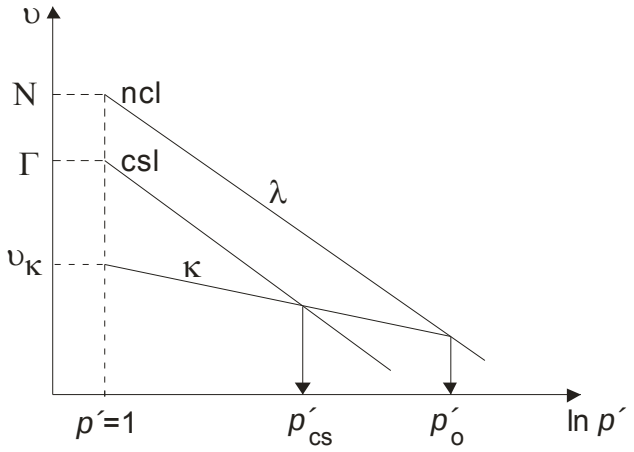

Fig. 2-7. Normal Compression, Critical State and Swelling Lines (After, Wood, 1990)

$$\kappa = \frac{C_S}{\ln 10} \tag{2-39}$$

The equation of a normal compression line is,

$$\upsilon = N - \lambda \ln p' \tag{2-40}$$

The swelling line is also straight in this form of the compression plane, as expressed in the following general equation,

$$\upsilon = \upsilon_\kappa - \kappa \ln p' \tag{2-41}$$

The linear relationship between specific volume υ and logarithm of mean effective stress p'_o during isotropic normal compression of the soil is expressed in Eq. (2-42),

$$\upsilon = N - \lambda \ln p'_o \tag{2-42}$$

Where N is a soil constant specifying the position of the isotropic normal compression line in the compression plane υ : ln p' then the magnitude of plastic volumetric strain is given by:

$$\delta\varepsilon_p^p = \left[(\lambda-\kappa)/\upsilon\right]\frac{\delta\, p_o'}{p_o'} \tag{2-43}$$

and the elements of the hardening relationship become:

$$\frac{\partial\, p_o'}{\partial\varepsilon_p^p} = \frac{\upsilon\, p_o'}{\lambda-\kappa} \tag{2-44}$$

$$\frac{\partial\, p_o'}{\partial\varepsilon_p^p} = 0 \tag{2-45}$$

Combining Eq. (2-32) and (2-33) can result in the following matrix equations.

$$\begin{bmatrix}\delta\varepsilon_p^e\\ \delta\varepsilon_q^e\end{bmatrix} = \begin{bmatrix}\kappa/\upsilon p' & 0\\ 0 & 1/3G'\end{bmatrix}\begin{bmatrix}\delta p'\\ \delta q\end{bmatrix} \tag{2-46}$$

$$\begin{bmatrix}\delta\varepsilon_p^p\\ \delta\varepsilon_q^p\end{bmatrix} = \frac{(\lambda-\kappa)}{\upsilon p'\left(M^2+\eta^2\right)}\begin{bmatrix}\left(M^2-\eta^2\right) & 2\eta\\ 2\eta & 4\eta^2/\left(M^2-\eta^2\right)\end{bmatrix}\begin{bmatrix}\delta p'\\ \delta q\end{bmatrix} \tag{2-47}$$

2.7. Soft–Soil-Creep Model (SSCM)

The formulation of the Soft-Soil-Creep model is based on the model parameters which are adopted from Vermeer and Neher, 1999 and, the manual of the Plaxis 3D-Foundation, version 1.5, 2006.

The greatest problem with erecting any structure on soft soil is that this material has a high degree of compressibility which includes not only primary but secondary compressions as well. Assuming the secondary compression is a small percentage of the primary compression, it is clear that creep is a prominent factor with a large primary compression. Indeed, large primary settlement is usually followed by substantial creep settlement in later years (Vermeer and Neher, 1999).

The Soft-Soil-Creep Model is suitable for estimating viscous effects, i.e. creep and stress relaxation. In fact, all soils exhibit some creep and primary compression is more often

than not followed by a certain amount of secondary compression. In such cases, it is desirable to estimate the creep from Finite Element Method (FEM) computations.

Buisman (1936) proposed the following equation to describe creep behaviour under constant effective stress.

$$\varepsilon = \varepsilon_c - C_B \log\left(\frac{t}{t_c}\right) \qquad \text{for: } t > t_c \qquad (2\text{-}48)$$

Where ε_c is the strain up to the end of consolidation, t the time measured from the beginning of loading, t_c the time to the end of primary consolidation and C_B is a material constant. For further consideration, it is convenient to rewrite this equation as:

$$\varepsilon = \varepsilon_c - C_B \log\left(\frac{t_c + t'}{t_c}\right) \qquad \text{for: } t' > 0 \qquad (2\text{-}49)$$

with $t' = t - t_c$ being the effective creep time.

Basing his work on that done by Bjerrum (1967) on creep, Garlanger (1972) proposed the creep equation that follows.

$$e = e_c - C_\alpha \log\left(\frac{\tau_c + t'}{\tau_c}\right) \qquad \text{with: } C\alpha = C_B\,(1 + e_0) \qquad \text{for: } t' > 0 \qquad (2\text{-}50)$$

Another slightly different possibility to describe secondary compression is by the form adopted by Butterfield (1979):

$$\varepsilon^H = \varepsilon_c^H - C \ln\left(\frac{\tau_c + t'}{\tau_c}\right) \qquad (2\text{-}51)$$

Where ε^H is the logarithmic strain defined as:

$$\varepsilon^H = \ln\left(\frac{V}{V_0}\right) = \ln\left(\frac{1+e}{1+e_0}\right) \qquad (2\text{-}52)$$

The subscript '0' denotes initial values while the superscript '*H*' is used to denote logarithmic strain, as originally used by Hencky. For small strains it is possible to show that:

$$C = \frac{C_\alpha}{(1+e_0).\ln 10} = \frac{C_B}{\ln 10} \tag{2-53}$$

This shows that the logarithmic strain is approximately equal to the engineering strain.

2.7.1. Variables τ_c and ε_c

By differentiating Eq. (2-51) with respect to time and dropping the superscript '*H*' to simplify notation, one finds:

$$-\dot{\varepsilon} = \frac{C}{\tau_C + t'} \qquad \text{or inversely:} \qquad -\frac{1}{\dot{\varepsilon}} = \frac{\tau_C + t'}{C} \tag{2-54}$$

This allows one to make use of the construction developed by Janbu, 1969, for evaluating the parameters *C* and τ_c from experimental data. Both the traditional way, as indicated in Figure 2-8(a), as well as the Janbu method as in Figure 2-8(b) can be used to determine the parameter *C* from an oedometer test with a constant load.

By taking into consideration classical literature, it is possible to describe the end of consolidation strain ε_c, by the following equation:

$$\varepsilon_c = \varepsilon_c^e + \varepsilon_c^c = -A \ln\left(\frac{\sigma'}{\sigma'_0}\right) - B \ln\left(\frac{\sigma_{pc}}{\sigma_{p0}}\right) \tag{2-55}$$

where ε = logarithmic strain

σ'_0 = initial effective pressure before loading

σ' = final effective loading pressure

σ_{p0} = pre-consolidation pressure before loading consolidation state

σ_{pc} = pre-consolidation pressure at the end of consolidation state

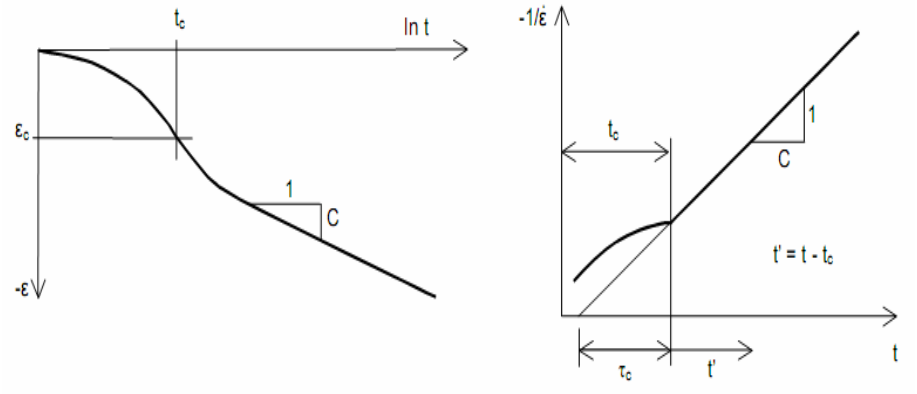

(a) (b)

Figure 2-8. Consolidation and Creep Behaviour in a Standard Oedometer Test
(After Vermeer and Neher, 1999)

In most literature on oedometer testing, the void ratio e is adopted instead of ε, and log instead of *ln*, and the swelling index C_r instead of A, and the compression index C_c instead of B. The above constants A and B relate to C_r and C_c and are expressed as:

$$A = \frac{C_r}{(1+e_0).\ln 10} \tag{2-56}$$

$$B = \frac{(C_c - C_r)}{(1+e_0).\ln 10} \tag{2-57}$$

Combining Eqs. (2-42) and (2-55) it follows that:

$$\varepsilon_c = \varepsilon_c^e + \varepsilon_c^c = -A \ln\left(\frac{\sigma'}{\sigma'_0}\right) - B \ln\left(\frac{\sigma_{pc}}{\sigma_{p0}}\right) - C \ln\left(\frac{\tau_c + t'}{\tau_c}\right) \tag{2-58}$$

Where ε is the total logarithmic strain due to an increase in effective stress from σ'_0 to σ' and a time period of $t_c + t'$. In Figure 2-9 the terms of Eq. (2-57) are depicted as a ε-lnσ diagram.

2.7.2. Differential Law for 1-D Creep

Vermeer and Neher (1999), adopted Bjerrum's idea to find an analytical expression for the quantity τ_c. In addition to Eq. (2-58) they therefore introduced the following to express the idealised stress-strain curve from an Oedometer test with the division of strain increments into elastic and a creep components where $t' + t_c$ = 1 day, thus arriving precisely on the *NC*-line:

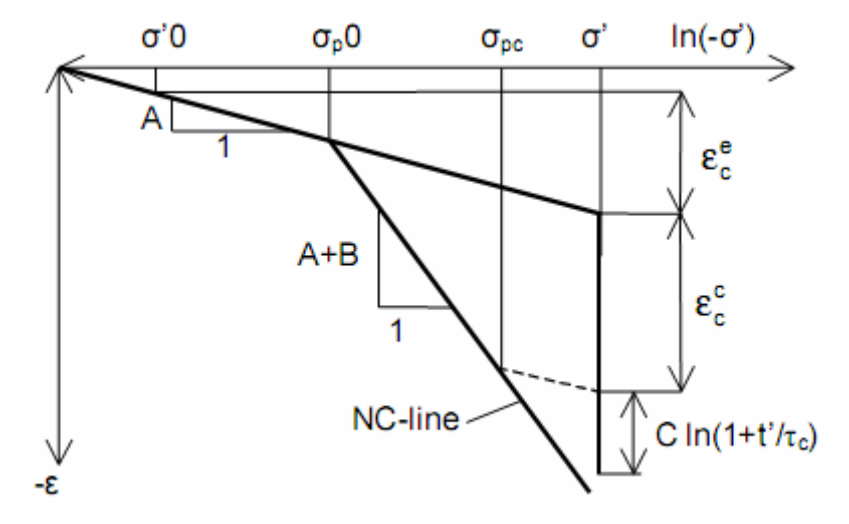

Figure 2-9 Idealised Stress-Strain Curve from an Oedometer Test with Division of Strain Increments into an Elastic and a Creep Component. For $t' + t_c$ = 1 day, one Arrives Precisely on the *NC*-line (After, Vermeer and Neher, 1999)

$$\varepsilon_c = \varepsilon_c^e + \varepsilon_c^c = -A \ln\left(\frac{\sigma'}{\sigma'_0}\right) - B \ln\left(\frac{\sigma_{pc}}{\sigma_{p0}}\right) \tag{2-59}$$

$$\sigma_p = \sigma_{p0} \exp\left(\frac{-\varepsilon^c}{B}\right) \tag{2-60}$$

where ε^c is negative so that σ_p exceeds σ_{p0}. The longer a soil sample is left to creep the larger σ_p grows. The time-dependency of the pre-consolidation pressure σ_p is now found by combining Eqs. (2-58) and (2-60) to obtain:

$$\varepsilon^c - \varepsilon_c^c = -B \ln\left(\frac{\sigma_p}{\sigma_{pc}}\right) = -C \ln\left(\frac{\tau_c + t'}{\tau_c}\right) \qquad (2\text{-}61)$$

In conventional Oedometer testing, the load is increased stepwise and each load step is maintained for a constant period of $t_c + t' = \tau$, where τ is precisely one day.

In this stepwise way of loading, the so-called normal consolidation line (*NC*-line) with $\sigma_p = \sigma'$ is obtained. On entering $\sigma_p = \sigma'$ and $t' = \tau - t_c$ into Eq. (2-60), it is found that:

$$B \ln\left(\frac{\sigma'}{\sigma_{pc}}\right) = C \ln\left(\frac{\tau_c + \tau - t_c}{\tau_c}\right) \qquad \text{for:} \quad \text{OCR} = 1 \qquad (2\text{-}62)$$

It is now assumed that $(\tau_c - t_c) << \tau$. This quantity can thus be disregarded with respect to τ and it follows that:

$$\frac{\tau}{\tau_c} = \left(\frac{\sigma'}{\sigma_{pc}}\right)^{\frac{B}{C}} \qquad \text{or:} \qquad \tau_c = \tau\left(\frac{\sigma_{pc}}{\sigma'}\right)^{\frac{B}{C}} \qquad (2\text{-}63)$$

Having derived the simple expression in Eq. (2-63) for τ_c, it is now possible to formulate the differential creep equation. To this end, Eq. (2-58) is differentiated to obtain:

$$\dot{\varepsilon} = \dot{\varepsilon}^e + \dot{\varepsilon}^c = -A\frac{\dot{\sigma}'}{\sigma'} - \frac{C}{\tau_c + t'} \qquad (2\text{-}64)$$

where $\tau_c + t'$ can be eliminated by means of Eq. (2-61) to obtain:

$$\dot{\varepsilon} = \dot{\varepsilon}^e + \dot{\varepsilon}^c = -A\frac{\dot{\sigma}'}{\sigma'} - \frac{C}{\tau_c}\left(\frac{\sigma_{pc}}{\sigma_p}\right)^{\frac{B}{C}} \qquad (2\text{-}65)$$

with:

$$\sigma_p = \sigma_{p0} \exp\left(\frac{-\varepsilon^c}{B}\right) \qquad (2\text{-}66)$$

Again it is recalled that ε^c is a compressive strain, being considered negative in this manual. Eq. (2-63) can now be introduced to eliminate τ^c and σ_{pc} to obtain:

$$\dot{\varepsilon} = \dot{\varepsilon}^e + \dot{\varepsilon}^c = -A\frac{\dot{\sigma}'}{\sigma'} - \frac{C}{\tau}\left(\frac{\sigma'}{\sigma_p}\right)^{\frac{B}{C}} \tag{2-67}$$

2.7.3. Three-Dimensional Model

On extending the 1D-model to general states of stress and strain, the well-known stress invariants for pressure *p* and deviatoric stress *q* are adopted. These invariants are used to define a new stress measure named p^{eq}:

$$p^{eq} = p' - \frac{q^2}{M^2\left(p' - c\cot(\phi)\right)} \tag{2-68}$$

Figure 2-10 shows that the stress measure p^{eq} is constant on the ellipses in the *p*-*q* plane. In fact, the ellipses are from the Modified Camclay Model as introduced by Roscoe and Burland (1968).

The soil parameter *M* represents the slope of the so-called '*critical state line*' as also indicated in Figure 2-10. We use the general 3D-definition for the deviatoric stress *q* and *M* as shown in Equation (2-68):

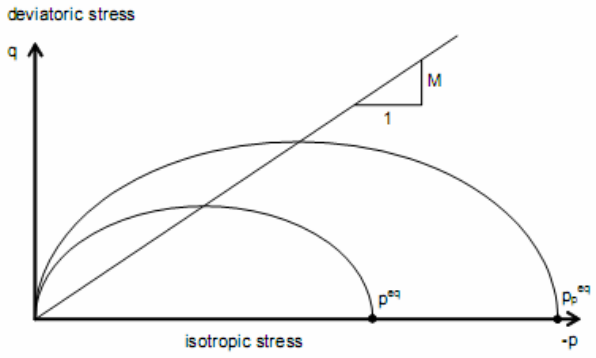

Figure 2-10 Diagram of p^{eq} -ellipse in a *p*-*q*-plane (After, Vermeer and Neher, 1999)

$$M = \frac{6\sin\phi_{cv}}{3-\sin\phi_{cv}} \tag{2-69}$$

Where ϕ_{cv} is the critical-void friction angle, i.e. the critical state friction angle. To extend the 1D-theory to a general 3D-theory, attention is now focussed on normally consolidated states of stress and strain as met in Oedometer testing. In such a situation, it yields $\sigma'_2 = \sigma'_3 = K_0^{NC} \sigma'_1$, and it follows from Eq. (2-68) that:

$$p^{eq} = \sigma' \left[\frac{1+2K_0^{NC}}{3} + \frac{3\left(1-K_0^{NC}\right)^2}{M^2\left(1+2K_0^{NC}\right)} \right] \tag{2-70}$$

$$p^{eq} = \sigma_p \left[\frac{1+2K_0^{NC}}{3} + \frac{3\left(1-K_0^{NC}\right)^2}{M^2\left(1+2K_0^{NC}\right)} \right] \tag{2-71}$$

Where $\sigma' = K_0^{NC} \sigma'_1$, and p_p^{eq} is a generalised pre-consolidation pressure, which is simply proportional to the one-dimensional one. For the known values of K_0^{NC}, p^{eq} can thus be computed from σ', and p_p^{eq} can be computed from σ_p. By omitting the elastic strain in the 1D-equation (2-67), introducing the above expressions for p^{eq} and p_p^{eq} and writing ε_v instead of ε it is found that:

$$-\dot{\varepsilon}_v^c = \frac{C}{\tau}\left(\frac{p^{eq}}{p_p^{eq}}\right)^{\frac{B}{C}} \tag{2-72}$$

where:

$$p_p^{eq} = p_{p0}^{eq} \exp\left(\frac{-\varepsilon_v^c}{B}\right) \tag{2-73}$$

For one-dimensional Oedometer conditions, this equation reduces to Eq. (2-67), so that one has a true extension of the 1D-creep model. It should be noted that the subscript '0' is once again used in the equations to denote initial conditions and that $\varepsilon_v^c = 0$ for time $t = 0$.

Instead of the parameters *A*, *B* and *C* of the 1D-model, we will now change to the material parameters κ^*, λ^* and μ^*, which fit into the framework of critical-state soil mechanics. Conversion between constants is as follows:

$$\kappa^* = 2A \;,\; B = \lambda^* - \kappa^* \;,\; \mu^* = C \tag{2-74}$$

On using these new parameters, Eq. (2-72) changes to become:

$$-\dot{\varepsilon}_v^c = \frac{\mu^*}{\tau}\left(\frac{p^{eq}}{p_p^{eq}}\right)^{\frac{\lambda^*-\kappa^*}{\mu^*}} \tag{2-75}$$

with:

$$p_p^{eq} = p_{p0}^{eq} \exp\left(\frac{-\varepsilon_v^c}{\lambda^*-\kappa^*}\right) \tag{2-76}$$

As yet the 3D-creep model is incomplete, as we have only considered a volumetric creep strain ε_v^c, whilst soft soils also exhibit deviatoric creep strains.

For introducing general creep strains, we adopt the view that a creep strain is simply a time-dependent plastic strain. It is thus logical to assume a flow rule for the rate of creep strain, as usually done in plasticity theory. For formulating such a flow rule, it is convenient to adopt the vector notation and to consider the principal directions as follows:

$$\underline{\sigma} = \begin{pmatrix}\sigma_1 & \sigma_2 & \sigma_3\end{pmatrix}^T \tag{2-77}$$

and:

$$\underline{\varepsilon} = \begin{pmatrix}\varepsilon_1 & \varepsilon_2 & \varepsilon_3\end{pmatrix}^T \tag{2-78}$$

Where *T* is used to denote a transpose. Similar to the 1D-model we have both elastic and creep strains in the 3D-model. Using Hooke's law for the elastic part, and a flow rule for the creep part, one obtains:

$$\underline{\dot{\varepsilon}} = \underline{\dot{\varepsilon}}^{e} + \underline{\dot{\varepsilon}}^{c} = \underline{\underline{D}}^{-1}\,\underline{\dot{\sigma}'} + \lambda\frac{\partial g^{c}}{\partial \underline{\sigma'}} \tag{2-79}$$

Where the elasticity matrix and the plastic potential function are defined as:

$$\underline{\underline{D}}^{-1} = \frac{1}{E_{ur}}\begin{bmatrix} 1 & -\nu_{ur} & -\nu_{ur} \\ -\nu_{ur} & 1 & -\nu_{ur} \\ -\nu_{ur} & -\nu_{ur} & 1 \end{bmatrix} \tag{2-80}$$

and:

$$g^{c} = p^{eq} \tag{2-81}$$

Hence we use the equivalent pressure p^{eq} as a plastic potential function for deriving the individual creep strain-rate components. The subscripts '*ur*' are introduced to emphasize that both the elasticity modulus and Poisson's ratio will determine unloading-reloading behaviour. Now it follows from the above equations that:

$$\dot{\varepsilon}_{v}^{c} = \dot{\varepsilon}_{1}^{c} + \dot{\varepsilon}_{2}^{c} + \dot{\varepsilon}_{3}^{c} = \lambda\,.\left(\frac{\partial p^{eq}}{\partial \sigma_{1}'} + \frac{\partial p^{eq}}{\partial \sigma_{2}'} + \frac{\partial p^{eq}}{\partial \sigma_{3}'}\right) = \lambda\,.\frac{\partial p^{eq}}{\partial p'} = \lambda\,.\,\alpha \tag{2-82}$$

Hence we define $\alpha = \partial p^{eq} / \partial p'$. Together with Eqs. (2-76) and (2-79) this leads to:

$$\underline{\dot{\varepsilon}} = \underline{\underline{D}}^{-1}\,\underline{\dot{\sigma}'} + \frac{\dot{\varepsilon}_{v}^{c}}{\alpha}\frac{\partial p^{eq}}{\partial \underline{\sigma'}} = \underline{\underline{D}}^{-1}\,\underline{\dot{\sigma}'} - \frac{1}{\alpha}\frac{\mu^{*}}{\tau}\left(\frac{p^{eq}}{p_{p}^{eq}}\right)^{\frac{\lambda^{*}-\kappa^{*}}{\mu^{*}}}\frac{\partial p^{eq}}{\partial \underline{\sigma'}} \tag{2-83}$$

where:

$$p_{p}^{eq} = p_{p0}^{eq}\,\exp\left(\frac{-\varepsilon_{v}^{c}}{\lambda^{*}-\kappa^{*}}\right) \tag{2-84}$$

or inversely:

$$-\varepsilon_v^c = (\lambda^* - \kappa^*) \ln\left(\frac{p_p^{eq}}{p_{p0}^{eq}}\right) \tag{2-85}$$

2.7.4. Formulation of Elastic 3D-Strains

When considering creep strains, it has been shown that the 1D-model can be extended to obtain a 3D-model, however, this has not yet been done for the elastic strains.

To get a proper 3D-model for the elastic strains as well, the elastic modulus E_{ur} has to be defined as a stress-dependent stiffness tangent according to the following equation:

$$E_{ur} = 3(1-2\nu_{ur}) K_{ur} = -3(1-2\nu_{ur})\frac{p'}{\kappa^*} \tag{2-86}$$

Hence, E_{ur} is not a new input parameter, but simply a variable quantity that relates to the input parameter κ^*. On the other hand, ν_{ur} is an additional true material constant. Similar to E_{ur}, the bulk modulus K_{ur} is stress dependent according to the rule $K_{ur} = -p'/\kappa^*$. Now the volumetric elastic strain for that can be derived:

$$\dot{\varepsilon}_v^e = \frac{\dot{p}'}{K_{ur}} = -\kappa^* \frac{\dot{p}'}{p'} \tag{2-87}$$

or by integration:

$$-\varepsilon_v^e = \kappa^* \ln\left(\frac{p'}{p_0'}\right) \tag{2-88}$$

In the 3D-model, the elastic strain is controlled by the mean stress p', rather than by principal stress σ' as in the 1D-model. However, mean stress can be converted into principal stress. For one-dimensional compression on the normal consolidation line, we have both $3p' = (1 + 2 K_0^{NC})\sigma'$ and $3p_0' = (1 + 2 K_0^{NC})\sigma_0'$ and it follows that $p'/p_0 = \sigma'/\sigma_0$. As a consequence we derive the simple rule $-\varepsilon_{vc} = \kappa^* \ln(\sigma'/\sigma_0')$, whereas the 1D-model involves $-\varepsilon_{vc} = A \ln(\sigma'/\sigma_0')$. It would thus seem that κ^* coincides with A. Unfortunately this line of

thinking cannot be extended towards over consolidated states of stress and strain. For such situations, it can be derived that:

$$\frac{\dot{p}'}{p'} = \frac{1+\nu_{ur}}{1-\nu_{ur}} \frac{1}{1+2K_0} \frac{\dot{\sigma}'}{\sigma'} \tag{2-89}$$

and it follows that:

$$-\dot{\varepsilon}_v^e = \kappa^* \frac{\dot{p}'}{p'} = \frac{1+\nu_{ur}}{1-\nu_{ur}} \frac{\kappa^*}{1+2K_0} \frac{\dot{\sigma}'}{\sigma'} \tag{2-90}$$

where K_0 depends to a great extent on the degree of over consolidation. For many situations, it is reasonable to assume K_0 = 1 and together with ν_{ur} = 0.2 one obtains $-2\varepsilon_v^e = \kappa^*$ ln (σ'/σ_0'). Good agreement with the 1D-model is thus found by taking $\kappa^* = 2A$.

2.7.5. Modified Swelling Index, Modified Compression Index and Modified Creep Index

These parameters can be obtained both from an isotropic compression test and an Oedometer test. When plotting the logarithm of stress as a function of strain, the plot can be approximated by two straight lines (Fig. 2-9). The slope of the normal consolidation line gives the modified compression index λ^*, and the slope of the unloading (or swelling) line can be used to compute the modified swelling index κ^*. Note that there is a difference between the modified indices κ^* and λ^* and the original Cam-clay parameters κ and λ. The latter parameters are defined in terms of the void ratio e instead of the volumetric strain ε_V. The parameter μ^* can be obtained by measuring the long term volumetric strain and plotting it against the logarithm of time (Fig. 2-8).

Relationship to Cam-clay parameters:

$$\lambda^* = \frac{\lambda}{1+e} \qquad \kappa^* = \frac{\kappa}{1+e}$$

$$\lambda^* = B + \kappa^* \qquad \kappa^* \approx 2A \qquad \mu^* = C$$

$$\lambda^* = \frac{C_c}{2.3(1+e)} \qquad \kappa^* \approx \frac{2}{2.3} \frac{C_r}{1+e} \qquad \mu^* = \frac{C_\alpha}{2.3(1+e)}$$

2.8. Prediction of Organic and Peat Soils Settlements

Compression of organic and peat soils are characterized by their excessive and long term settlements which are caused by creep under a constant vertical effective stress. In many cases structures built over these layers yield relatively small primary settlements early on but have significantly greater secondary compression with the expulsion of water from micropores or viscous deformation of the soil structure. The creep law for clay first proposed by Buisman (1936) may be extended by researchers to determine the secondary compression.

Edil and Dhowian (1979), Edil and Mochtar (1984) improved the theoretical model proposed by Gibson and Lo (1961) to represent the compression behaviour of peat. This model has been found to give satisfactory results in representing the one-dimensional compression of peat under a given increment of stress. The model utilizes three empirical parameters pertaining to the primary compression, the secondary compression, and the rate of secondary compression, respectively. The time-dependent strain, $\varepsilon(t)$, may be written as

$$\varepsilon(t) = \Delta\sigma \left[a + b \left(1 - e^{-(\lambda/b)t}\right]\right. \qquad (2\text{-}91)$$

where $\Delta\sigma$ = stress increment
a = primary compressibility
b = secondary compressibility
λ/b = rate factor for secondary compression
t = time

The method uses a plot of logarithm of strain rate versus time (log $(\Delta\varepsilon/\Delta t)$ versus t). A convenient method of analysis of a given set of vertical strain-time data in order to determine the empirical parameters (a, b, and λ) was described by Edil and Dhowian, 1979. This should result in a straight line for the time range corresponding to the secondary compression if the soil conforms to the basic assumptions made in the model. The slope and intercept of this best-fit line yield the values of a, b and λ as follows:

$$\text{Slope of the line} = -0.434\ (\lambda/b) \qquad (2\text{-}92)$$

$$\text{Intercept of the line} = \log\ (\Delta\sigma\ \lambda) \qquad (2\text{-}93)$$

$$a = \varepsilon(t)/\Delta\sigma - b + be^{-(\lambda/b)t_k} \quad (2\text{-}94)$$

Where t_k is the last time a reading of compression is taken. When H is the soil layer thickness, then the settlement of the layer can be written as:

$$s = \varepsilon(t) \,.\, H \quad (2\text{-}95)$$

CHAPTER III

EXPERIMENTAL SETUP AND MODEL CONFIGURATION

3.1. General

The experimental program of this study is directed toward establishing an understanding of the capacity of the tiang tongkat foundation and its load-transfer behaviour over Pontianak soft organic soil. The physical and mechanical properties tests were carried out at both the Soil Mechanic Laboratories of Tanjungpura University Pontianak-Indonesia and IFGT TUB Freiberg-Germany.

Tested for their properties were commercially available Kaolin and natural soils from eight fields in Pontianak city. Samples were taken from 28 boreholes which varied in depth from 1 to 42 m in the following 8 fields: Perdana, A. Yani II, Terminal – Siantan, Ramayana, Yos Sudarso, Danau Sentarum, BNI-46 Tanjungpura and Astra – A. Yani. Since the soil at every site is different, the soil properties must be determined by laboratory or field tests. More than 180 specimens were tested for their mechanical properties. As the ground water level was high, often nearing ground surface, all of the samples had 100% degree of saturation (Sr) at about 0 to 2 m depth. The laboratory results were used in the Finite Element Plaxis 3-Dimensional Foundation program with a variety of tiang tongkat foundation models.

3.2. Physical Properties

All soil is made up of three basic constituents i.e. solids, liquids, and gases. Solids may be either mineral or organic matter, or both with their pore spaces filled with water and/or air. If all of the pore spaces are filled by water, the soil is saturated. The purpose of the physical property tests is to obtained adequate information relating to behaviour of the soil, in order to facilitate the design of foundation. These properties may be classified as classification and behavioural properties. To describe any soil, the following may be tested:

- water content, W_n
- unit weight, γ
- specific gravity, G_S
- Atterberg limits
- sieve analysis
- organic content, OC
- degree of saturation, S_r

3.3. Mechanical Properties

Consolidation of a sample produces increased density, a small decrease in water content, and an increase in shear strength. The increase in shear strength will be partly due to the decrease in water content, resulting in a closer spacing of clay particles so that the interparticle attraction is larger, as well as partly due to the interlocking effect from the denser particle arrangement. At the end of consolidation, the excess pore pressure produced by the consolidation stresses should be approximately zero which is the definition of end of consolidation (Bowles, 1979).

The most important aspect in geotechnical engineering is soil shear strength which affects slope stability as well as the types of foundations and retaining walls designed. If the load or stress in a foundation or earth slope is increased until the deformations become unacceptably large, it can be said that the soil of the foundation or slope has failed. The shear strength of a soil is the ultimate or maximum shear stress the soil can withstand (Holtz and Kovacs,1981).

Three main mechanical property tests are commonly used to examine the mechanical behaviour of soils and, in particular, to investigate their strength and deformations during loading. They are the consolidation, direct shear and triaxial tests. The consolidation test is carried out to obtain soil data which are used in predicting the rate of settlement. The most important soil parameter furnished by a consolidation test is the compression index, C_c, which indicates the compressibility of the specimen. The shear strength of cohesive soil is determined by the direct shear and triaxial tests so that cohesion, c and the internal friction angle, ϕ can be measured.

3.3.1. Direct Shear Test

A series direct shear tests were carried out on specimens of a 20 mm height and 40 cm^2 area. The specimen was put into a shear box with filter papers positioned at the top and bottom of the soil specimen separating the specimen from the porous stones at each end to prevent particles from being forced into the pores of the stones. The porous stones were kept in distilled water for a sufficient time to reach saturation. The box was then mounted on a loading frame with vertical deflection and horizontal displacement dial gauges properly adjusted to give accurate dial readings while under application of a load. Shearing tests were conducted with 50 kN/m^2, 100 kN/m^2 and 200 kN/m^2 normal stresses respectively.

3.3.2. Consolidation Test

These series of tests were carried out on specimens that were prepared similar to those in the direct shear test. Each ring with the sample prepared as described in Section 3.3.1 above was placed in a consolidation cell. The cell was then mounted on a loading frame with a vertical deflection dial gauge properly adjusted to give a proper dial reading under application of load. The load increment ratio was uniform with loads from 25 kN/m^2 to 800 kN/m^2 being applied for 24 hours. Particularly for Kaolin with sand, the maximum loading was 1200 kN/m^2. Once reaching the maximum loads for both natural soils and Kaolin, the load was decreased to 25 kN/m^2 after a period of 24 hours.

3.3.3. Triaxial Test

Triaxial compression tests were conducted on only 6 specimens from the fields of Astra – A. Yani and Perdana of Pontianak while another series was conducted on 12 specimens of Kaolin. Cylindrical specimens of 50 mm diameter and 100 mm depth were used for these tests. Pore water pressures were measured at both the top and the bottom of each specimen. The consolidated undrained, *CU*, and consolidated drained, *CD*, with normal and over consolidations (*NC* and *OC*, respectively) were carried out. Both total and effective stresses could be calculated during shear and at failure.

In the *NC* series, the specimen was isotropically consolidated under the desired effective stresses, σ'_3 where the stresses were 300 kN/m^2, 450 kN/m^2 and 600 kN/m^2 respectively. After consolidation was completed, the specimen was loaded to failure by increasing the deviator stress, (σ'_1 - σ'_3). In the *OC* series, the tests were conducted with 3, 6 and 12 over consolidated ratios, n_p, respectively. Before being loaded, the specimen was isotropically consolidated to maximum 600 kN/m^2 effective stress and then unloaded to 50 kN/m^2, 100 kN/m^2 and 200 kN/m^2 respectively.

The *CU* test was used on Pontianak soft organic soils. The selections were based on, first, the average topography in Pontianak which is low being near sea level, and second, the water content, W_n, is high. The *CU* and *CD* tests were carried out on Kaolin.

3.4. Kaolin Preparation

Nowadays, Kaolin is widely used as material for soft soil models. Kaolin clay is a versatile industrial material which has many trade names as it is produced around the world. In this study, the laboratory tests were carried out on commercially available Kaolin H 1 which is specially used to model super soft soil. The mineralogical properties of this material are potassium-feldspar = 6%, kaolinite = 90%, quartz = 3% and other minerals = 1%. To more accurately mimic the real conditions in Pontianak, the Kaolin was mixed with a fraction of sand and had a high water content.

Firstly, the sand was considered fine after passing through a 0.2 mm sieve and was mixed by a weight ratio of 15% of the total weight of Kaolin. After that, the Kaolin and sand were mixed with approximately 110% water with an electric mixer for 30 minutes to achieve a homogeneous sample where the water content, W_n, after consolidation would remain higher than the liquid limit, *LL*. The reason for this was that most of the water content, W_n, from the Pontianak soft organic soil samples were higher than their liquid limits, *LL*. The water content was measured before and after each test.

After achieving a homogeneous sample, the slurry was poured into a white steel tube of a 100 mm in diameter and 250 mm in length which had been placed vertically onto an automatic Oedometer apparatus. Firstly, the sedimentation process (settling time) of about 24 hours of the slurry was carried out. During this time of the flocculation and settling stages, particles in the mixture flocculate in such a way that flocks are formed, after which uniform

aggregates of the flocks settle onto the seabed (Imai, 1980). Following the settling time, the water separates from the deposit. However, loads cannot yet be applied to the slurry before or even during this process, as the sample does not have enough strength to support any load, often overflowing immediately after a load is applied.

Once the settling time was completed, the preconsolidation process of the Kaolin sample was carried out by applying a series of loads which ranged from 11 kN/m^2 to 300 kN/m^2 with a load increment ratio (*LIR*) of 2. Each pressure was applied 24 hours so that 90% consolidation was achieved with drainage being permitted from the top and bottom of the deposit. After the preconsolidation test, the total deformation of the Kaolin was from 40% to 55% of the initial height. Figure 3-1 shows the apparatus used for this process.

Fig. 3-1. Preconsolidation Tests of Kaolin

3.5. Field Load Tests

The quick maintained load (QML) test was used to determine the load capacity of foundations in Pontianak city. During a full scale load test, three types of foundations (mini pile, T1, mini pile with a pair of horizontal mini beams, T2, and mini pile with two pairs of horizontal mini beams, T3) were subjected to failure in compression. These models are shown in Figure 3-2. Whereas in Figure 3-2(a) the square mini pile was 10 cm width and 140 cm long, in Figures 3-2(b) and (c) this was combined with horizontal beams 4 cm by 8 cm width and 60 cm long to be used as full scale models.

Three full scale models were tested in Perdana conducted by Sentanu, Noviarty and Suhendra, 2002, and another two models were also tested in Untan field conducted by Triyanti and Hadianto, 2002, respectively, which did not include the testing of the mini pile, T1. The ground water level for both fields located about 0.20 to 0.30 m below the ground surface. Before the tests, all of the models were driven into the ground at a selected depth and allowed sufficient time of about 30 days for dissipation of excess pore water pressures resulted from the pile driving operation. The settlement at each stage of loading was taken at intervals of 5 minutes. The soil properties of both sites are classified as organic clay which having 117.73 % and 102.97 % water content, 13.55 and 16.40 kN/m^3 unit weight, 7 and 13 kN/m^2 cohesion and 12 and 10º friction angle. The physical properties of both in-situ for full scale load tests are listed in Table 3-1.

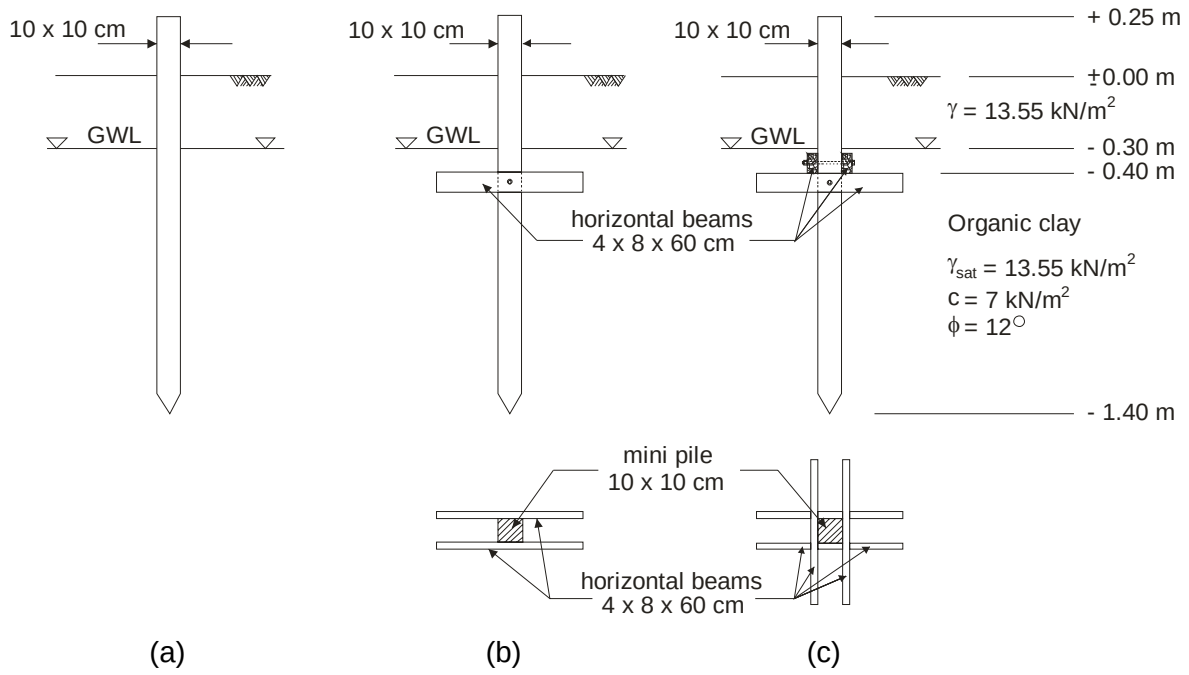

Fig. 3-2. Models of Field Load Tests: (a) mini pile, T1, (b) mini pile with a pair of horizontal beams, T2, (c) mini pile with two pairs of horizontal beams, T3

Table 3-1. Physical Properties of In-situ Full Scale Load Tests

Properties	**Site names**	
	Perdana	Untan
Soil classification	Organic clay	Organic clay
Water content, W_n (%)	117.73	102.97
Unit weight, γ_{sat} (kN/m^3)	13.55	16.40
Cohesion, c' (kN/m^2)	7	13
Friction angle, ϕ'	12	10
Foundation type	Mini pile, Tiang tongkat	- Tiang tongkat

3.6. Tiang Tongkat Foundation Models

Figure 3-3 illustrates the basic models of the tiang tongkat foundation that were used for finite element simulation. Similar to the field load test models, four basic foundation models used are as follows:

P1 (Fig. 3-3(a)), mini pile,

P2-1 and P2-2 (Fig. 3-3(b) and (c)), tiang tongkat with a pair of horizontal beams,

P3-1 and P3-2 (Fig. 3-3(d) and (e)), tiang tongkat with two pairs of horizontal beams and,

P-4 (Fig. 3-3(f)), pile combined with square floor.

All piles varied from 10, 12 and 14 cm in width, *D*, and 140 cm, 260 cm and 380 cm in total length, *L*t. Two different horizontal beams were used with the tiang tongkat. In the foundation models of P2 through to P4, each beam of *B* length (from 50 to 110 cm) was coupled with either one or two pairs of horizontal beams of *B1* width (4, 10, 15 cm) or of *B2* width (10, 20, 30 cm).

Each foundation was subjected to vertical and inclination point loads to failure in compression. The foundations were placed at the centre of a small excavation at a 40 cm depth so that the embedment lengths, *L*, of the piles were 100 cm, 220 cm and 340 cm respectively. The water table in each case was considered to be 30 cm below ground surface. The characteristics of the tiang tongkat foundations for each field and their parameters are listed in Table 3-2 and Table 3-3.

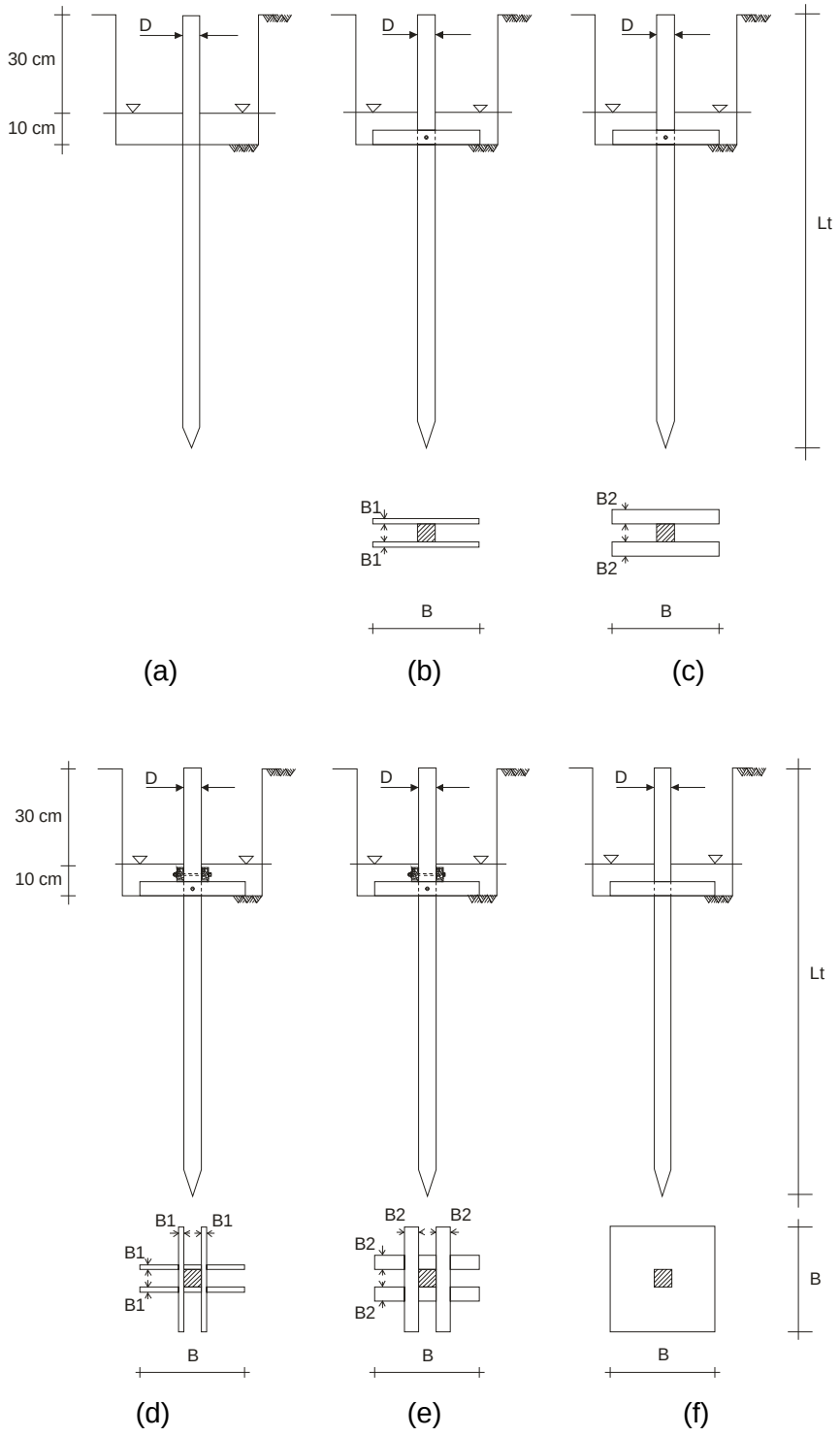

Fig. 3-3. Finite Element Models of the Tiang Tongkat Foundation
(a) mini pile, P1, (b) and (c) mini pile with a pair of horizontal beams, P2-1 and P2-2
(d) and (e) mini pile with two pairs horizontal beams, P3-1 and P3-2
(f) mini pile combined with square floor, P4

Table 3-2. Characteristics of Tiang Tongkat Foundations for each Field

No.	Site names	Tiang Tongkat Foundations Dimensions				
		D (cm)	*Lt* (cm)	*B1* (cm)	*B2* (cm)	*B* (cm)
1	Perdana	10	140	4	10	60
		10	260	10	20	80
		10	380	15	30	100
2	A. Yani II	12	140	4	10	50
		12	260	10	20	70
		12	380	15	30	90
3	Terminal-Siantan	14	140	4	10	70
		14	260	10	20	90
		14	380	15	30	110
4	Ramayana	10	140	4	10	50
		10	260	10	20	70
		10	380	15	30	90
5	Yos Sudarso	12	140	4	10	70
		12	260	10	20	90
		12	380	15	30	110
6	Danau Sentarum	14	140	4	10	60
		14	260	10	20	80
		14	380	15	30	100
7	BNI46-Tanjungpura	10	140	4	10	70
		10	260	10	20	90
		10	380	15	30	110
8	Astra-A. Yani	12	140	4	10	60
		12	260	10	20	80
		12	380	15	30	110
9	Kaolin with sand	14	140	4	10	50
		14	260	10	20	70
		14	380	15	30	90

Table 3-3. Parameters of Tiang Tongkat Foundations

Parameters	Unit	Mini pile	Horizontal beam/ Floor
Material model		Linear elastis	Linear
Type of material behaviour		Non-porous	-
γ_{unsat}	kN/m^3	19	19
E	kN/m^2	1.25E+07	1.25E+07
ν		0.15	0.15
A	m^2	-	0.024

CHAPTER IV

CHARACTERIZATION OF SOILS

4.1. Material Characterization of Pontianak Soft Organic Soils

Most of the Pontianak samples were blackish brown, blackish grey to dark black in colour and had an acidic smell. Of the two fields tested, the organic content, *OC*, of about 10% was found. Loss on ignition was somewhat varied when the samples were oven-dried at 550 °C for the duration of 4 hours. Although the percentage of this content is not high, this value significantly influences the behaviour of soil, as organic matter tends to make a soil weaker and more compressible.

4.1.1. Physical Properties

Fig. 4-1 shows the grain size distribution of Pontianak soft organic soils which is combined both sieve and hydrometer tests. These are classified as fine grain soils because most of the samples having average 84 % pass through sieve No. 200. As shown in Fig. 4-2 on the plasticity chart, the plotted characteristics of the soils lay above and below the A-line. The plasticity index, *PI*, and liquid limit, *LL*, varied widely ranging from 5 to 35% and 20 to 70 % respectively. Based on visual observation, organic content, *OC*, and grain size distribution as well as according to ASTM Standard D2487-00, these soils are classified as organic soil.

Generally, organic silt deposits seem dominantly near the ground surface and are about 6 to 8 m thick. Organic clay is located below this layer. The sandy soil layer is found at about 15 to 30 m depth. At several locations near the Kapuas river, however, it is located at about 5 to 10 m depth. Sand layer is located at about 30 m depth.

The relationship of physical properties against depth is shown in Fig. 4-3. The water content, W_n, varies widely ranging from 25 to 200% but decreases with greater depth. Of all the samples collected, only a few borepoints showed higher than 200% water content. This value could be separated into two depths. From surface to about 15 m depth, the water content ranged from 50 to 100% while deeper than 15 m, the range was from 25 to 50% (see Fig. 4-3(a)). Water content is one of the easiest properties to obtain and is also one of the

most useful as much research has shown it to be a good indicator of the shear strength of saturated clay (Lambe, 1951).

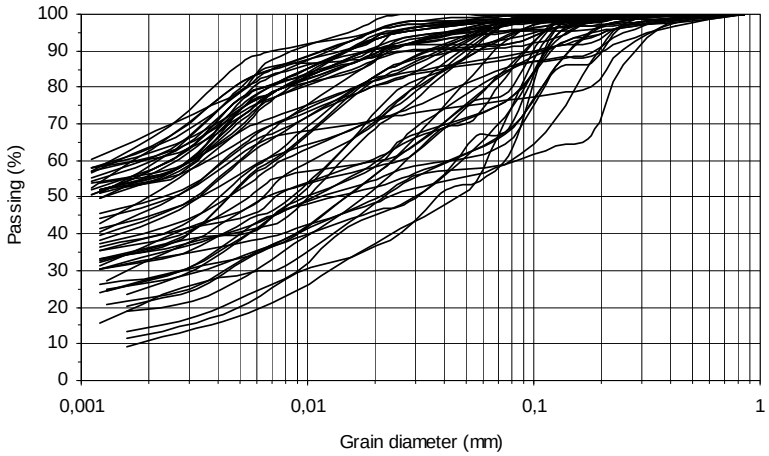

Fig. 4-1. Grain Size Distribution of Pontianak Soft Organic Soil

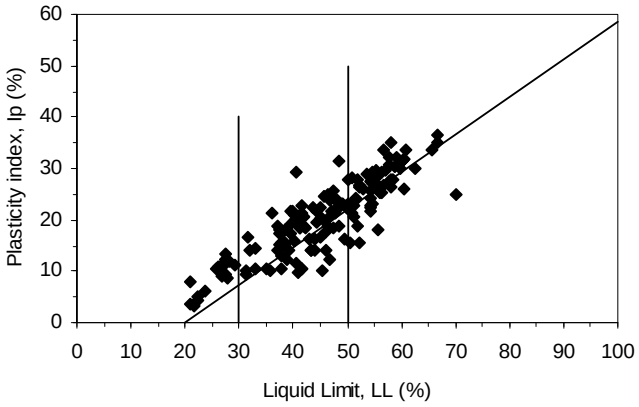

Fig. 4-2. Plasticity of Pontianak Soft Organic Soil

Overall, the water content, W_n, of Pontianak soft organic soil was higher than its liquid limit, *LL*. A cohesive soil with water content higher than its liquid limit is defined as super soft clay. This definition includes very sensitive clays after they have been disturbed. Super soft clay is neither a liquid nor a solid; it is a material with characteristics bordering between the two. It may be defined as a soil with no practical bearing capacity, often displaying a fluid-like consistency and behaviour (Fakher and Jones, 1996).

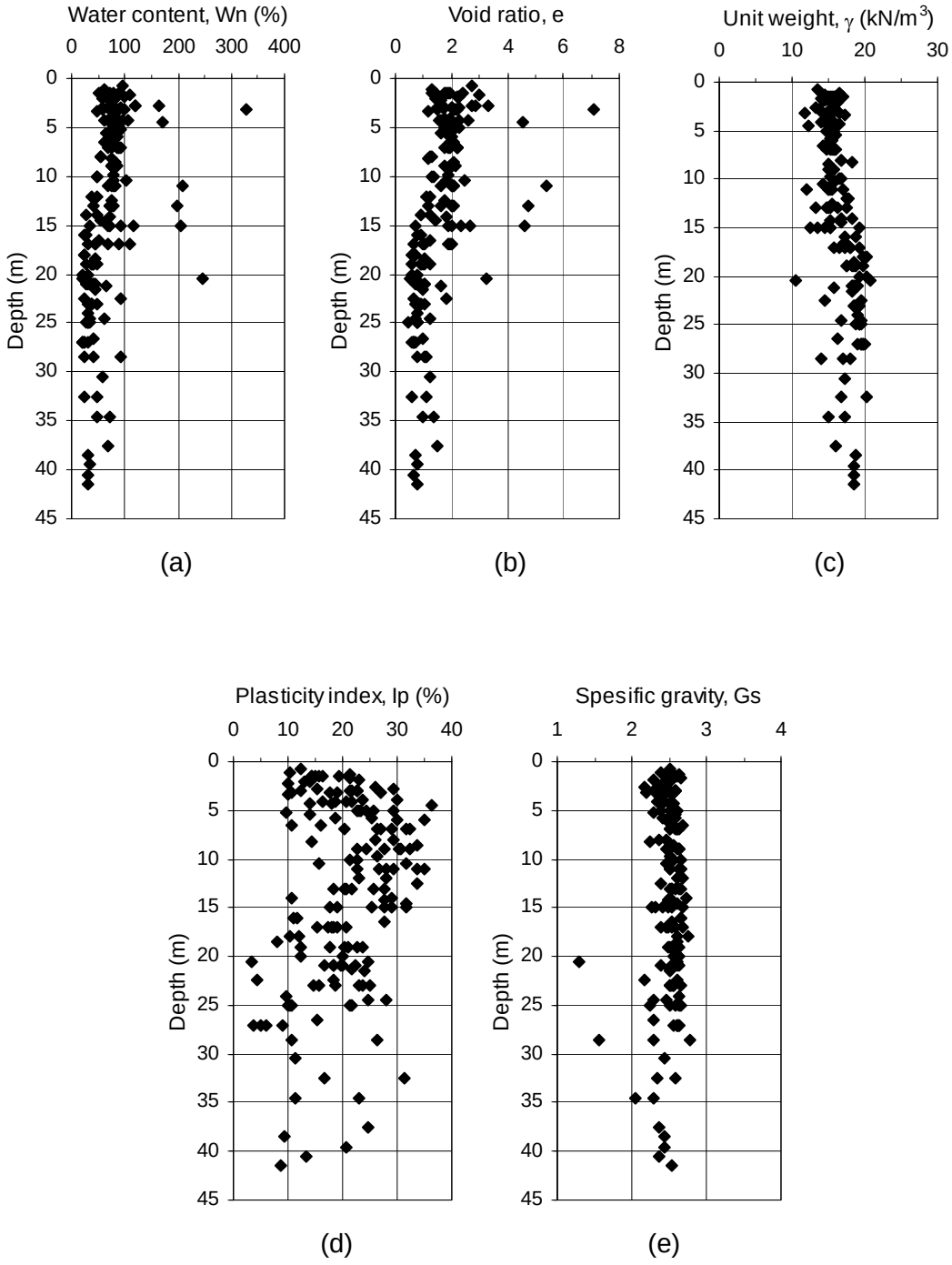

Fig. 4-3. Physical Properties of Pontianak Soft Organic Soil

According to Fig. 4-3(b) above, the void ratio, *e*, tends to decrease with depth, ranging from 1.5 to 3 until 15 m depth whereas several borepoints show higher than 3, and then decreasing to a constant value of about 1.5 below 15 m. The natural void ratio, *e*, of amorphous peats, on the other hand, is much lower down to a value of 2 (Hillis and Brawner, 1961). For slightly organic clay, a natural void ratio, *e*, less than 2 is expected. It can be seen in Fig. 4-3(c) that unit weight, γ, is relatively constant ranging from 14 to 18 kN/m^3, increasing slightly to 19 kN/m^3 at 15 m depth and deeper.

The plasticity index of Pontianak soft organic soil in Fig. 4-3(d) shows a widely scattered pattern ranging from 10 to 35% until 15 m depth and then decreasing sightly from 5 to 30% deeper than 15 m. As shown in Fig. 4-3(e), the specific gravity, G_S, is generally constant ranging from 2.2 to 2.6 as depth increases. In the literature the range of specific gravities, G_S, is from 1.1 to 2.5 for peats (Muskeg Engineering Handbook, 1969) and it could be slightly higher for some organic soils with low organic content.

Table 4-1 below summarizes Figures 4-2 and 4-3. Most of the samples have a 100 % degree of saturation which influences such fundamental soil properties as permeability, shear strength, and compressibility. The liquidity index, *LI*, is over 2 at below 15 m depth, with several locations having ranges from 6 to 8. However, the average *LI* is about 2.06. These values show that the soil could be considered extremely sensitive to breakdown of the soil structure and that it would be essentially a very viscous liquid when sheared. In an undisturbed state, this soil may be stable; however, a sudden shock may transform them into a liquid state. Such soils are called sensitive clays (Das, 1983).

Table 4-1. Properties of Pontianak Soft Organic Soil

Properties	**Pontianak Soft Organic Soil**
Water Content, W_n (%)	25 – 200
Void Ratio, *e*	1.5 – 3
Specific Gravity, G_S	2.2 – 2.6
Saturated Unit Weight, γ_{sat} (kN/m^3)	14 – 19
Liquid Limit, *LL* (%)	22 – 70
Plastic Limit, *PL* (%)	17 – 35
Plasticity Index, *PI* (%)	5 – 35
Average Liquidity Index, *LI*	2.06

4.1.2. Compression Characteristics

When soils undergo loading, because of their relatively low permeability, their compression is controlled by the rate at which water is squeezed out of the pores. The slope e versus log σ' plot for normally consolidated soil is referred to as the compression index, C_c. In order to characterize the Pontianak soft organic soil compressibility behaviour, a series of incremental load Oedometer tests were carried out on specimens prepared from intact samples collected at different depths. The load increment ratio was uniform where loading was 25 kN/m^2 to 800 kN/m^2. Some of the 1-D Oedometer tests results are shown in Fig. 4-4.

The compression index, C_c varies widely with increasing depth, however the depth does not influence of C_c. The top layer that is 10 m thick is highly compressible ranging from 0.5 to 1.38 with an average value of about 0.8 but it becomes significantly less compressible at below this layer ranging from 0.2 to 0.5 with an average value are about 0.3. Similar to the compression index, the recompression index, C_s decreases with greater depth. This value ranges widely from 0.03 to 0.25.

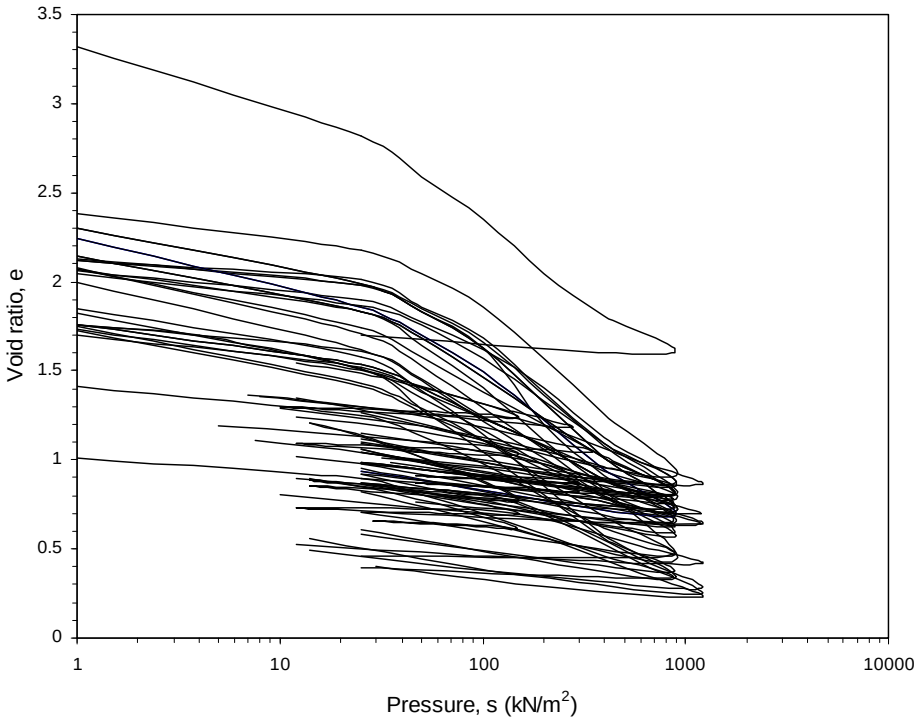

Fig. 4-4. 1-D Oedometer Tests of Pontianak Soft Organic Soil

4.1.3. Over Consolidated Ratio

The over consolidated ratio, *OCR*, is defined as the ratio between the preconsolidation stress and the effective in-situ stress. *OCR* is a state parameter that indicates the amount of overconsolidation of the soil (Brinkgreve, 2001). This value notably reduces with depth. Pontianak soft organic soils are heavily over consolidated from ground surface to about 5 m depth due to the wetting and drying cycles during deposition. The over consolidation ratio, *OCR*, ranges 2 to 11 at this layer. Slightly over consolidated with *OCR* ranges from 1.3 to 2 are found at about 5 to 20 m depth.

4.1.4. Shear Strength Characteristics

A soil's shear strength which is the internal frictional resistance of a soil to shearing forces is the most important aspect in geotechnical engineering. The shear strength of saturated soil is dependent on the effective stress acting on the soil particles, the soil type, and the soil structure. Shear strength is basically the measure of the maximum or ultimate stress a material can sustain. It is a fundamental property required in the analysis of construction projects over peat and organic soils.

The shear test was used to determine the shear strength of Pontianak soft organic soil. This test was conducted on 154 specimens of which some representative measurements are shown in Fig. 4-5. Generally, the effective internal friction angle, ϕ', ranges from 3º to 19º and cohesion, c', ranges from 5 to 15 kN/m^2. It was found that these values remain constant until 15 m depth and then increase at greater depth. The change of the effective internal friction angle, ϕ', and cohesion, c', against depth are shown in Fig. 4-6. It can be seen that most of the samples have nearly similar slopes. This would be expected because the soils have very similar basic physical properties. However, there is considerable difference in the position of the shear resistance curves which is caused by a variation in cohesion which is related to the density, moisture content and plasticity.

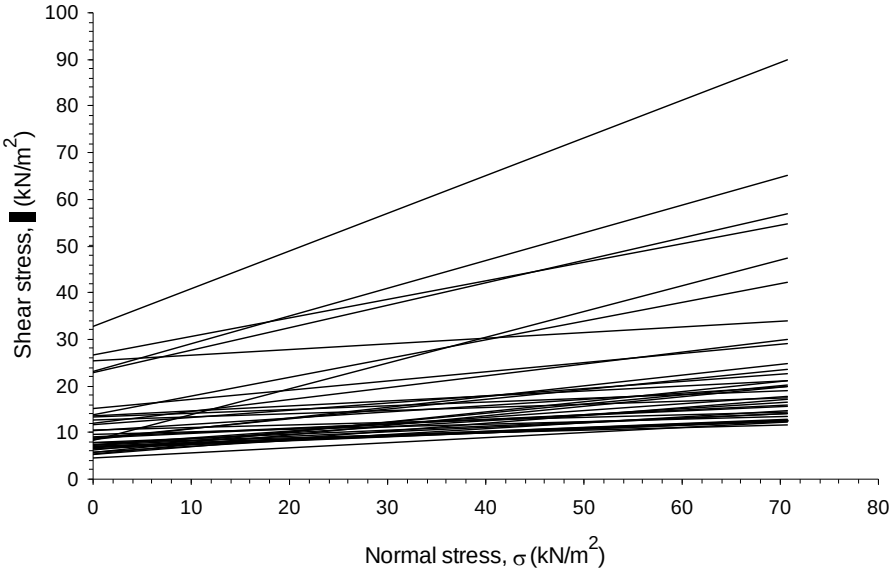

Fig. 4-5. Shear Tests of Pontianak Soft Organic Soil

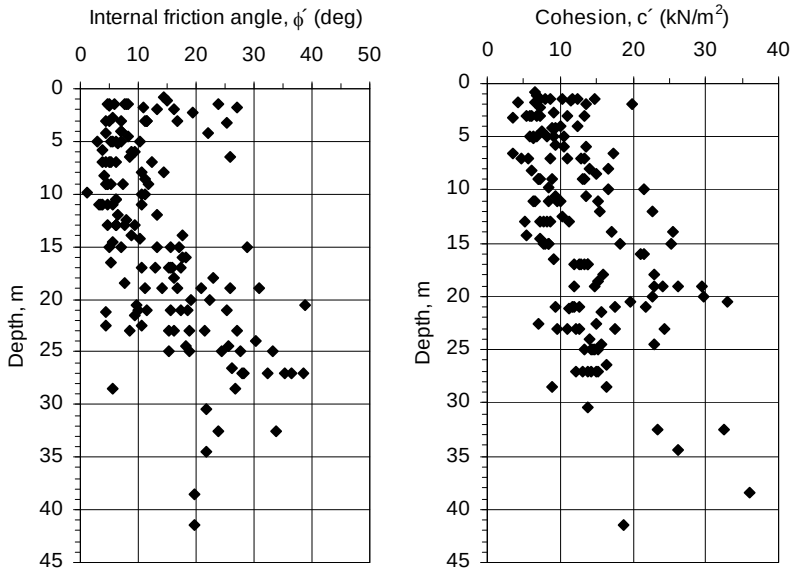

Fig. 4-6. Shear Strength Characteristics of Pontianak Soft Organic Soil against Depth

Besides the direct shear test, the triaxial compression test was also carried out to measure the shear strength of the soil. This test was conducted on 6 specimens located in the 2 fields of Perdana and Astra-A Yani. A specimen with a 50 mm diameter and 100 mm high was used. Pore water pressures were measured at the top and bottom of the specimens. The consolidated undrained, *CU*, tests with normal and over consolidations (*NC* and *OC*) were

carried out. The *CU* condition was taken based on, first, the average topography in Pontianak which is low and near sea water level, second, the water content, W_n, which is high. Both total and effective stresses were calculated during shear and at failure.

In the *NC* series, the specimen was first isotropically consolidated under the desired consolidation stresses, σ'_3. The isotropic pressures were 300 kN/m^2, 450 kN/m^2 and 600 kN/m^2 respectively. After consolidation was complete, the specimen was loaded to failure in undrained shear.

In the *OC* series, the tests conducted with over consolidated ratios, n_p were 3, 6 and 12 respectively. All specimens were isotropically consolidated to maximum effective stress 600 kN/m^2 and then unloaded isotropically to a mean effective stress 50 kN/m^2, 100 kN/m^2 and 200 kN/m^2 respectively.

Fig. 4-7 shows the curve of deviator stress, q, against vertical strain, ε_a, the maximum value being denoted by $q_f = (\sigma'_1 - \sigma'_3)_f$. In the *NC* series, the deviator stresses at failure, q_f, were 238.38 kN/m^2, 352.21 kN/m^2, 530.30 kN/m^2 respectively while the mean effective stresses at failure, p'_f, were 269.31 kN/m^2, 369.46 kN/m^2, 633.40 kN/m^2 respectively. In the *OC* series, q_f, were 210.68 kN/m^2, 288.61 kN/m^2, 408.76 kN/m^2 respectively and p'_f, were 132.1 kN/m^2, 201.26 kN/m^2, 309.3 kN/m^2 respectively.

The Mohr failure envelopes of both normal and over consolidated tests can be seen in Fig. 4-8. Based on these results, both effective cohesion, c', and effective internal friction angle, ϕ', on *NC* and *OC* tests were obtained as follows, c'_{NC} = 16.5 kN/m^2 ; ϕ'_{NC} = 20.31° ; c'_{OC} = 27 kN/m^2 ; ϕ'_{OC} = 28.26° respectively. The slope of the *OC* samples higher than that of the *NC* samples. Soil strength can be expressed as an effective friction component, which is a function of the effective normal stress added to the effective cohesion component, which is a function of the void ratio. The *OC* samples clearly have a higher void ratio, *e*, than the *NC* samples. Hence, the shear strength of the *OC* tests was higher than *NC* tests.

All of the compression triaxial tests lie on the critical state line with *M* gradient at about 0.6222. The shear strength parameters of the Pontianak soft organic soil are c' = 66.10 kN/m^2 and ϕ' = 16.37° respectively. The results are presented in the form of $p' - q$ plot in Fig. 4-9.

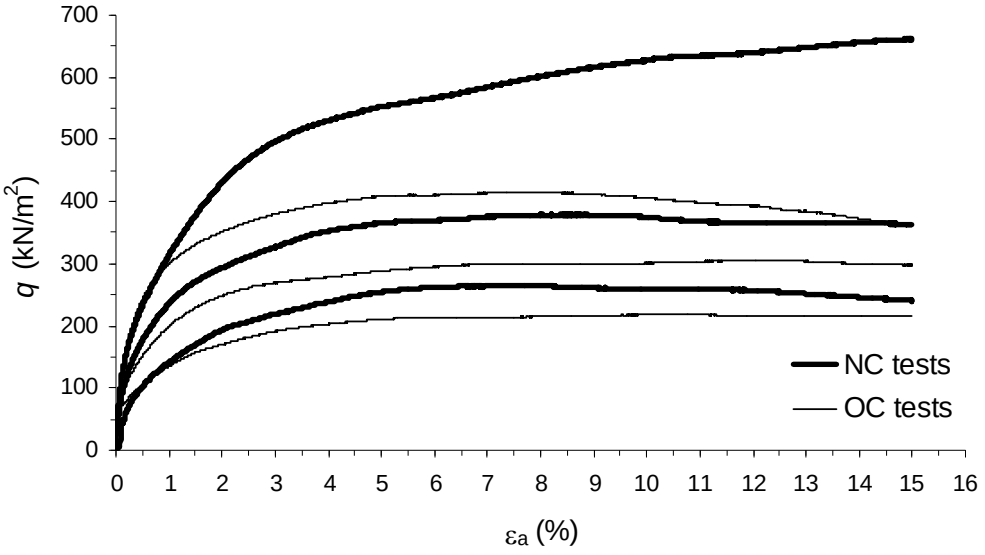

Fig. 4-7. Response to shearing on Pontianak soft organic soils for *NC-CU* tests

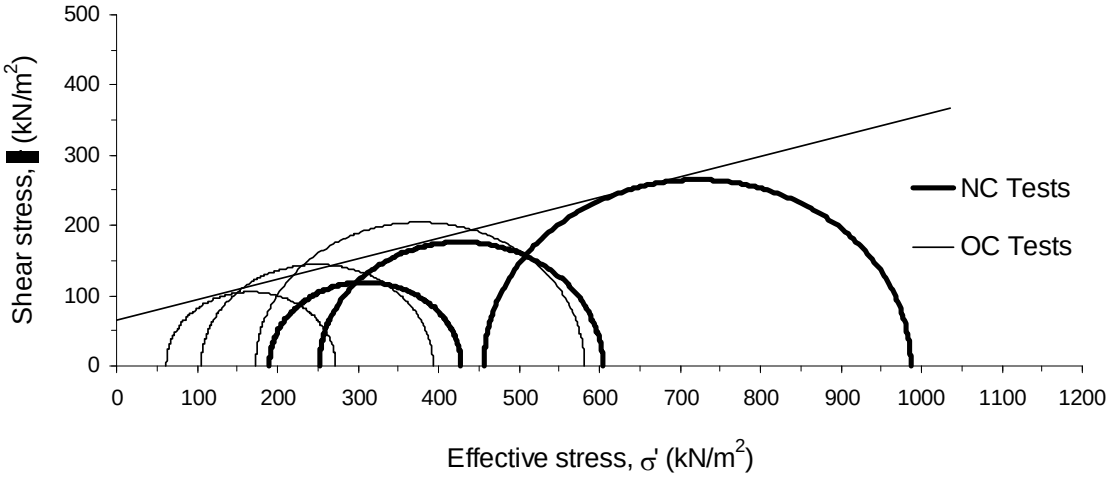

Fig. 4-8. Mohr Failure Envelopes for Normal and Over consolidated Pontianak Soft Organic Soils

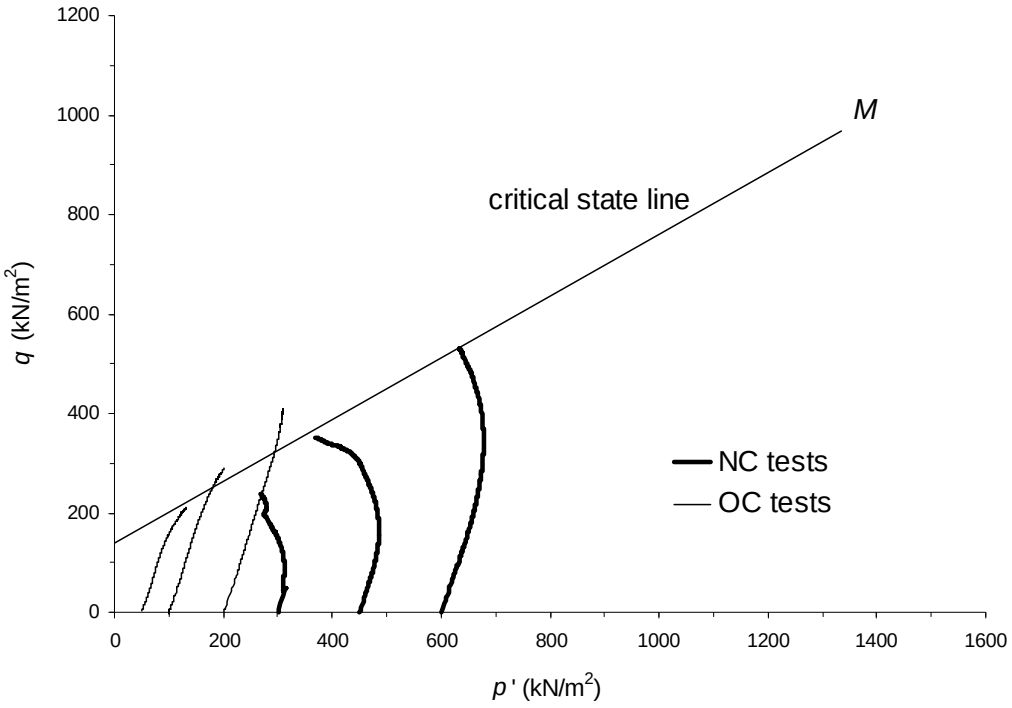

Fig. 4-9. Critical State Line of Pontianak Soft Organic Soil

4.2. Material Characterization of Kaolin

Commercially available Kaolin H 1 was modified and used to simulate Pontianak's super soft soil in this study.

4.2.1. Physical Properties

Grain size distributions of Kaolin, that is mixed with a 15% sand fraction, attains an overall mixture of 20% fine sand, 50% silt and 30% clay. The Kaolin consistency limits are a 41% liquid limit, *LL*, a 25% plastic limit, *PL*, and a 16% plastic index, *PI*. Based on these parameters, this soil is classified as silt with sand. The physical properties of Kaolin are listed in Table 4-2.

Table 4-2. Physical Properties of Kaolin

Properties	Kaolin
G_S	2.6
W_n (%)	40
LL (%)	41
PL (%)	25
PI (%)	16
S_r (%)	100

4.2.2. Compression Characteristics

In Figure 4-10 that follows, the void ratio versus effective vertical consolidation pressure of Kaolin plots the different preconsolidation pressures, water content, W_n, and void ratio, *e*. This figure clearly demonstrates that soil with low preconsolidation pressure has a higher water content as well as a higher void ratio. This can be seen in sample E4-1(0) which has an 86.19 % water content, W_n, and a 1.804 void ratio, *e*, as the soil was not subjected preconsolidation pressure. On the other hand, an increase in preconsolidation pressure will decrease water content, W_n, and void ratio, *e* as shown in sample EKS-13(300). These results show that high pressure will squeeze out more water decreasing the void ratio so that strength of soil will increase. However, the compression index, C_c, does not increase significantly, remaining quite stable at 0.3 for all of the samples.

4.2.3. Shear Strength Characteristics

Based on the Mohr circle, the undrained shear strength of Kaolin has 18º, effective internal friction, ϕ'_U, and 12 kN/m^2, effective cohesion, c'_U. The other drained shear strength has 14.33º, effective internal friction, ϕ'_D, and 20 kN/m^2, effective cohesion, c'_D. The relationship between effective stress, σ', and effective shear stress, τ', of Kaolin is shown in Fig. 4-11.

The compression triaxial *CU* and *CD* tests lie on the critical state line with *M* gradient being about 0.55. The effective internal friction, ϕ' and the effective cohesion, c' are quite similar with their results being determined by the Mohr circle. The shear strength parameters

of Kaolin are c' = 23.67 kN/m^2 and ϕ' = 14.37°. Fig. 4-12 shows the critical state line gradient of Pontianak soft organic soil and Kaolin with sand. The gradient of Pontianak soft organic soil is shown to be steeper than that of Kaolin.

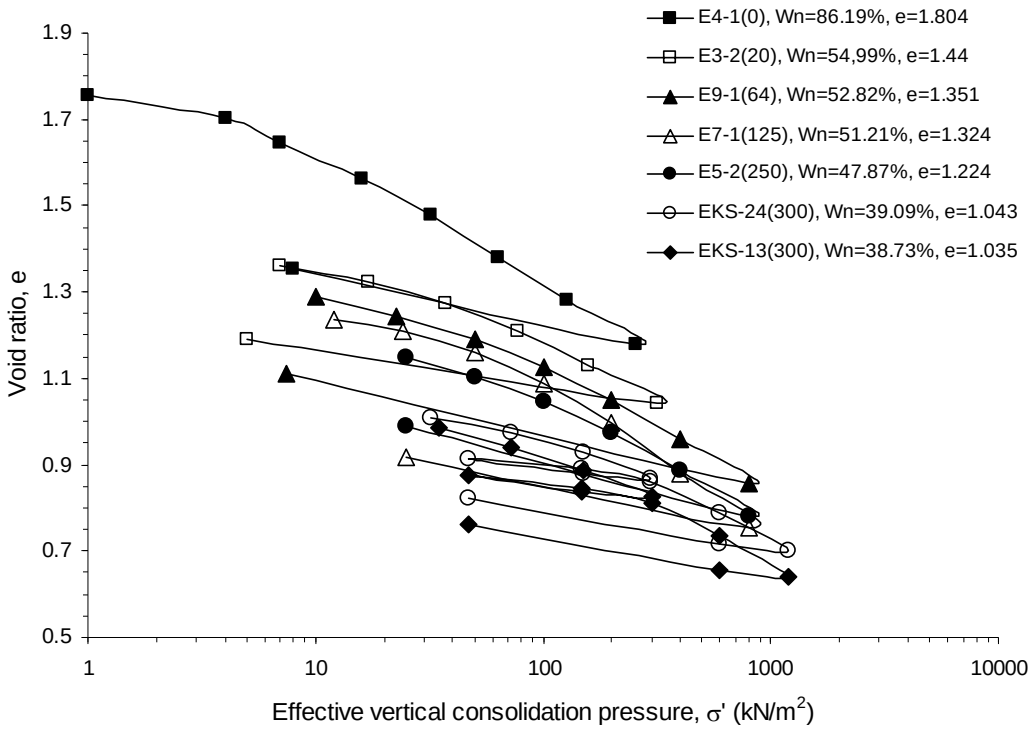

Fig. 4-10. Void Ratio versus Effective Vertical Consolidation Pressure

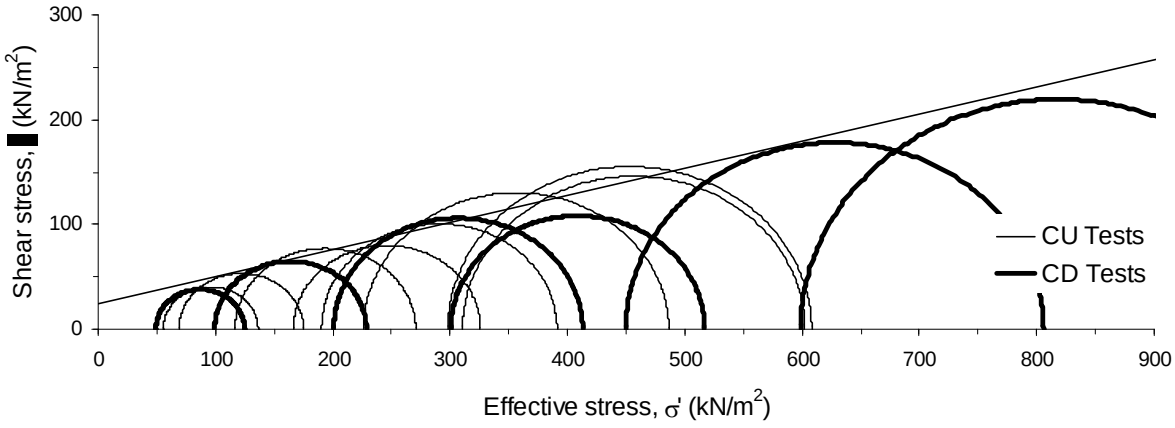

Fig. 4-11. Relationship between Effective Stress, σ', and Effective Shear Stress, τ', of Kaolin with Sand

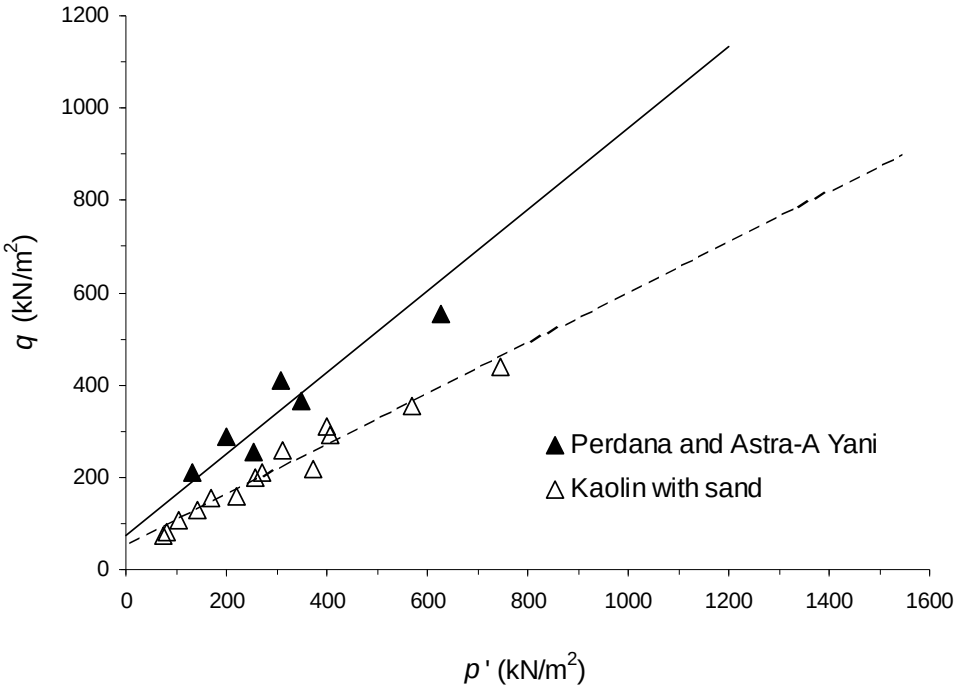

Fig. 4-12. Critical State Line Gradient of Kaolin with Sand

CHAPTER V

MATERIAL DATA SETS

5.1. General

The aim of this chapter is to present parameters' formulations for predicting load-settlement behaviour of traditional foundations and their load transfers in which all the interactions between plate or horizontal beams, pile and soil are simultaneously considered. The soil parameter models considered in this thesis are described. A tiang tongkat foundation of any dimension is constructed over different fields. The foundation was modelled as three-dimensional linear elastic and the Pontianak soft organic soil was modelled as undrained Soft-Soil-Creep Model, SSCM. The SSCM was selected to account viscous effects, i.e. creep and stress relaxation. In fact, all soils exhibit some creeps and primary compression is thus followed by a certain amount of secondary compression. All of the 324 models were simulated by means of the Plaxis 3-Dimensional Foundation Program.

Eight fields in Pontianak and an artificial soil of Kaolin were used as undrained Soft-Soil-Creep models. As explained above, the piles have 140 cm, 260 cm and 380 cm total length, *L*t, in order to avoid any influence on the boundaries; the soil mesh of 300 to 500 cm width and 400 to 1200 cm depth were used. The soft organic soil layer in Pontianak is thick and has a sand layer found at 15 to 30 m depth. Because these models are relatively small, the soil was considered to be a single slightly over consolidated layer.

Based on the laboratory and field load test results, some parameters were the same for all materials, i.e. over consolidated ratio, *OCR*; Poisson ratio, ν'; coefficient of lateral earth pressure, K_0; interface strength, R_{inter}; and Skempton *B*-parameter. The other parameters such as basic stiffness parameters, empirical parameters of primary, secondary and rate of secondary compressions were different for each location. The following section presented all assumptions and determinations of the parameters used to analyze the behaviour of tiang tongkat.

5.2. Overconsolidated Ratio, *OCR*

The top layer of Pontianak city is heavily over consolidated ratio. *OCR* varies from 2 to 11 at this layer as described in Section 4.1.3. Within this range, the soil behaviour will be stiffer. In fact, as shown from its physical and mechanical properties tests, the soil behaviour is soft. In this case, the soil is said to be in the state of normal consolidation, which would imply *OCR* = 1.0. This is exactly what happens in Cam-Clay type of models. In order for the preconsolidation stress to follow the effective stress level, time is needed. Hence by loading the soil very quickly, the *OCR* value can (temporary) become less than 1.0. On the other hand, if the load remains constant, the creep process continues by time, which results in a gradual increase of the preconsolidation stress and *OCR*. Particularly in the top layer (just below the ground surface), crust forming may occur, which is associated with relatively stiff and strong behaviour. The reason for this can be drying of the soil, variations of the phreatic level, temporary loads, temperature changes, etc. Nevertheless, these soils are still considered to be normally consolidated, but the actual *OCR* value is often higher than 1.0 (Brinkgreve, 2001).

The creep process starts immediately without additional loading, whereas the settlement velocity depends on the *OCR* value. The use of *OCR* value 1.0 in the K_0 procedure may lead to excessive initial settlement velocities. Hence, the initial *OCR* value larger than 1.0 is generally recommended. Therefore, for such problems it is recommended to use a slightly increased *OCR* value to generate the initial stress state. In the reality, however, most soils tend to show a slightly increased pre-consolidation stress in comparison with the initial effective stress (PLAXIS, 2006).

From explanations above, it can be concluded that an initial *OCR* value of 1.5, to be used in the K_0 procedure, would be a good choice. This value is slightly lower than in-situ; however it can represent soft organic soil which has excessive and long term settlement characteristics.

5.3. Poisson's Ratio

The lateral strain, ε_h at any point in a soil sample is proportional to the axial strain, ε_a at the same point if the material is linearly elastic. The ratio of these strains is a property of the material known as effective Poisson's ratio, ν' expressed as,

$$\nu' = \frac{\varepsilon_h}{\varepsilon_a} \tag{5-1}$$

Based on elasticity theory, we get

$$\Delta p' = K' \Delta \varepsilon_v \tag{5-2}$$

where $\Delta p'$ = increment effective mean stress

K' = effective bulk modulus

$\Delta \varepsilon_v$ = increment volumetric strain

The effective bulk modulus, K' is related to effective elasticity modulus, E' and Poisson's ratio, ν', may be written as

$$K' = \frac{E'}{3(1-2\nu')} \tag{5-3}$$

According to the triaxial test on Perdana samples, K', E' and ν' were 31,000 kN/m^2, 900 kN/m^2 and 0.35 respectively. However, different Poisson's ratio which determined from Eq. (5-3), gives ν' = 0.495. Therefore, the average Poisson's ratio ν' ≈ 0.4 is taken as the parameter design.

5.4. Coefficient of Lateral Earth Pressure, K_0

The coefficient of lateral earth pressure, K_0 in over consolidated soils is larger than in normally consolidated soils. This effect is automatically taken into account for advanced soil models when generating the initial stresses using the K_0-procedure. The basic formula is based on Jaky's correlation, K_0 = 1 – sin ϕ'. However, the Pontianak soft organic soil behaviour shows the internal friction angle, ϕ', is small which K_0 will be relatively high and increasing the lateral stress of soil. Hence, to reduce the affecting of lateral stress, determining of K_0 was changed to Hooke's law which is based on Poisson ratio, ν'.

$$K_0 = \frac{\nu'}{1-\nu'} \tag{5-4}$$

where ν' = effective Poisson's ratio

Based on the laboratory test, the Poisson's ratio ν' is taken 0.4 and K_0 is equal to 0.667.

5.5. Strength Reduction Factor, R_{inter}

A relative movement between a pile and soil produces shear stress along the interface of the pile and the soil. Such movement can be induced by a push-load on the pile pressing it down into the soil, or by a pull-load moving it upward (Fellenius, 1984). In addition to the soil properties, the interface properties from the soil will reduce the strength of soil-structure. The main interface parameter is the strength reduction factor R_{inter}.

The Coulomb criterion is used to distinguish between elastic and plastic behaviours of the interface strength. For the interface to remain elastic the shear stress τ is given by:

$$|\tau| < \sigma_n \tan\phi_i + c_i \tag{5-5}$$

where σ_n = effective normal stress

ϕ_i = friction angle of the interface

c_i = cohesion

For plastic behaviour τ is computed using following equation:

$$|\tau| = \sigma_n \tan\phi_i + c_i \tag{5-6}$$

The strength properties of interfaces are linked to the strength properties of a soil layer. The interface properties are calculated from the soil properties and the strength reduction factor by applying the following rules:

$$c_i = R_{inter}\, c_{soil} \tag{5-7}$$

$$\tan \phi_i = R_{inter} \tan \phi_{soil} \leq \tan \phi_{soil} \quad (5\text{-}8)$$

The strength reduction factor, R_{inter} in Eq. (5-7) and (5-8) can be calculated by the field load test result. According to Figure 5-1(a) about shear strength along the pile, the side friction force of it is,

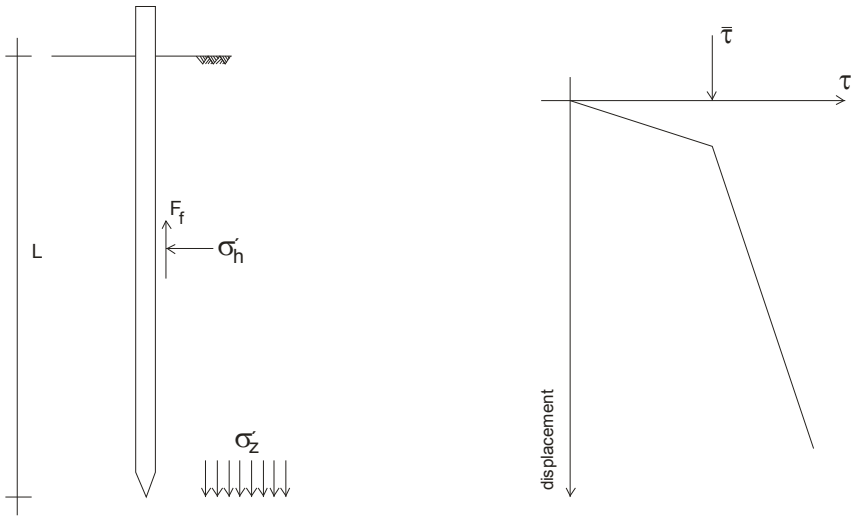

(a) (b)

Fig. 5-1. Strength along the pile, (a) side friction force, (b) the relationship between shear stress against displacement

$$F_f = \tau_f \, . \, A \quad (5\text{-}9)$$

where τ_f = side friction resistance

A = area of pile skin

Adopting Eq. (5-6) to determine the shear strength of soil,

$$\tau_f = K_0 \sigma_z' \tan \phi' + c'$$

$$= \sigma_z' (K_0 \tan \phi' + c'/\sigma_z') \quad (5\text{-}10)$$

where K_0 = the coefficient of lateral earth pressure

σ_z' = effective overburden pressure

ϕ' = effective internal friction angle of soil

c' = effective cohesion of soil

Eq. (5-10) can be simplified as,

$$\tau_f = \beta\, \sigma_z' \tag{5-11}$$

where $\beta = K_0 \tan \phi' + c'/\sigma_z'$ (5-12)

Based on the relationship between shear stress against displacement (Figure 5-1(b)), we can determine the ultimate shear resistance of soil, $\bar{\tau}$,

$$\bar{\tau} = \beta \sigma_z' \tag{5-13}$$

Furthermore, the strength reduction factor, R_{inter} can be determined by combining Eq. (5-12) to Eq. (5-13),

$$\bar{\tau} = \left[K_0 R_{inter} \tan \phi' + \frac{R_{inter} c'}{\sigma_z'} \right] \sigma_z' \tag{5-14}$$

where $$R_{inter} = \frac{c_i}{c'_{soil}} = \frac{\tan \phi_i}{\tan \phi'_{soil}} \tag{5-15}$$

c_i = interface cohesion

ϕ_i = interface friction angle

The result of strength reduction factor, R_{inter} on Pontianak soft organic soils give the value about 0.35 which is smaller than that found in literature which ranges from ½ to ⅔.

5.6. Skempton *B*-Parameter

Soil is an assemblage of discrete particles, together with variable amounts of water and air. In a saturated soil the voids are completely filled with water. The interaction between the soil structure and the pore fluid, whether water or a combination of water and air, is responsible for the behaviour of a soil mass. The relationship between pore pressure changes and changes in total stress in a soil can be expressed in term of the pore pressure coefficient *B* which was defined by Skempton, 1954.

The component of pore pressure change, Δu, due to the isotropic stress change, $\Delta\sigma$, is related to that change by the coefficient *B*, defined by following equation:

$$\Delta u = B \,.\, \Delta\sigma \tag{5-16}$$

$$B = \Delta u / \Delta\sigma \tag{5-17}$$

For the particular samples, test results appear to be explained reasonably well by the elementary Mohr-Coulomb model in combination with the standard Plaxis option on undrained behaviour.

$$E^u = \frac{1-\nu'}{1-2\nu'} 2G \tag{5-18}$$

where E^u = undrained elasticity modulus
G = shear modulus

On using the measured *B* factor, Vermeer, 2000, computed the undrained Poisson's ratio ν^u. According to the basics of elasticity theory:

$$\frac{E^u}{E'} = \frac{\Delta\sigma}{\Delta\sigma'} = \frac{\Delta\sigma}{\Delta\sigma - \Delta u} = \frac{1}{1-B} \tag{5-19}$$

where E' = effective elasticity modulus
$\Delta\sigma'$ = effective stress change

Combining equations for E^u and E', the constant *G* drops out and we get,

$$\frac{E^u}{E'} = \frac{1-\nu^u}{1-2\nu^u}\,\frac{1-2\nu'}{1-\nu'} \tag{5-20}$$

Inserting $E'/E^u = 1 - B$, it follows that

$$\nu^u = \frac{\nu' + B(1-2\nu')}{1+B(1-2\nu')} \tag{5-21}$$

For full saturation with $B = 1$, this equation yields the logical result of $\nu^u = 0.5$. If there is no pore water at all, i.e. $B = 0$, we get another trivial result of $\nu^u = \nu'$. However, to prevent numerical difficulties for nearly incompressible material with $\nu^u = 0.5$, Poisson's ratio ν^u is equal to 0.495. The use of a constant undrained Poisson's ratio implies a *B* factor of

$$B = \frac{\nu^u - \nu'}{(1-2\nu')(1-\nu^u)} \approx \frac{0.98-2\nu'}{1-2\nu'} \tag{5-22}$$

If we substitute $\nu' = 0.4$ (Section 5.3.), therefore *B* factor is 0.9.

5.7. Basic Stiffness Parameters

Most of Cam Clay parameters used as the design parameters on Plaxis 3D finite element were determined from Oedometer tests. The void ratio, *e* can be calculated for each load increment when soil is applied to additional loads. A type of graph to illustrate the data from these tests is an arithmetic plot of the void ratio versus logarithmic scale of vertical effective stress. According to Fig. 5-2, the change of void ratio, Δe can be obtained as,

$$\Delta e = C_c\, \Delta \log \sigma_v' \tag{5-23}$$

where C_c = compression index

σ_v' = vertical effective stress

The compression index, C_c is measured in Oedometer tests, together with other stiffness related parameters such as the swelling index, C_s and the preconsolidation stress. If the 10-log scale of vertical effective stress changed to natural logarithm, we can get reformulate the change of void ratio,

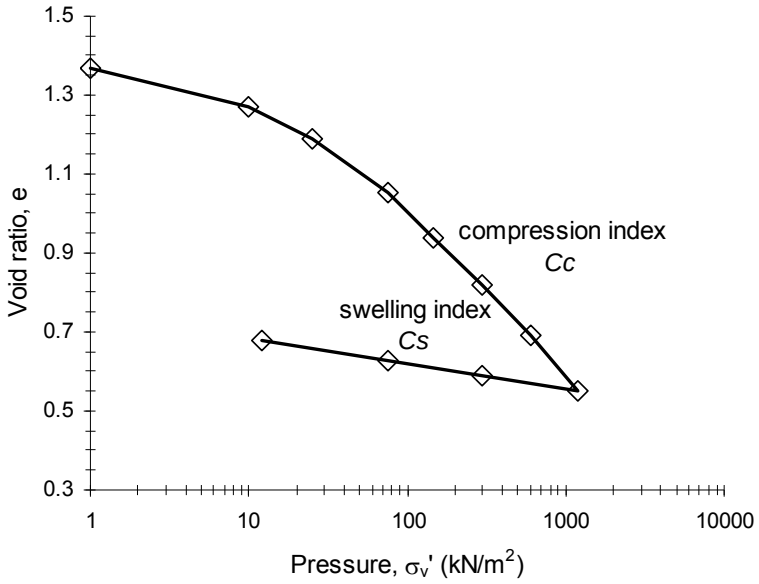

Fig. 5-2. One dimensional compression curve

$$\Delta e = - \lambda \, \Delta \ln \sigma_v' \qquad (5\text{-}24)$$

where $\lambda = Cc/\ln 10$ (5-25)

The modified compression index, λ^* is used in all advanced Plaxis models. It shows relationship between the traditional compression index, C_c and the modified one, λ^*. The index is expressed by equation

$$\lambda^* = \frac{\lambda}{(1+e)} = \frac{Cc}{(1+e)\ln 10} \qquad (5\text{-}26)$$

$$\lambda^* = \frac{Cc}{2.3(1+e)} \qquad (5\text{-}27)$$

Similarly, the so called swelling index, C_s will be used as an alternative input parameter for the unloading-reloading which is expressed as

$$Cs = \frac{\Delta e}{\Delta \log \sigma_v'} \tag{5-28}$$

and after 10-log changed to natural logarithm, we get

$$\kappa = Cs/\ln 10 \tag{5-29}$$

Furthermore, the modified swelling index, κ^* can be written by following equation

$$\kappa^* = \frac{\kappa}{(1+e)} = \frac{Cs}{(1+e)\ln 10} \tag{5-30}$$

$$\kappa^* = \frac{Cs}{2.3(1+e)} \tag{5-31}$$

Garlanger, 1972 proposed a creep equation as expressed in Eq. (2-50),

$$e = e_c - C_\alpha \log\left(\frac{\tau_c + t'}{\tau_c}\right) \tag{2-50}$$

$$C_\alpha = \frac{\Delta \mathrm{e}}{\Delta \log t} \tag{5-32}$$

where C_α = creep index

e = void ratio

e_c = void ratio up to the end of consolidation

τ_c ; t_c = consolidation time

t' = $t - t_c$ = effective creep time

t = time

Eq. (5-32) reformulated by changing 10-log scale of time to natural logarithm as,

$$\mu = C_\alpha / \ln 10 \tag{5-33}$$

The modified creep index, μ^* can be expressed as,

$$\mu^* = \frac{\mu}{(1+e)} = \frac{C_\alpha}{(1+e)\ln 10} \tag{5-34}$$

$$\mu^* = \frac{C_\alpha}{2.3(1+e)} \tag{5-35}$$

According to Plaxis, 2006, the ratio between modified compression index and modified creep index, λ^*/μ^* ranges 15 to 25. Hence this ratio was taken 20 as a parameter design. All of parameters used for calculation are given in Table 5-1 for different fields and Kaolin with sand respectively.

5.8. Empirical Parameters for Primary Compression, Secondary Compression and Rate of Secondary Compression

The separation of primary consolidation and secondary compression and their treatment by the Terzaghi consolidation theory and the Buisman secondary compression method, as is often done with inorganic soils, appears to be inappropriate for peats. In an attempt to represent the settlement-time curve as a whole, a rheological model proposed by Gibson and Lo has been used to represent the compression behaviour of peat (Edil and Mochtar, 1984).

A rheological model as proposed by Gibson and Lo, 1961, and shown in Fig. 5-3 has been found to give satisfactory results in representing the one-dimensional compression of peat under a given increment of stress. As expressed in Eq. (2-91), the time-dependent strain, $\varepsilon(t)$, may be rewritten again as

$$\varepsilon(t) = \Delta\sigma [a + b\ (1 - e^{-(\lambda/b)t})] \tag{2-91}$$

Table 5-1. Soil Properties for the Eight Fields in Pontianak and Kaolin

Parameters	Unit	Site names				
		Perdana	A. Yani II	Terminal-Siantan	Ramayana	Yos Sudarso
Soil Classification		Organic clay	Organic silt	Organic clay	Organic silt	Sandy organic silt
Material model		Soft Soil Creep Model	Soft Soil Creep Model	Soft Soil Creep Model	Soft Soil Creep Model	Soft Soil Creep Model
Type of material behaviour		Undrained	Undrained	Undrained	Undrained	Undrained
Water content, *Wn*	%	117.73	169.98	81.57	90.77	91.02
Void ratio, *e*		2.545	3.318	2.073	1.85	1.021
Soil weight above phreatic level, γ_{unsat}	kN/m^3	13.55	12.3	15.24	15.59	14.06
Soil weight below phreatic level, γ_{sat}	kN/m^3	13.55	12.3	15.24	15.59	14.06
Permeability, $k_x = k_y = k_z$	m/day	3.69E-05	5.08E-05	4.36E-06	2.18E-04	3.04E-04
Young modulus, E_{ref}	kN/m^2	900	1073	650	690	1100
Poisson's ratio, ν'		0.4	0.4	0.4	0.4	0.4
Modified compression index, λ^*		0.148	0.076	0.095	0.12	0.073
Modified compression index, κ^*		0.026	0.008	0.028	0.029	0.018
Modified creep index, μ^*		0.0074	0.0038	0.0047	0.006	0.0037
Cohesion, c_{ref}	kN/m^2	7	7.5	15	6	9
Friction angle, ϕ	deg.	12	8	1	5	6
Lateral earth pressure coeff., K_0		0.667	0.667	0.667	0.667	0.667
Overconsolidation ratio, *OCR*		1.5	1.5	1.5	1.5	1.5

Table 5-1. (continued)

Parameters	Unit	Site names			
		Danau Sentarum	BNI46-Tanjungpura	Astra-A.Yani	Kaolin
Soil Classification		Organic silt	Sandy organic silt	Sandy organic silt	Silt with sand
Material model		Soft Soil Creep Model	Soft Soil Creep Model	Soft Soil Creep Model	Soft Soil Creep Model
Type of material behaviour		Undrained	Undrained	Undrained	Undrained
Water content, *Wn*	%	118.92	71.01	58.22	38.91
Void ratio, *e*		2.316	1.768	1.466	1.039
Soil weight above phreatic level, γ_{unsat}	kN/m^3	13.7	15.55	16.49	17.78
Soil weight below phreatic level, γ_{sat}	kN/m^3	13.7	15.55	16.49	17.78
Permeability, $k_x = k_y = k_z$	m/day	2.10E-04	7.81E-04	8.22E-05	4.14E-05
Young modulus, E_{ref}	kN/m^2	782	871	1166	3111
Poisson's ratio, ν'		0.4	0.4	0.4	0.4
Modified compression index, λ^*		0.08	0.132	0.074	0.061
Modified compression index, κ^*		0.012	0.014	0.019	0.018
Modified creep index, μ^*		0.004	0.0065	0.0037	0.0006
Cohesion, c_{ref}	kN/m^2	9	7	16.5	5
Friction angle, ϕ	deg.	5	19	20.31	18.86
Lateral earth pressure coeff., K_0		0.667	0.667	0.667	0.667
Overconsolidation ratio, *OCR*		1.5	1.5	1.5	1.5

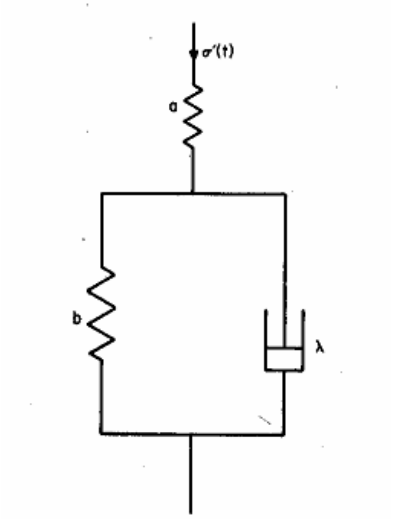

Fig. 5-3. Rheological model for secondary compression
(After, Edil and Mochtar, 1984)

where $\Delta\sigma$ = stress increment
a = primary compressibility
b = secondary compressibility
λ/b = rate factor for secondary compression
t = time

A convenient method of analysis of a given set of vertical strain-time data for determining the empirical parameters (a, b and λ) was described by Edil and Dhowian, 1979, and Edil and Mochtar, 1984. The Method uses a plot of logarithm of strain rate versus time (log ($\Delta\varepsilon/\Delta t$) versus t). Fig. 5-4 shows strain rate curves from Perdana and Untan fields which samples were loaded a 300 kN/m^2 with loading period of precisely 7 days. The thin line indicates strain rate curve of Perdana and the thick one is Untan. These should result in a straight line for the time range corresponding to the secondary compression if the soil conforms to the basic assumptions made in the model. The slope and intercept of this best-fit line yield the value of a, b and λ as follows:

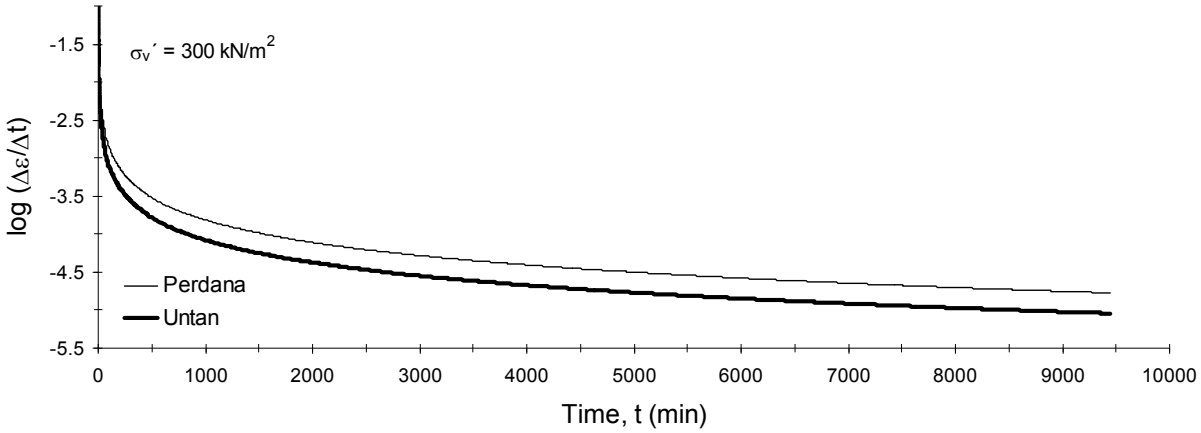

Fig. 5-4. Strain rate logarithm versus time for Perdana and Untan fields

Slope of the line = -0.434 (λ /b) (5-36)

Intercept of the line = log ($\Delta\sigma$ λ) (5-37)

$$a = \varepsilon(t)/\Delta\sigma - b + be^{-(\lambda/b)t} \quad (5\text{-}38)$$

Table 5-2 shows the empirical parameters of primary compression, *a*, secondary compressions, *b*, and rate of secondary compression, λ /*b* for both Perdana and Untan fields.

Table 5-2. Empirical parameters of *a*, *b* and λ/*b* for Perdana and Untan fields

Empirical Parameters	**Fields**	
	Perdana	**Untan**
a (m^2/kN)	0.000085112	0.000043587
b (m^2/kN)	0.00146538	0.00083808
λ /*b*	0.00014353	0.0001121

CHAPTER VI

RESULTS AND ANALYSIS

6.1. Load-settlement Verification

The load-settlement-curve of Perdana field tests with models of mini pile, T1, mini pile with a pair of horizontal beams, T2, and mini pile with two pairs of horizontal beams, T3 are shown in Figure 6-1(a), (b) and (c) respectively, whereas the Untan field used only T2 and T3 models shown in Figure 6-2(a) and (b). The performance of field measurements and their two analyses i.e. the Soft Soil Creep Model (SSCM) and Edil et al on both fields were compared. The solid lines indicate the measurements; the dashed lines are the results from the SSCM and the dotted lines indicate the analysis with Edil et al.

The Perdana field shows that the SSCM and Edil et al. are fairly similar seemingly underestimating the measurements in foundation model T1, and then significantly differ after applying a 1.6 kN load (Figure 6-1(a)). In foundation model T2, Edil et al seems to underestimate overall at lower level loads and closes to measurements up to 2.5 kN, while SSCM is similar to measurements at initial loads and overlapping up to 3 kN (Figure 6-1(b)). The analyses and measurements are similar in that after 4 kN of load, separation of SSCM overestimates at higher load levels in foundation model T3 (Figure 6-1(c)).

Figure 6-2 shows the comparison between analyses and measurement in Untan field. There is a good agreement between the results of different analyses and those of the field load tests. The SSCM, Edil et al and measurements are close together up to 6 kN and 9 kN in T2, T3 foundation models respectively as shown in Figure 6-2(a) and (b). Moreover, both analyses move away from measurement at higher level loads where SSCM remains higher than Edil et al.

Edil et. al and SSCM have different theoretical approaches to creep. Edil et al adopted the rheological model of Gibson and Lo (1961) in which the structural viscosity is assumed to be linear. They assumed that the parameters for the primary and secondary compressibility depend on the stress level and the rate factor for secondary compression, λ/b, which is strongly non-linear with time for inorganic clay. This factor indicated that there was no simple correlation between the laboratory and the field data for the peat and organic soils. This is

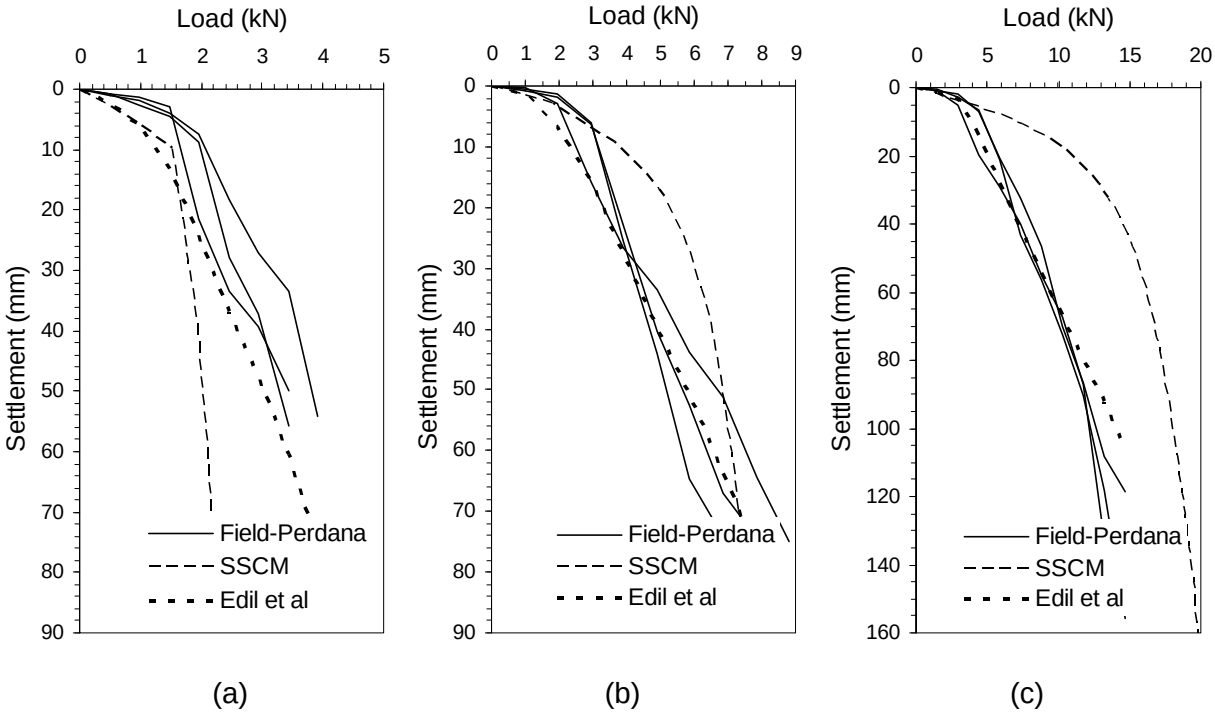

Fig. 6-1. Load-settlement Curve of Foundation Models in Perdana
(a) mini pile, T1, (b) mini pile with a pair horizontal beams, T2
(c) mini pile with two pairs of horizontal beams, T3

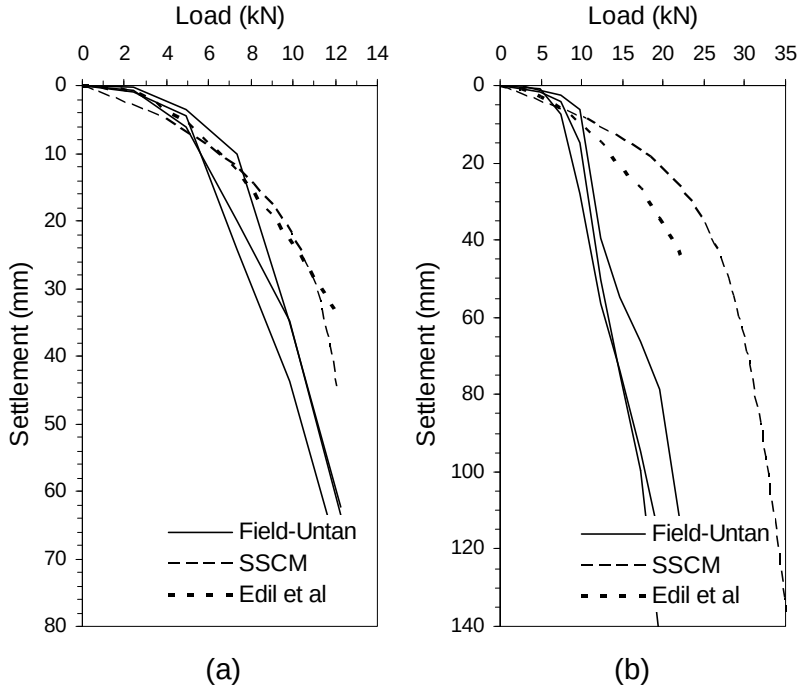

Fig. 6-2. Load-settlement-curve of foundation models in Untan
(a) mini pile with a pair horizontal beams, T2
(b) mini pile with two pairs of horizontal beams, T3

expected in view of the possible non-linearity of λ which represents the structural viscosity of soil during secondary compression.

The calculation using Edil et al (1979, 1984) showed the load-settlement curve to underestimate field measurements. The primary compressibility, "*a*", was significantly high and dominantly increased as the settlement of soil became more excessive. In reality, the primary consolidation of peat is ill-defined and takes place relatively quickly but the secondary compression is significant both in rate and accumulated magnitude (Edil and Mochtar, 1984). Edil et al recommended the using of simple rheological model for predicting of peat or organic settlements; however their equation only used for embankment which does not account of friction affect as occurred in tiang tongkat foundation. An empiric approach of parameter "*a*", was taken to reduce its value by multiplying it with 0.1. Although, in general the calculation results are still quite lower than measurement as shown in Figure 6-1(a) and (b) and Figure 6-2, however using the new parameter "*a*", provides good agreement to estimate the load-settlement for both Perdana and Untan fields.

The SSCM is an extension of the Soft Soil model to estimate creep, i.e. secondary compression in very soft soils which includes time and strain rate effects. This model assumes that logarithmic strain includes deformation during consolidation and the secondary compression per logarithmic time increment which is described by the modified creep index μ^*. The isotropic consolidation is reached after creep has occurred, this is based on the assumption that consolidation occurs in less than one day.

The Soft Soil Creep Model, SSCM, shows significantly different results for both Perdana and Untan fields with the numerical analysis higher than field measurements. Where the T1 and T2 models had a small *Ab*/*Ap* ratio, the SSC models were close to measurements. However, in T3 which had a higher horizontal beam area, the SSC models move away from measurement with an increase in ratio *Ab*/*Ap* as shown in Figures 6-1 and 6-2. These analyses are significantly higher on the model with a higher base area and load level. The ratio *Ab*/*Ap* influences contact area of soil and the pore water pressure at the base of the horizontal beams. The ground water level was found almost near the ground surface in these fields; hence, the pore water pressure in the SSCM is completely incompressible. In full scale models, the thick layers of in-situ organic soil are about 20 m depth, while in numerical models 4 m depth was considered, besides using a coarse mesh these calculations. El-Mosallamy, 1999, reported in his study that the Plaxis 3D FE-Foundation analyses showed stiffer behaviour at higher load levels. He also stated that the slight deviation of axial capacity is not strongly influenced by the mesh refinements. On the other hand, the capacity of the

foundation is strongly influenced by several factors, among which are the meshes refinements, the initial stress state and the modelling scheme.

There are many empirical methods available to determine the axial capacity of a foundation from load-settlement data. Generally, the ultimate capacity of a foundation used in design may be one whose values: (1) determine the load that corresponds to the point at which the settlement curve has a significant change in slope (commonly called the tangent method); (2) a calculated value, given by the sum of the end-bearing and shaft resistance; or (3) the load at which a settlement of 15% of the diameter or diagonal dimension occurs (when point (1) is not clear). Method (1) has been used to predict the axial capacity of foundation 3D FE models as the ultimate axial capacity; which is based on the elastic plastic theory that the ultimate axial capacity is determined by a significant change between the elastic and plastic parts.

Based on the tangent method; the axial capacity increases with an increase in the area ratio of the horizontal beam over pile skin, *Ab*/*Ap*. As shown in Table 6-1, the test results of Untan are higher than those of Perdana by approximately 2 times. This difference is due to the properties of the Untan soil which is better than Perdana's as it has a lower water content, as well as a higher unit weight and cohesion. The high capacity of Untan also shown in Table 5-2, whereas the empirical parameters of *a*; *b*; and λ/b of the Untan field smaller than Perdana field.

Subsequently, the ultimate settlement was selected to determine the axial capacity of tiang tongkat foundation calculated by SSCM and Edil et al. For the foundation design, the load-settlement curves as described in Figures 6-1 and 6-2 can be used to find the ultimate settlement and their corresponding load levels. The settlement of the tested foundations was measured at about 6 mm which was considered to be acceptable for the tiang tongkat foundation design.

Table 6-1 lists comparisons of axial capacity of the tiang tongkat foundations among their measurements, SSCM and Edil et al. Generally, it can be seen that errors in the Edil et al analyses of Perdana are slightly higher than those found at Untan while SSCM errors seem constant in these fields. The comparisons show that the errors from SSCM and Edil et al are 12.7% and 15.7% respectively, indicating that the present method has adequate accuracy.

The analytical solution of the ultimate axial capacity, *F*, is average of the three values derived from Terzaghi, Meyerhof and Hansen respectively. These results indicate that the analytical solutions were higher than the field tests. Table 6-2 shows the comparison of axial capacity of tiang tongkat foundation between measurements and analytical solutions. These differences appear significantly high because the common equation does not take into

account the affect of creep that is present in organic or peat soils. Peat and organic soils are well known for their high compressibility and long-term settlement. In many cases, the majority of settlement results from creep at a constant vertical effective stress. The difficulty and inability to apply conventional settlement-prediction methods such as Terzaghi's consolidation theory to peat material is well explained in Edil et al, 1979 and 1984. The primary reason for such difficulty is the relatively large secondary compression that occurs in peat or organic soils in compression.

Table 6-1. Axial Capacity Comparison of Tiang Tongkat Foundations between Measurements and SSCM and Edil et al

Methods	Perdana			Untan		Average Error (%)
	T1 (kN)	T2 (kN)	T3 (kN)	T2 (kN)	T3 (kN)	
Measurement	1.6	2.6	3.9	5.6	8.2	
SSCM	1.2	2.7	4.2	4.5	7.6	12.7
Edil et al	1.2	2	3.4	5.1	7.5	15.7

Table 6-2. Axial Capacity Comparison between Measurements and Analytical Solutions *

Methods	Perdana			Untan	
	T1 (kN)	T2 (kN)	T3 (kN)	T2 (kN)	T3 (kN)
Measurement	1.6	2.6	3.9	5.6	8.2
Analytical solutions*)	2.2	13.5	23.6	21.2	37

*Terzaghi, Meyerhof and Hansen

6.2. Numerical Simulation of the Tiang Tongkat Foundation

In this section, the results of 3D Finite Element-analysis of tiang tongkat foundation on Pontianak's 8 fields and Kaolin are presented. The 324 models were divided into 6 types of foundation i.e. P1, P2-1, P2-2, P3-1, P3-2 and P4 as shown in Figure 3-3. The input parameters for all applied models are different for each field and summarized in Tables 3-2, 3-

3 and 5-1 where the type of material behaviour for all fields were undrained. The loads are modelled as vertical or inclination point loads at the pile top and distributed loads at the horizontal beam respectively. In particular, the distributed load was given as a surcharge stress based on the unit weight of the soil and the embedment depth of the horizontal beam.

The calculation consists of 3 phases. The initial phase consists of the generation of initial stresses using the K_0 procedure. The following phases consist of the installation of the foundation which is left to recover for an assumed period of 30 days, and the subsequent loading of structural elements. The pore water pressure is generated based on a phreatic level. When the geometry of a foundation model is complete, the 2D finite element mesh is generated before generating a full 3D mesh. The 2D mesh generation process is based on a robust triangulation principle that searches for optimised triangles resulting in an unstructured mesh. The 3D mesh is created by connecting the corners of the 2D triangular elements to the corresponding points of the corresponding elements in the network plane. In this way a 3D mesh, composed of 15-noded wedge elements is formed.

6.2.1. Vertical Point Load

The tiang tongkat foundation models were subjected to vertical point loads at the top of the pile and other surcharge loads at the horizontal beams. Figure 6-3 shows the generated 3D mesh of the soil model with an embedded tiang tongkat foundation subjected to loading.

Figure 6-4 shows the results a series of load-settlement behaviours of the tiang tongkat foundations at Yos Sudarso field. This series of models was subjected to vertical point and distributed loads while soil parameters were taken from Yos Sudarso field as listed in Table 5-1. Figure 6-4(a), (b) and (c) show the curves of foundations with a 12 cm pile width, *D*, and 100 cm, 220 cm and 340 cm pile lengths, *L*, while possessing horizontal beam lengths, *B*, are 70 cm, 90 cm and 110 cm respectively.

Unique trends in the grouping of the curves can be seen. The first and weakest group consists of P1, while the second intermediate group consists of P2-1 and P2-2 with the third group of P3-1, P3-2 and P4 exhibiting the strongest behaviour. The axial loads differed from each other in that P1 < P2 < P3 < P4 as shown in Figure 6-4(a), (b) and (c) respectively. The increase in the axial capacity of the tiang tongkat foundation is due to significant increases in horizontal beam area which then increases the contact area between soil and structure at the end bearing of the base. It can also be seen from Figure 3-3 and Table 3-2 that the horizontal

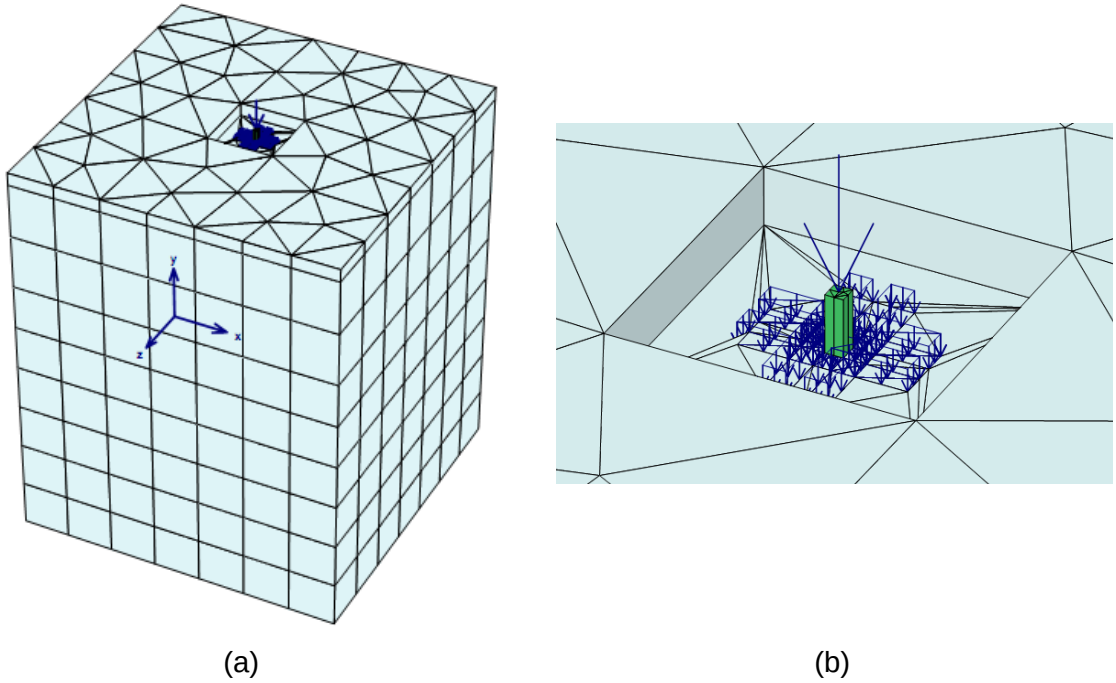

(a) (b)

Fig. 6-3. Generated 3D Mesh Subjected to Vertical and Distributed Loads
(a) 3D FE of soil model, (b) foundation loading in detail

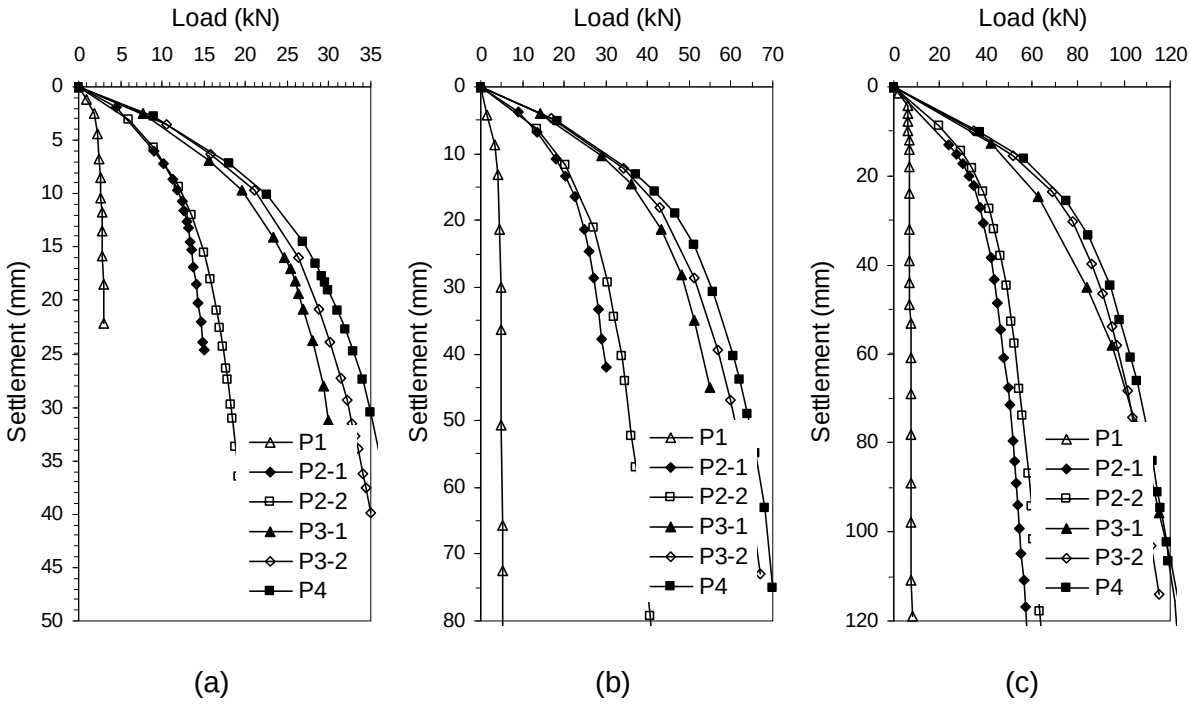

(a) (b) (c)

Fig. 6-4. Load-settlement behaviour of Tiang Tongkat Foundations on Yos Sudarso Field Subjected to Vertical Point Load, pile width, D = 12 cm
(a) L = 100 cm, (b) L = 220 cm and (c) L = 340 cm

beam area of P1 < P2-1 < P2-2 < P3-1 < P3-2 < P4. On the other hand, we can say that the axial capacity of a foundation increases with increasing of ratio horizontal beam area over pile skin, *Ab*/*Ap* for the constant pile length, *L.* It can be seen that the load-settlement curve for foundation models P2-1 and P2-2 are the same for up to 11 kN, 20 kN and 35 kN and models P3-1, P3-2 and P4 are the same for up to 15 kN, 30 kN and 45 kN with pile length, *L* = 100 cm, 220 cm and 340 cm respectively. Based on the results above, the shortest pile reaches to its ultimate axial capacity first followed by the longer piles.

6.2.2. Inclination Point Load

Besides vertical point loads, the tiang tongkat foundation models were also subjected to inclination point and surcharge loads. The 3D Finite element model and its detailed view of foundation loading for inclination point loads are shown in Figure 6-5(a) and (b). The inclination load was a result of both vertical and horizontal point loads on top of the pile. The soil parameters of this model were taken from Yos Sudarso field (Table 5-1) with pile width, *D* = 12 cm.

The load-settlement behaviour of the foundation subjected to inclination load is presented in Figure 6-6. Similar to foundations subjected to vertical point loads, the inclination capacity of a foundation increases with increasing ratio *Ab*/*Ap*, which is represented by an increase of the horizontal beam area for constant pile length, *L*. The curve of the load-settlement of the tiang tongkat foundations with 100 cm, 220 cm and 340 cm pile lengths, *L* are presented in Figures 6-6(a), (b) and (c) respectively. As in Figure 6-4, the curves show the same unique trend of grouping in the same manner as when under a vertical point load. The first and weakest group consists of P1, while the second intermediate group consists of P2-1 and P2-2 with the third group of P3-1, P3-2 and P4 exhibiting the strongest behaviour.

The inclination loads (as in the vertical point loads) differed from each other where P1 < P2 < P3 < P4 as shown in Figures 6-6(a), (b) and (c) respectively. It can be seen that the load-settlement curve for foundation models P2-1 and P2-2 are same for up to 10 kN, 15 kN and 25 kN and models P3-1, P3-2 and P4 are the same for up to 13 kN, 16 kN and 30 kN with pile lengths, *L* = 100 cm, 220 cm and 340 cm respectively. Moreover, the longer piles reach higher ultimate inclination capacities than the shorter piles. If we compare the results of Figures 6-4 with 6-6, it seems that the axial capacities are higher than the inclination capacities.

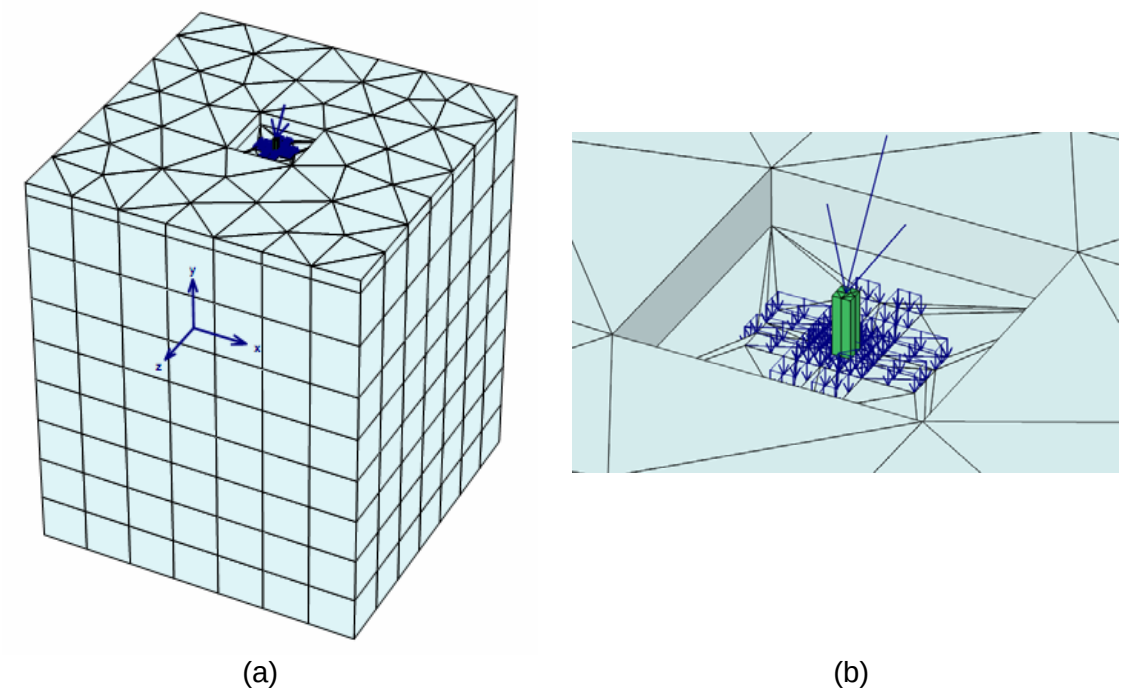

Fig. 6-5. Generated 3D mesh subjected to inclination and distributed loads
(a) 3D FE of soil model, (b) detail of foundation loading

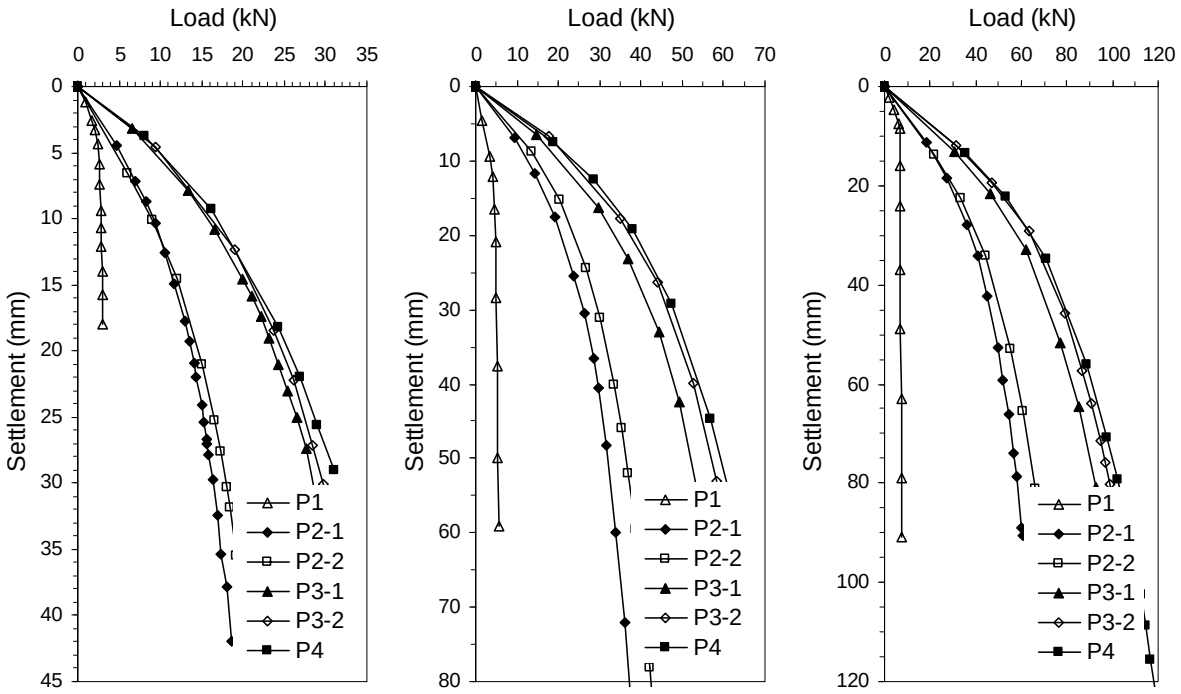

Fig. 6-6. Load-settlement behaviour of tiang tongkat foundation on Yos Sudarso field subjected to inclination point load, (a) *L* = 100 cm, (b) *L* = 220 cm and (c) *L* = 340 cm

From the analysis above, we can say that horizontal beam area affects the inclination capacity of a tiang tongkat foundation under constant pile length. Increasing this area will increase the capacity of the foundation. There are many theories concerning the analysis of single pile and pile groups subjected to lateral loads by researchers e.g. Poulos, 1971, and Banerjee and Davies, 1978, reported the elastic solution for a laterally loaded pile; Maharaj, 2003, wrote about the load-deflection response of a laterally loaded single pile using nonlinear finite element analysis. Increasing the thickness and size of the pile cap has been found to increase the lateral load carrying capacity of a pile significantly. This is more effective for shorter piles than for longer piles. By increasing the length of pile, the lateral load carrying capacity of pile cap system as a whole increases.

6.2.3. Deformation Behaviour of Tiang Tongkat Foundations

The displacements and deformed mesh of tiang tongkat foundation are discussed in this section. Only Danau Sentarum field is described here with the foundation models of P1, P2-1, P3-1 and P4 subjected to vertical and inclination point loads. The foundation pile length, L, is 340 cm and pile width, D, is 14 cm. Contour lines of equal settlement around the foundation are presented in this section to demonstrate the 3D results. The differences between failure surfaces for each type of tiang tongkat foundation are discussed. The displacement shadings at failure of model, around the foundation and foundation cross sections are shown in Figures 6-7 through to 6-14 respectively. The results from the numerical models describe the effects of horizontal beam or square floor combined with mini piles were significant to the failure surface.

On mini pile, P1, the shear zone is not developed, as depicted in Figure 6-7. The strength reduction factor of Pontianak soft organic soil, R_{inter}, is 0.35, smaller than the common interface friction angle between structure and soil as explained in Chapter III, which produces too small a shaft resistance on the pile. The behaviour of soil particles around the pile is similar to the results reported by Irsyam (1992) who studied the effects of smooth plates on sand, and Uesugi et al (1988) who studied the effects of surface roughness on pullout resistance and grain displacement respectively. The sand is sheared uniformly without developing a shear zone; therefore, the displacement of the interface consists mostly of particles slipping on the metal surface. The plate behaves as a smooth surface and the interface friction angle may be less than one half of the particle-to-particle friction angle (Yoshimi and Kishida, 1981).

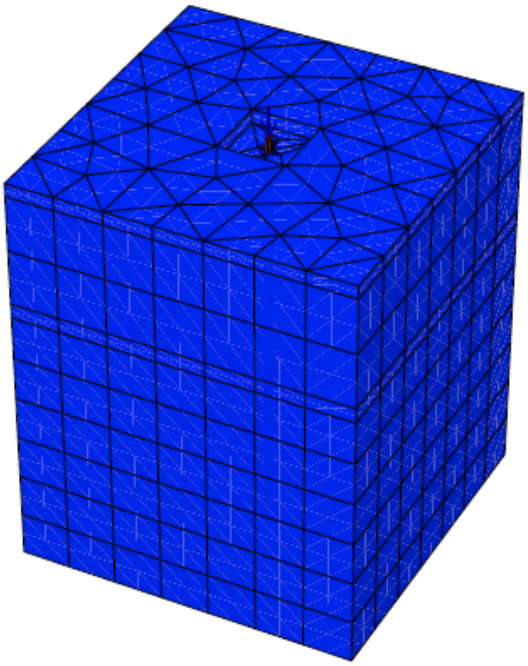

(a)

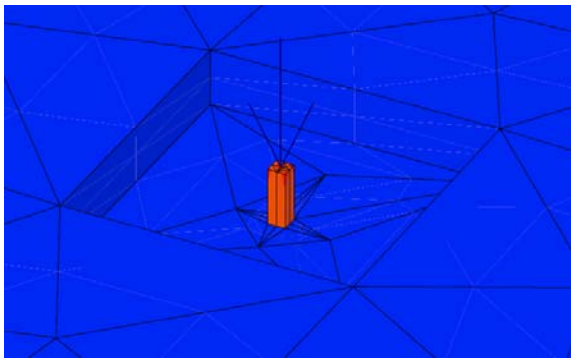

(b)

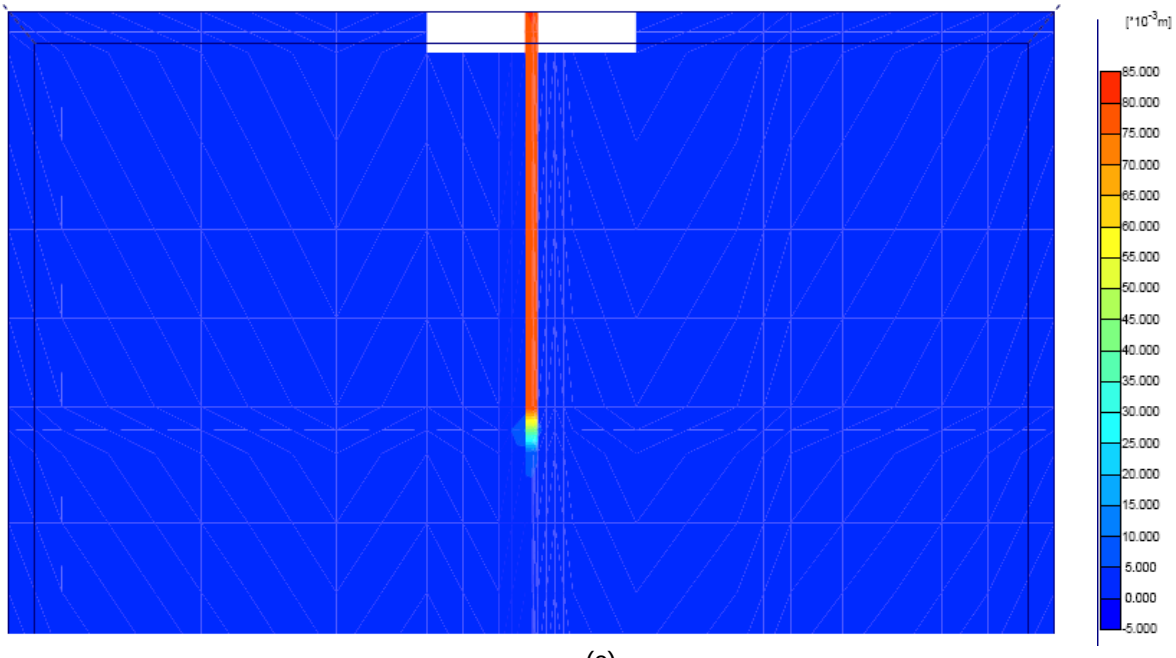

(c)

Fig. 6-7. Displacement of Mini Pile, P1 Subjected to Vertical Load
(a) displacement shadings of mesh, (b) displacement around top pile,
(c) cross section of pile

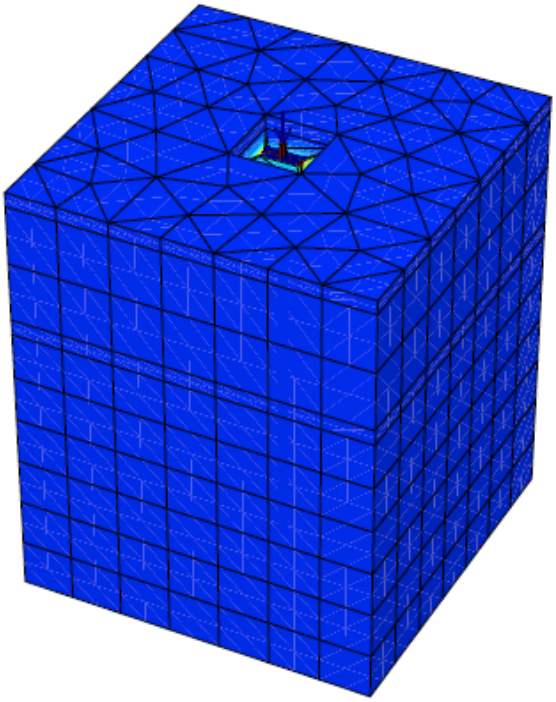

(a)

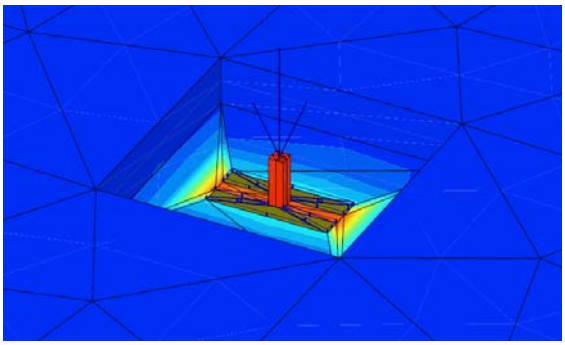

(b)

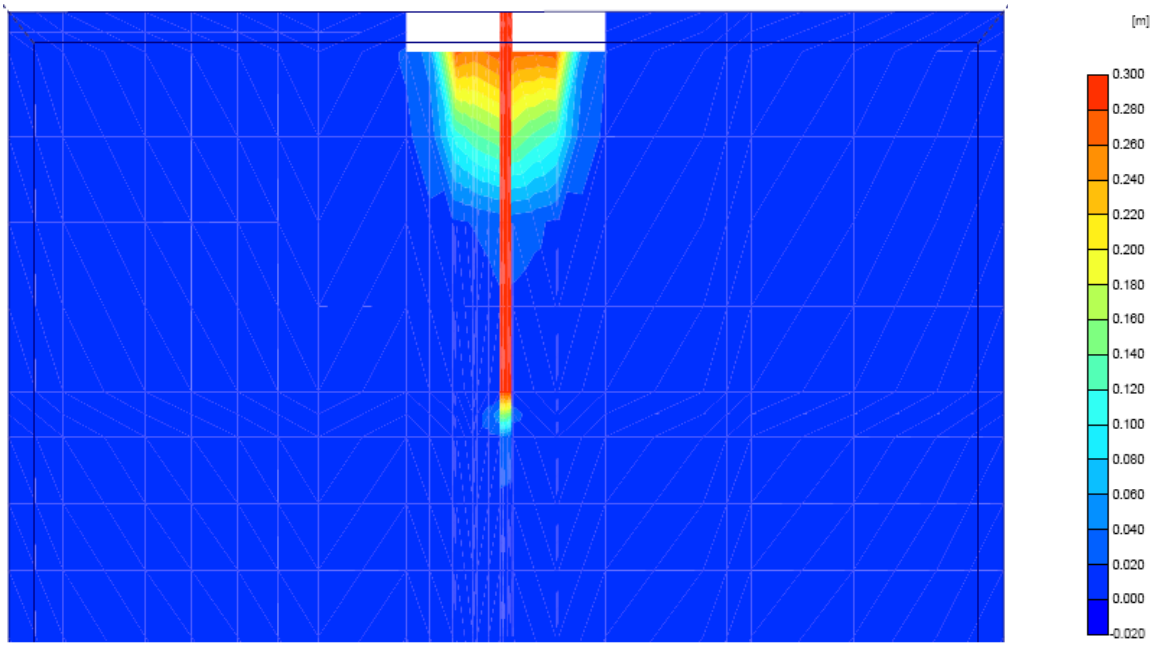

(c)

Fig. 6-8. Displacement of Tiang Tongkat Foundation with a Pair Horizontal Beams, P2-1 Subjected to Vertical Load, (a) displacement shadings of mesh, (b) displacement around horizontal beam, (c) cross section of tiang tongkat foundation

An important observation could be made in soil fabric at failure for the tiang tongkat foundation with horizontal beam, P2-1. When loading begins, the soil at the horizontal base will be pushed downward into a new position. On the other hand, the soil particles will be in an arrangement with the surrounding particles to slide and move along with the adjacent particles. After some movement, frictional resistance in the particles is built up, rearranging and relocating soil particles into new positions of equilibrium in the direction offering the least resistance to shear. Therefore, frictional resistance in the aggregate is built up gradually and consists of setting up normal stresses in the grain structure as the grains push or slide along (Cornforth, 1964). The relatively high shear zone is found at the bottom of the horizontal base. Irsyam, 1992 defined the high shear zone is the area in which the positives volumetric strain increment is distinctly higher from the surrounding regions. Because the soil is very soft, it requires less shearing resistance and reaches its maximum shear stress without passing a peak value as shown in Figure 4-7 above.

The continuous shearing will change the void ratio and the thickness of the shear zone, localize particle deformations, and form a failure surface. The process continues until, after considerable displacement, a failure surface is completely formed. The shear zone is localized around a horizontal base, whereas the surface with less shear resistance is formed slightly outward from the base, and a constant residual shear stress develops. This shape occurs by the small base area of the pair of horizontal beams, P2-1, for the tiang tongkat foundation as shown in Figure 6-8. The constant residual shear resistance is attributed to the full formation and mobilization of passive resistance and also the friction between the soil and the base (Irsyam, 1992).

In foundation models that have larger horizontal beam areas such as P3-1 and P4, the initial loading pushes soil particles into new positions. Therefore, frictional resistance in the particle is built up gradually and the particles push and slide along, so that interparticle forces are generated at contact points within the assembly. Continuous shear will alter the equilibrium condition thereby prompting the grains to slide into new positions of equilibrium in directions offering the least resistance to shear. A relatively high shear zone occurs just below the base, which represents the region in which shear stresses along the particle contacts have already reached limiting equilibrium. Because the horizontal base area of these models is large, the number of particle contacts will be higher. The base area of P4 is larger than P3-1, and as a result, the shear zone of P4 will be larger than P3-1, and of course both their zones will be larger than P2-1. The complete formation of a failure surface may be associated with the establishment of constant residual shear resistance. The difference of shear zone between P3-1 and P4 models demonstrate in Figure 6-9 and Figure 6-10.

The shear zones of the P3-1 and P4 models seem relatively large which correlates with their high capacity. As mentioned in section 4.4, the soil layer is saturated and the ground water level found high, hence, the pore water pressure in SSCM is completely incompressible. Furthermore, the Plaxis 3D FE-Foundation analyses show stiffer behaviours at higher load levels, as reported by El-Mosallamy, 1999.

Shear zone behaviour of mini pile, P1, was the same when subjected to inclination and vertical point loads. This is due to the soil being very soft, so that, with small R_{inter} and shaft area, the shear zone is not formed. The behaviour of tiang tongkat foundation models, P2-1, P3-1 and P4 subjected to inclination loads are similar to the vertical load except that the shear zone inclined in the direction of the long side of the horizontal base. The relatively high shear zone occurs in front of the foundation. All of the deformations on foundations subjected to inclination loads are shown from Figures 6-11 to 6-14.

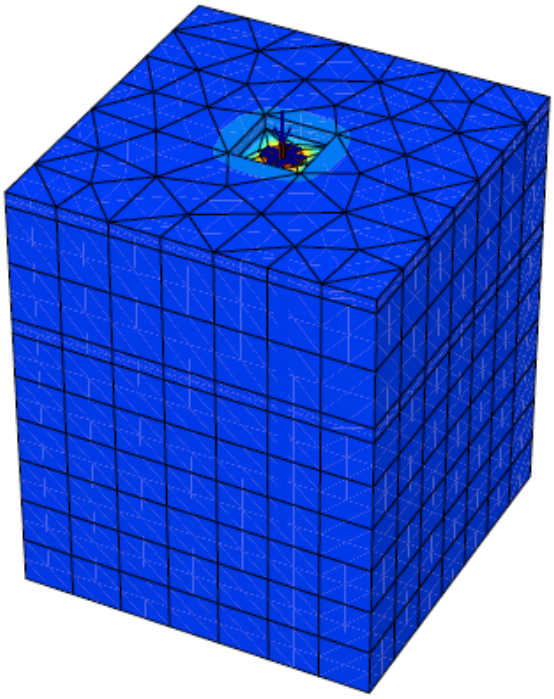

(a)

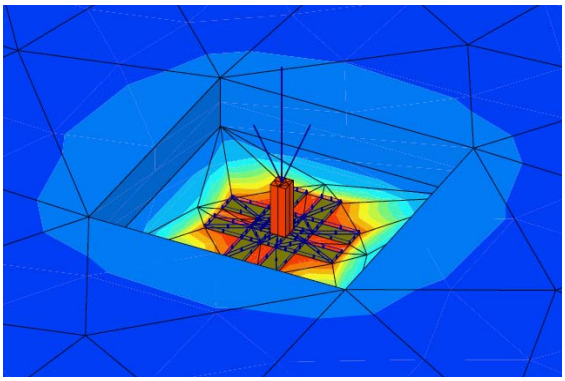

(b)

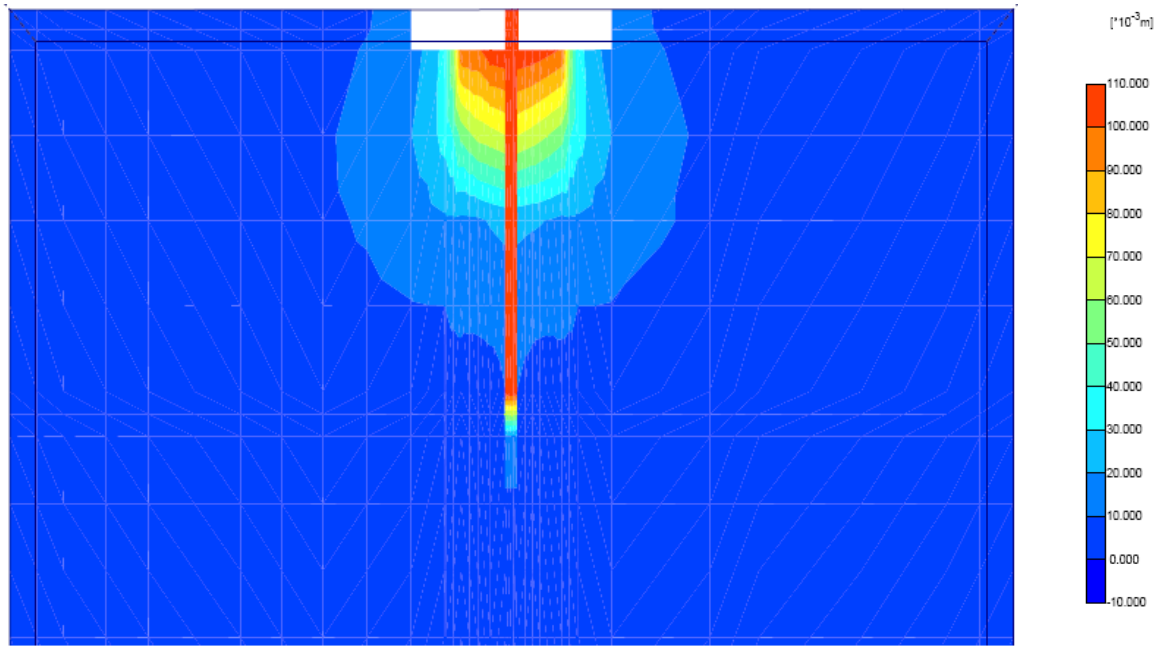

(c)

Fig. 6-9. Displacement of Tiang Tongkat Foundation with Two Pairs of Horizontal Beams, P3-1 Subjected to Vertical Load, (a) displacement shadings of mesh, (b) displacement around horizontal beam, (c) cross section of the tiang tongkat foundation

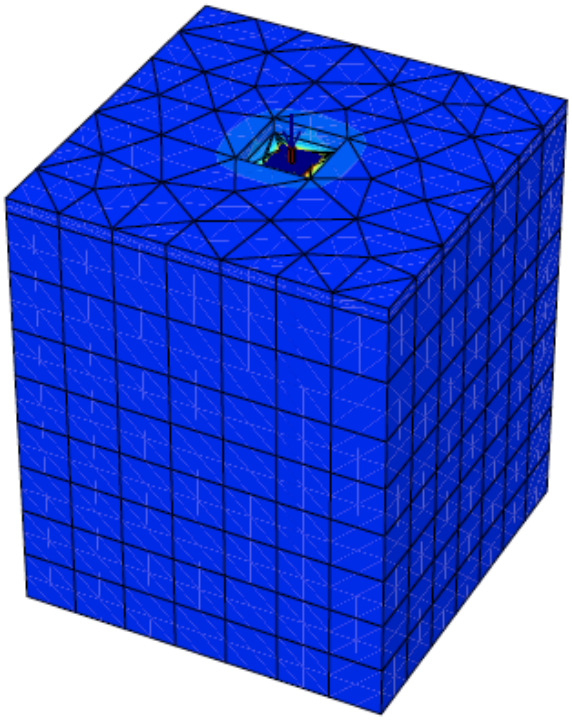

(a)

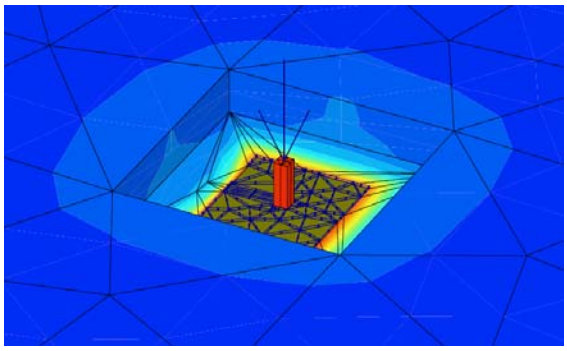

(b)

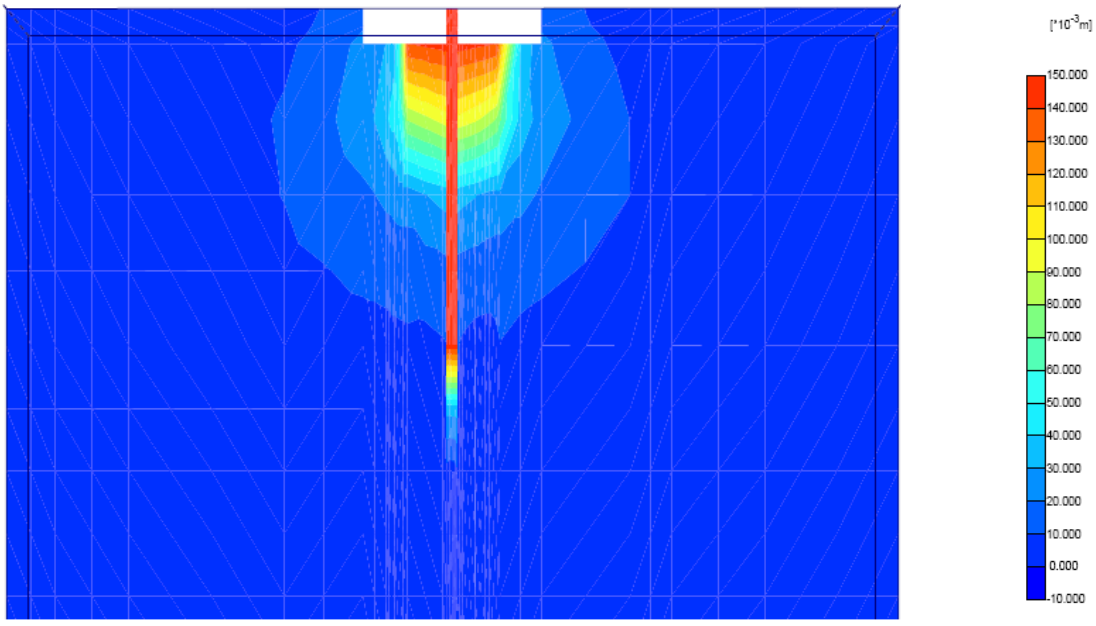

(c)

Fig. 6-10. Displacement of Combined Mini Pile with Square Floor,
P4 Subjected to Vertical Load, (a) displacement shadings of mesh,
(b) displacement around square floor, (c) cross section of the tiang tongkat foundation

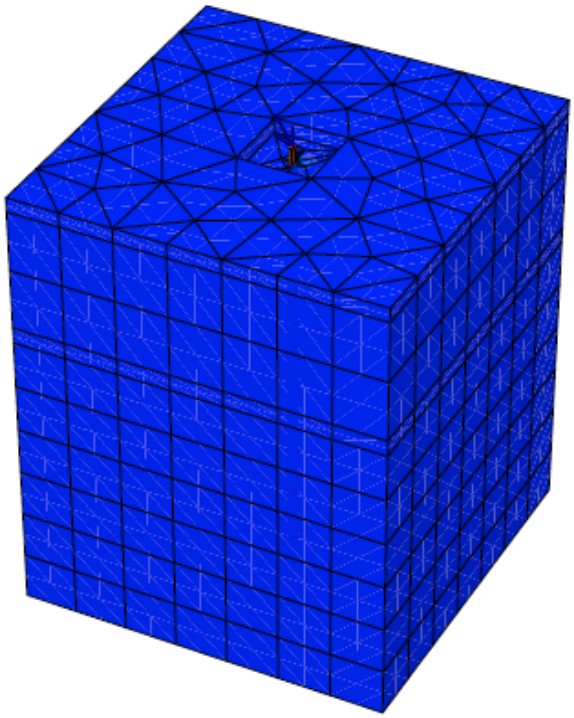

(a)

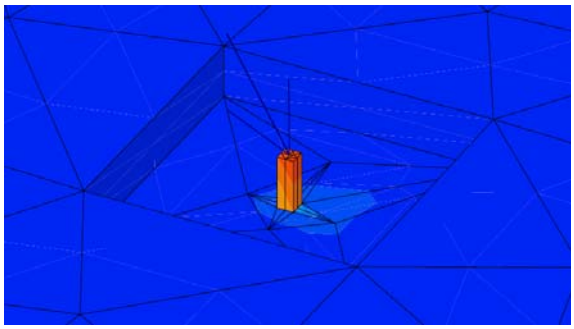

(b)

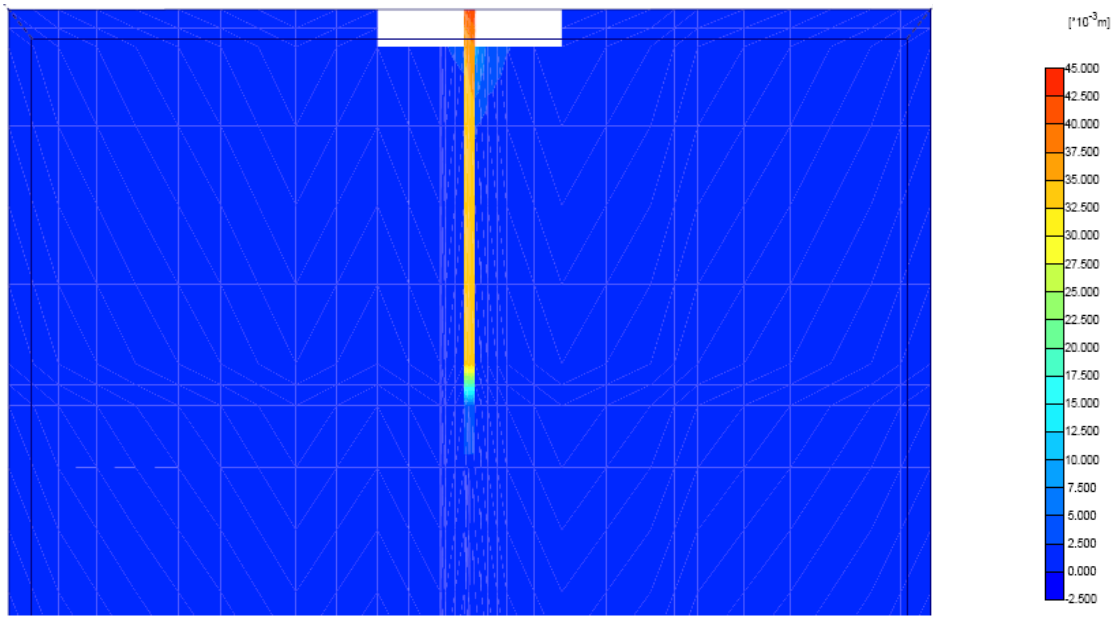

(c)

Fig. 6-11. Displacement of Mini Pile, P1 Subjected to Inclination Load
(a) displacement shadings of mesh, (b) displacement around top pile, (c) cross section of pile

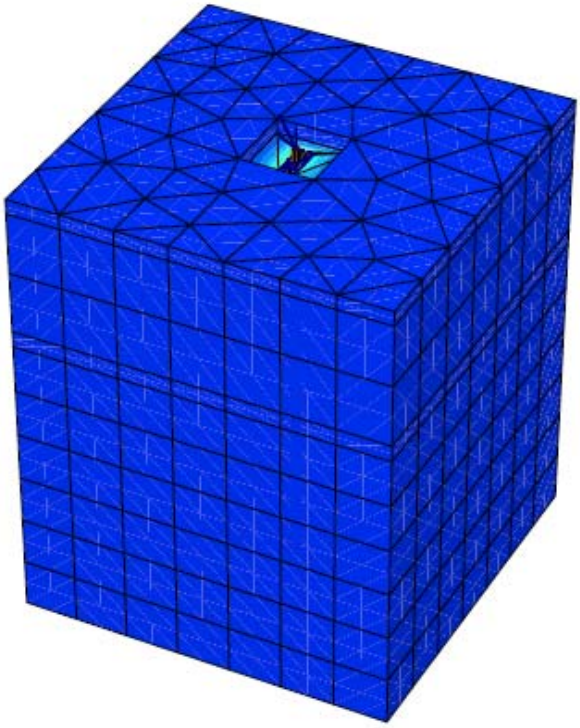

(a)

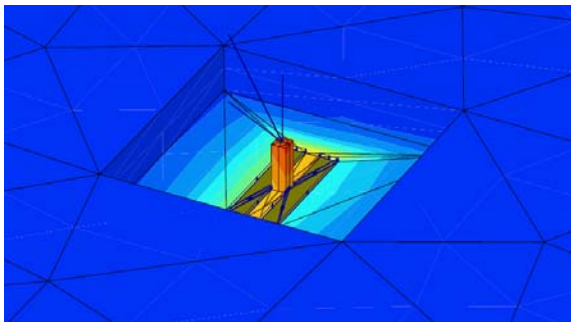

(b)

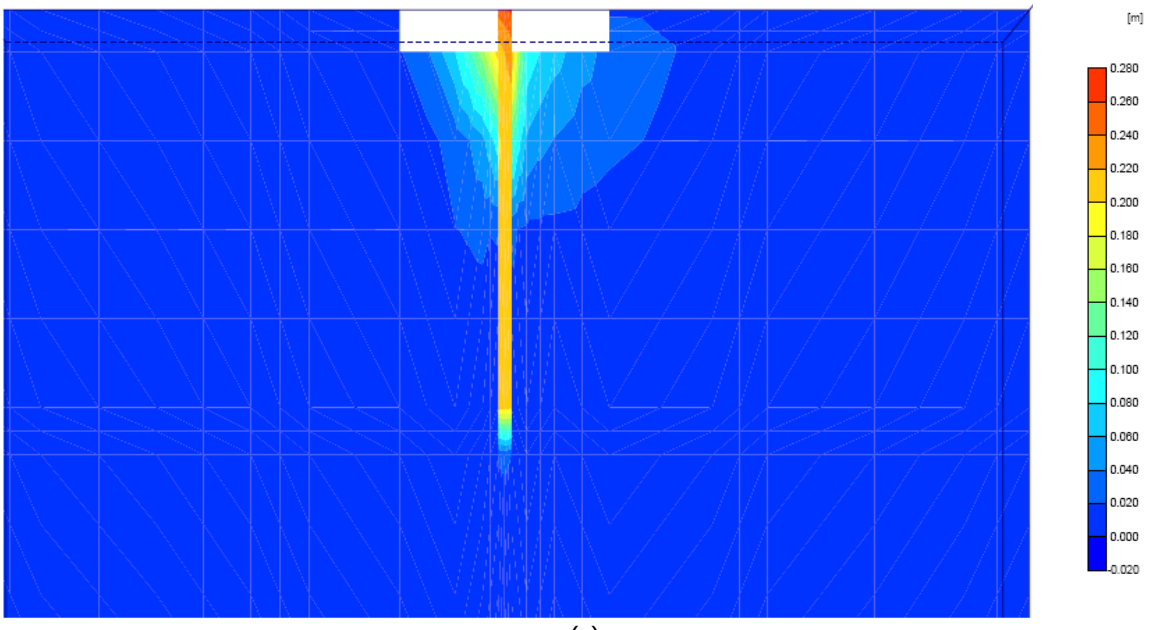

(c)

Fig. 6-12. Displacement of Tiang Tongkat Foundation with a pair Horizontal Beams, P2-1, Subjected to Inclination Load, (a) displacement shadings of mesh, (b) displacement around horizontal beam, (c) cross section of the tiang tongkat foundation

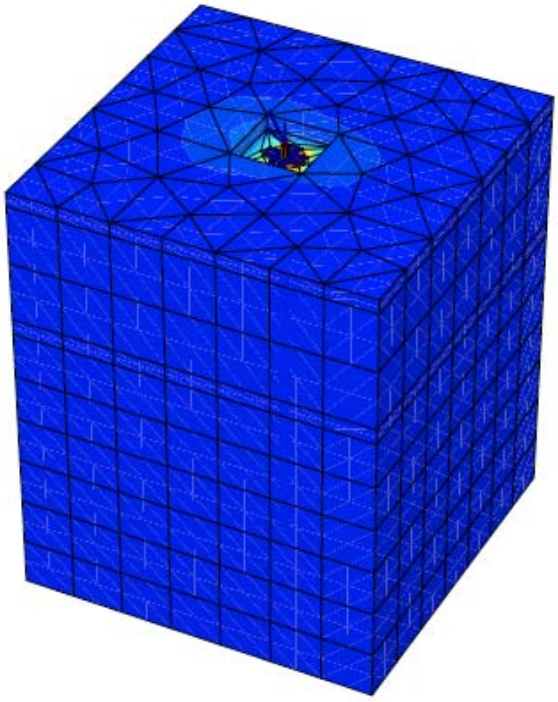

(a)

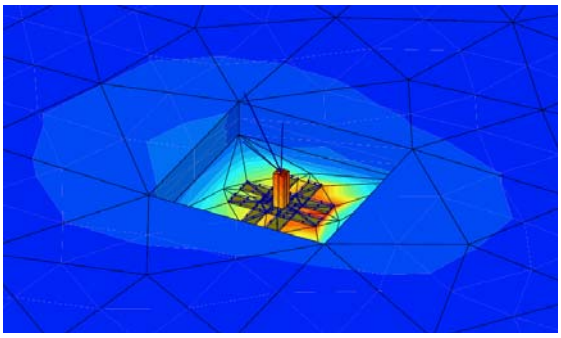

(b)

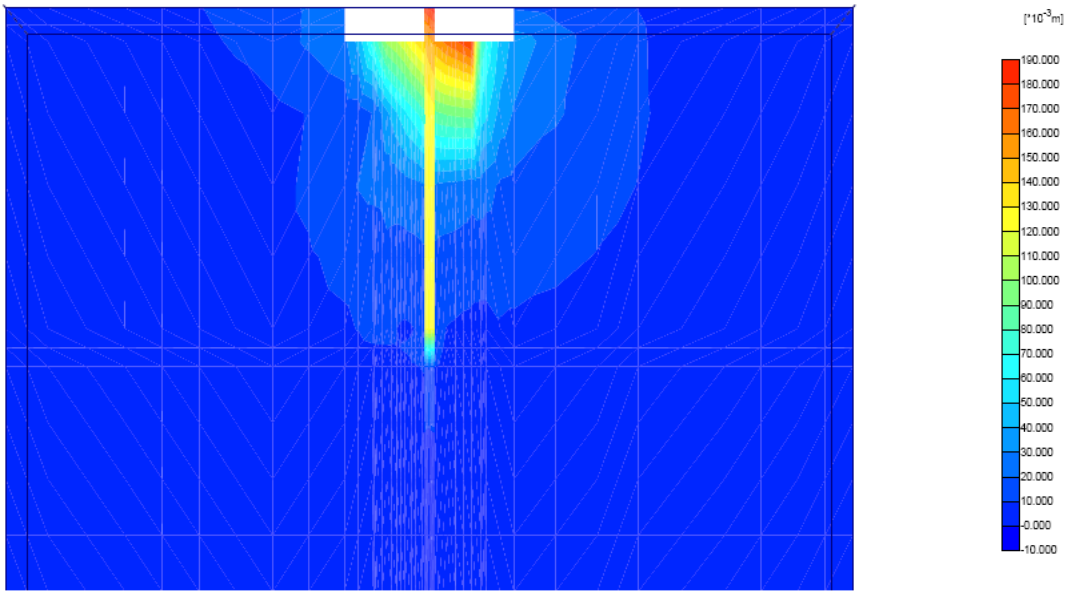

(c)

Fig. 6-13. Displacement of Tiang Tongkat Foundation with two pairs of horizontal beams, P3-1, Subjected to Inclination Load, (a) displacement shadings of mesh, (b) displacement around horizontal beam, (c) cross section of the tiang tongkat foundation

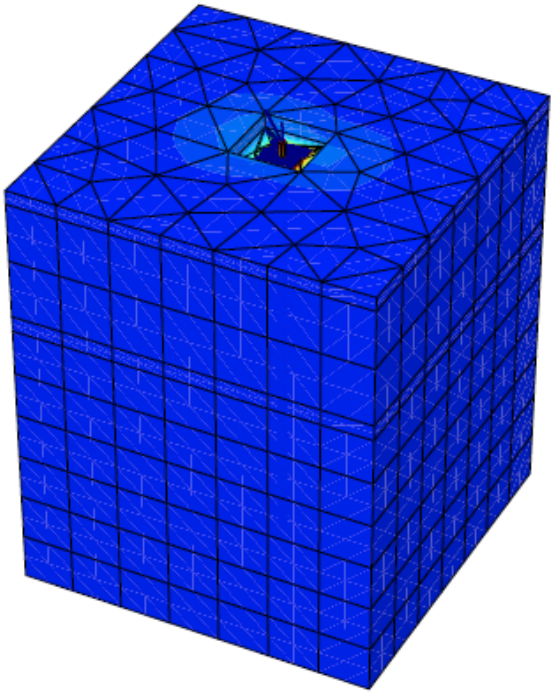

(a)

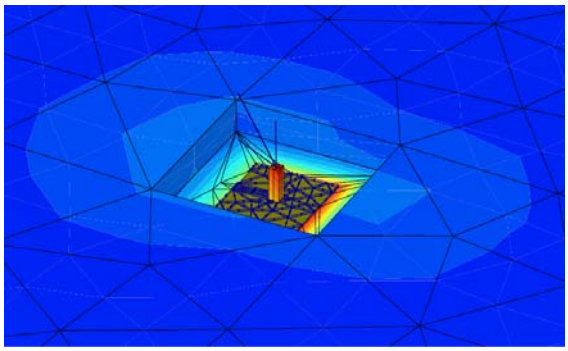

(b)

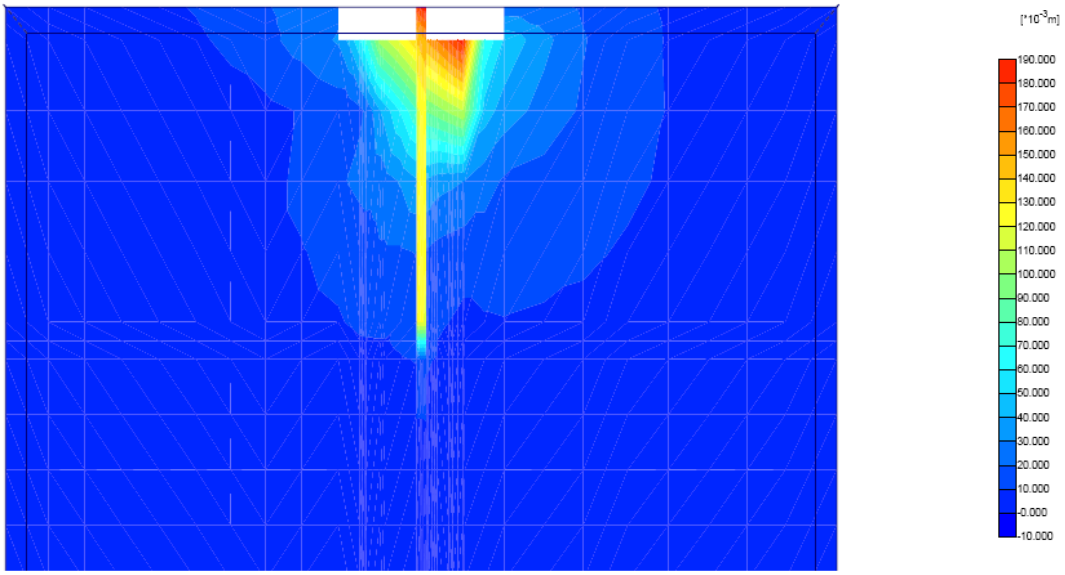

(c)

Fig. 6-14. Displacement of Combined Mini Pile with Square Floor, P4, subjected to inclination load, (a) displacement shadings of mesh, (b) displacement around square floor, (c) cross section of the tiang tongkat foundation

CHAPTER VII

DESIGN

7.1. General

Estimation of the capacity of tiang tongkat foundation over Pontianak soft organic soils for eight natural fields and Kaolin with sand will be demonstrated. Each field such as Perdana, A. Yani II, Terminal-Siantan, Ramayana, Yos Sudarso, Danau Sentarum, BNI46-Tanjungpura, Astra-A.Yani and Kaolin with sand differ in behaviour which are showing the relationship between area ratio, *Ab*/*Ap* and load, *F*. These results were obtained from several variations of traditional floating wood foundations in Pontianak city by mean of PLAXIS 3D Finite Element. The axial and inclination capacities are determined from ultimate settlement which was measured at about 6 mm from field tests as explained in Section 6-1.

Subdividing of groups of ratio *Ab*/*Ap* against load, *F*, is also described. These curves are based on shear strength of soils such as cohesion, *c*, and internal friction angle, ϕ, of the soils. The purpose of these relationships is to estimate the foundation capacity in a practical manner.

7.2. The Capacity of Tiang Tongkat Foundation on Each Field

The relationship of ratio, *Ab*/*Ap* against load, *F*, for eight natural fields such as Perdana, A. Yani II, Terminal-Siantan, Ramayana, Yos Sudarso, Danau Sentarum, BNI46-Tanjungpura, Astra-A.Yani and Kaolin with sand shown in Figure 7-1 through to 7-9 respectively. Two types of capacities are illustrated in these figures which thick lines indicate axial capacity and the thin ones are inclination capacity. Both axial and inclination capacities consist of three pile length, *L* such as 100 cm, 220 cm and 340 cm respectively. Each field corresponds to three basic stiffness parameters known as modified compression index, λ^*, modified swelling index, κ^* and modified creep index, μ^* whereas these parameters listed in Table 5-1.

It can be seen from Fig. 7-1 through to 7-9 that they show the axial capacity of a foundation increases with increasing of ratio horizontal beam area over pile skin, *Ab*/*Ap* for the

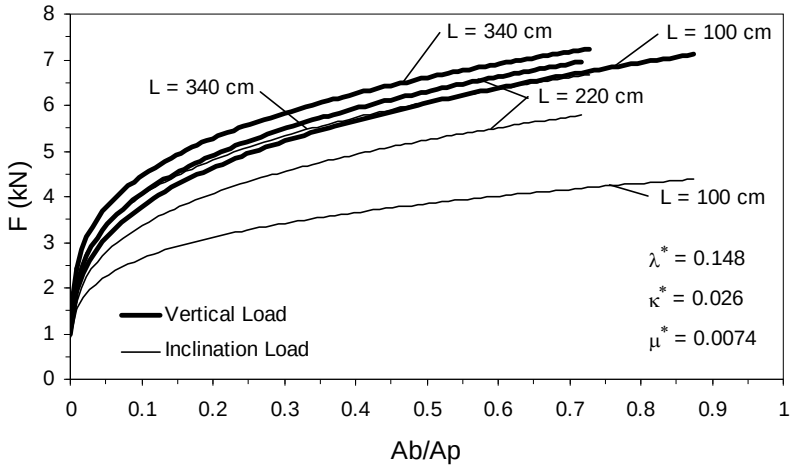

Fig. 7-1. Axial and Inclination Capacities of Tiang Tongkat Foundations on Perdana Field

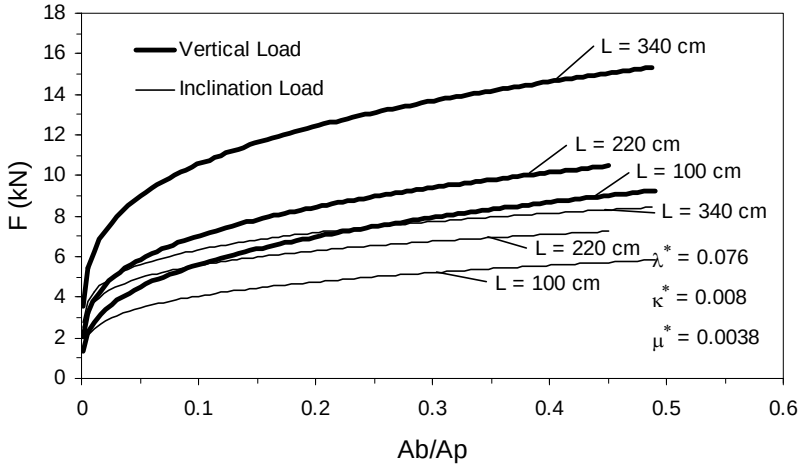

Fig. 7-2. Axial and Inclination Capacities of Tiang Tongkat Foundations on A.Yani II Field

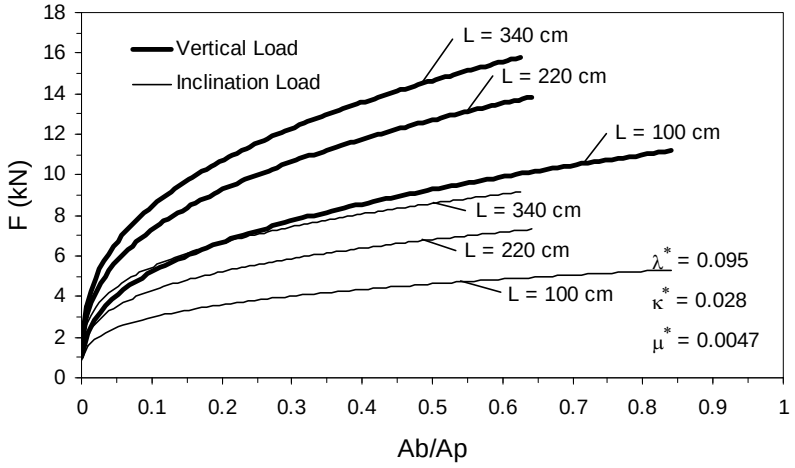

Fig. 7-3. Axial and Inclination Capacities of Tiang Tongkat Foundations on Terminal-Siantan Field

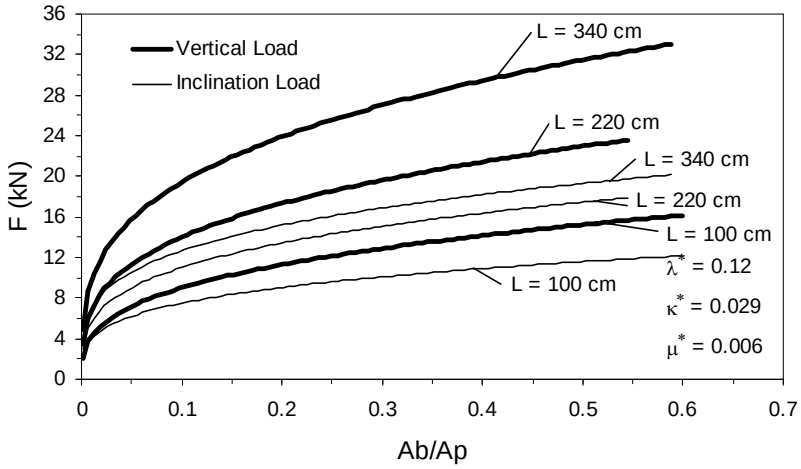

Fig. 7-4. Axial and Inclination Capacities of Tiang Tongkat Foundations on Ramayana Field

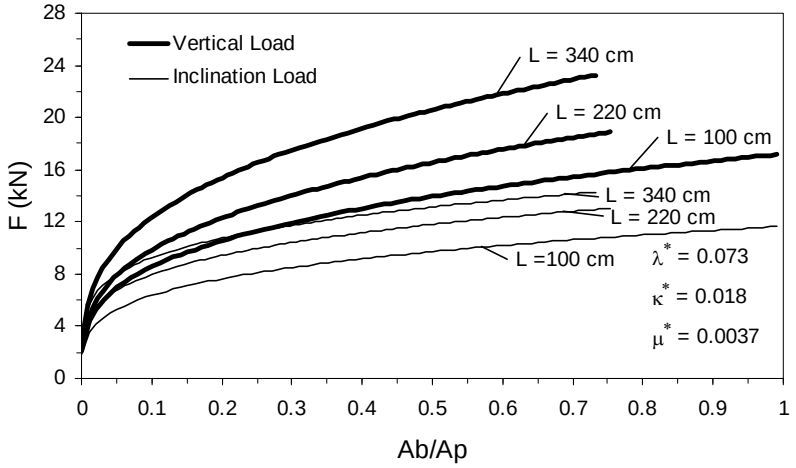

Fig. 7-5. Axial and Inclination Capacities of Tiang Tongkat Foundations on Yos Sudarso Field

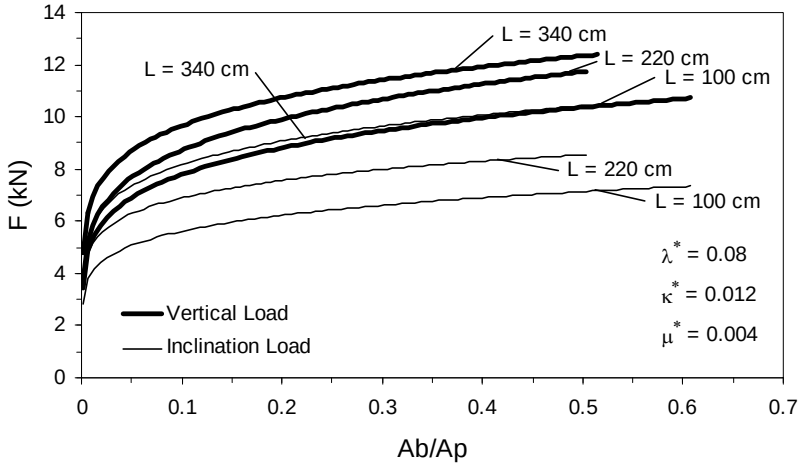

Fig. 7-6. Axial and Inclination Capacities of Tiang Tongkat Foundations on Danau Sentarum Field

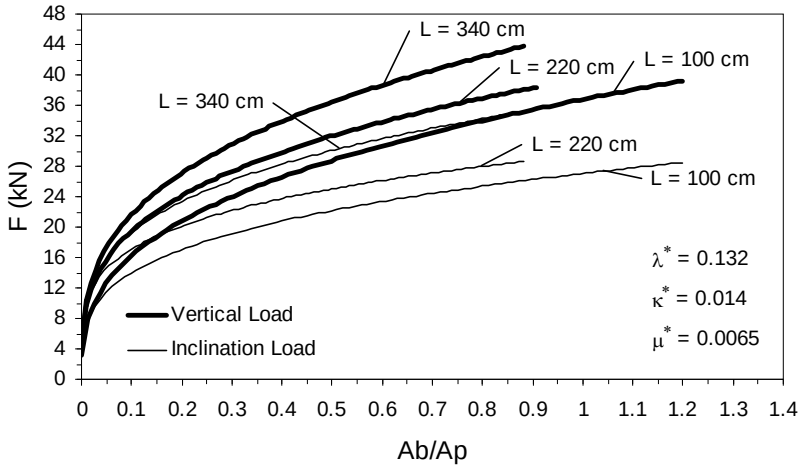

Fig. 7-7. Axial and Inclination Capacities of Tiang Tongkat Foundations on BNI46-Tanjungpura Field

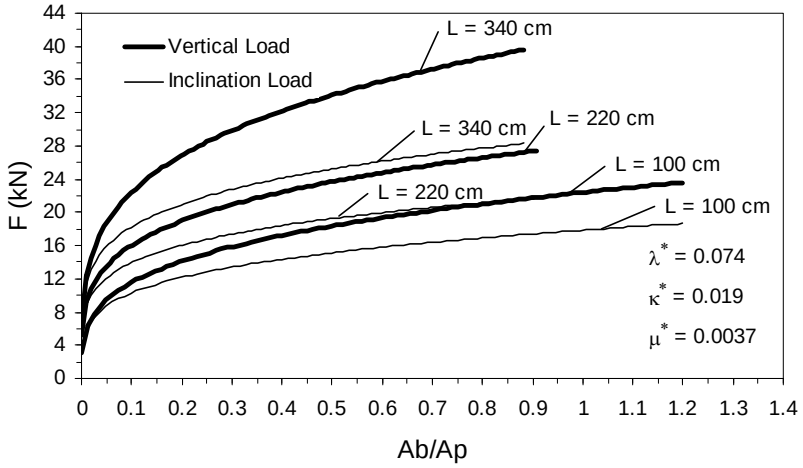

Fig. 7-8. Axial and Inclination Capacities of Tiang Tongkat Foundations on Astra-A.Yani Field

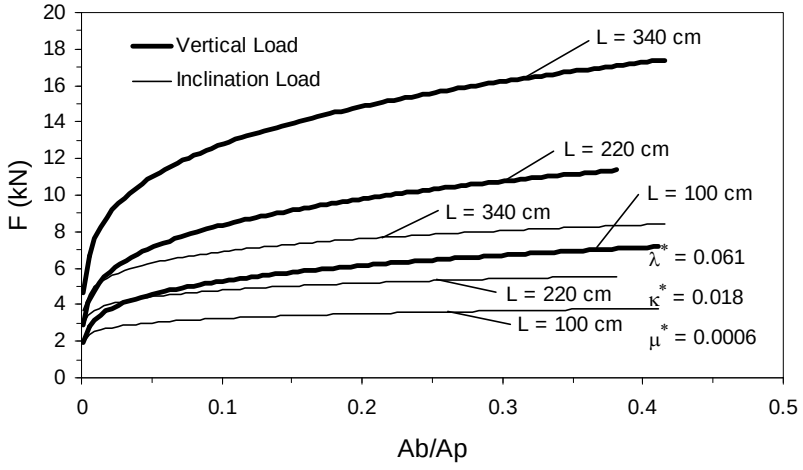

Fig. 7-9. Axial and Inclination Capacities of Tiang Tongkat Foundations on Kaolin with sand

constant pile length, *L*. The numerical results of these foundation models demonstrate the axial capacity higher than inclination capacity. Moreover, Perdana field shows lowest capacity which is its three basic stiffness parameters generally highest. As shown in Fig. 7-1, the modified compression index, λ^* = 0.148, the modified swelling index κ^* = 0.026 and the modified creep index, μ^* = 0.0074, besides, the water content, *Wn* is high at about 117.73 %. The capacity of foundation in Perdana field corresponds to shear strength of soils which is also influenced by extreme water content.

The intermediate capacities with quite similar behaviour is demonstrated on A.Yani II, Terminal-Siantan, Ramayana, Yos-Sudarso and Danau Sentarum fields as shown in Fig. 7-2 through to 7-6 respectively. These basic stiffness parameters range, λ^* = 0.073 – 0.12, κ^* = 0.008 – 0.029 and μ^* = 0.0037 – 0.006, whereas water content, *Wn*, ranges 81.57% to 169.98%. In fact, Kaolin with sand (Fig. 7-9) included in this group with λ^* = 0.061, κ^* = 0.018 and μ^* = 0.006, however its water content, *Wn*, is particularly different with 38.91%. This difference is caused by their strength factors which are related to the minerals involved and interrelation of water content and density. As explained in Chapter IV, the natural field of soils in Pontianak contains organic content and Kaolin with sand is inorganic soil.

The highest capacities are BNI46-Tanjungpura and Astra-A.Yani fields as demonstrate in Fig. 7-7 and 7-8 respectively. The basic stiffness parameters are λ^* = 0.074 – 0.132, κ^* = 0.014 – 0.019 and μ^* = 0.0037 – 0.0065 whereas the water content, *Wn* varies 58.22% to 71.01%. Generally, the basic stiffness parameters of these fields are not significantly different from other ones. However their water content, *Wn* is the lowest among all, which plays an important role to influence shear resistance of the foundation. Besides initial density, the shear resistance is dependent upon the initial water content.

7.3. The Using Graph of Axial Capacity for Practical Manner

A higher *Ab*/*Ap* ratio does not significantly contribute to an increase in the axial capacity compared to an increase in pile length, *L*. which affects pile shaft resistance to a much greater degree thereby increasing the total axial capacity of a foundation. The comparisons of axial capacity, *F*, of different pile lengths are shown in Figure 7-10. The influence of pile length to increase the capacity of foundation is similar with piled raft foundation which has been described by many researchers such as Davis and Poulos, 1972, Burland et al, 1977 and Liang et al, 2003. In this concept, piles are provided to control

settlement rather than carry the entire load. This foundation has been proved to be an economical way to improve the serviceability of foundation performance by reducing settlement to acceptable levels.

Based on the shear strength of soils and R-squared of the statistical analysis, the SSCM results are divided into three groups of parameters which are, (a) c = 5 – 9 kN/m^2, ϕ = 5 – 19º; (b) c = 15 kN/m^2, ϕ = 1º and (c) c = 16.5 kN/m^2, ϕ = 20.31º, where each group is shown in Figure 7-10(a), (b) and (c) respectively. The selecting of shear strength parameters are caused that they can be determined easily by engineer and these curves can be used to estimate the capacity of foundation in practical manner. It can be seen the differences in axial capacity, *F*, among (a), (b) and (c) groups in Figure 7-10. The lowest capacity shown in group (b), while the intermediate in group (a) and the group (c) demonstrating the highest capacity. Moreover, at the three groups' results, a sharp increase in axial capacity, *F*, occurs up to 0.2 *Ab*/*Ap* and then slightly increase with higher *Ab*/*Ap*.

Here again the ratio *Ab*/*Ap* does not have a significant influence when inclination capacity is increased compared to when pile length, *L*, is increased. The comparison of inclination capacity, *F*, with difference pile lengths are shown in Figure 7-11 whereas when the value of *Ab*/*Ap* remains the same, the capacity, *F*, increases with increases in pile length. Similar to the axial capacity, the SSCM results in this inclination load also divided into three groups of soil properties which are, (a) c = 5 – 9 kN/m^2, ϕ = 5 – 19º; (b) c = 15 kN/m^2, ϕ = 1º and (c) c = 16.5 kN/m^2, ϕ = 20.31º, where each group is shown in Figure 7-11(a), (b) and (c) respectively.

The differences in inclination capacity, *F*, among (a), (b) and (c) groups can be seen in Figure 7-11. The lowest capacity shown in group (b), while the intermediate in group (a) and the group (c) demonstrating the highest capacity. These soil properties also represent the shear strength of the soil. Besides, from three groups' results, a sharp increase in inclination capacity, *F*, occurs up to 0.2 *Ab*/*Ap* and then slight increase with higher *Ab*/*Ap*.

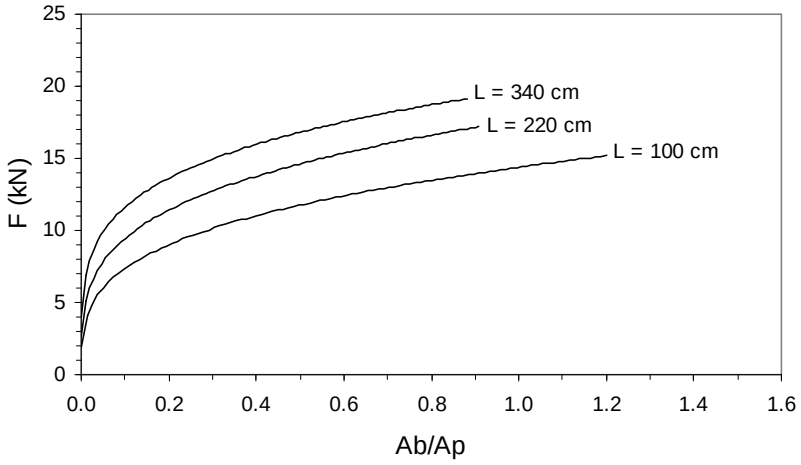

(a)

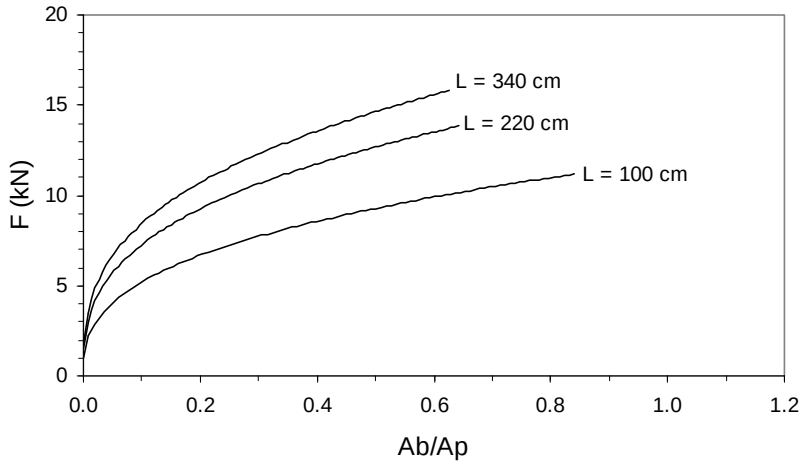

(b)

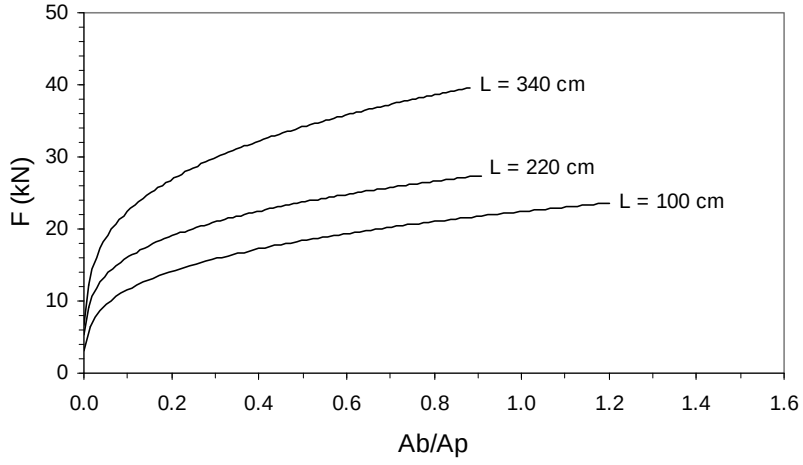

(c)

Fig. 7-10. Axial Capacity of Tiang Tongkat Foundations Subjected to Vertical Point Loads, (a) c = 5 – 9 kN/m^2, ϕ = 5 – 19º; (b) c = 15 kN/m^2, ϕ = 1º; (c) c = 16.5 kN/m^2, ϕ = 20.31º

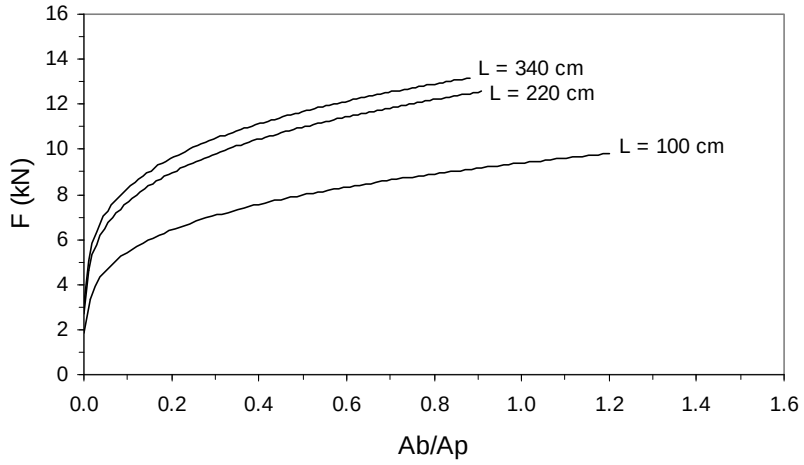

(a)

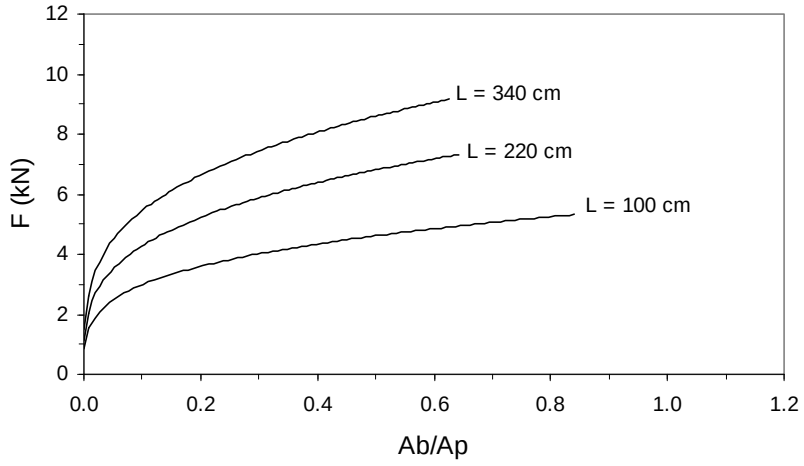

(b)

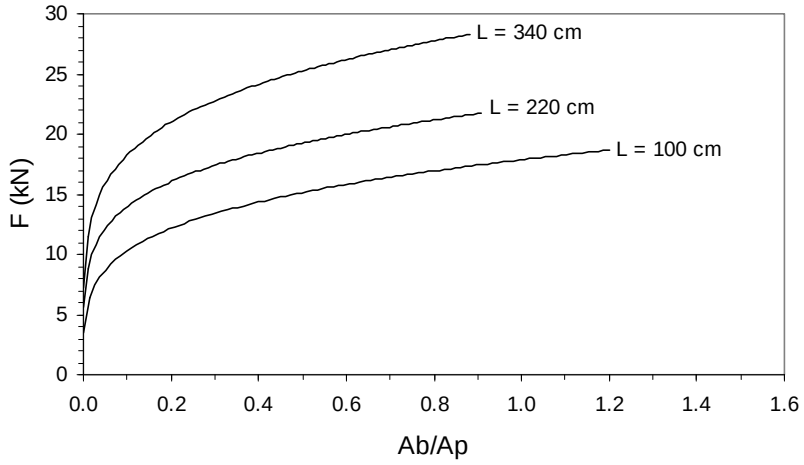

(c)

Fig. 7-11. Inclination Capacity of Tiang Tongkat Foundations Subjected to Inclination Point Loads, (a) c = 5 – 9 kN/m^2, ϕ = 5 – 19º; (b) c = 15 kN/m^2, ϕ = 1º; (c) c = 16.5 kN/m^2, ϕ = 20.31º

CHAPTER VIII

CONCLUSIONS and RECOMMENDATIONS

8.1. Conclusions

1. When examining the load settlement results of Perdana field, the analytical solutions of both the SSCM and Edil et al were lower than measurements of the mini pile, T1. For longer piles in foundation models T2 and T3, however, Edil et al seemed to only slightly underestimate measurements while the SSCM and measurement were similar up to 3 kN of load and then separate further at higher load levels. These separations could be most clearly seen in the T3 model where Edil et al underestimates and the SSCM overestimates in-situ measurements. When the Untan field was examined, there was good agreement between the results of different analyses and those, the field load tests. The SSCM, Edil et al and measurements were similar to each other up to 6 kN and 9 kN in T1, T2 foundation models respectively. Moreover, both analyses move away from measurement at higher-level loads where the SSCM still remains higher than analysis of Edil et al.
2. The primary compressibility, "*a*", in the Edil et al formula was significantly high and causing the settlement to be more excessive. In reality, the primary consolidation of peat takes place relatively quickly and the secondary compression is significant both in rate and accumulated magnitude. An empiric approach of parameter, "*a*", had been taken to reduce its value by multiplying it with 0.1 thereby providing Edil et al with a good agreement to estimate load-settlement for both Perdana and Untan fields.
3. Soft Soil Creep Model was similar to measurements with small ratio *Ab*/*Ap* in foundation models, T1 and T2, however in foundation model, T3, with its higher ratio tends to overestimate *Ab*/*Ap* increases. The ratio *Ab*/*Ap* influences contact area of soil and pore water pressure at the base of horizontal beams. This is due to the fact that the pore water pressure in the SSCM is completely incompressible with a higher ratio *Ab*/*Ap*. Moreover, the SSCM shows stiffer behaviour at higher load levels. The capacity of the foundation is strongly influenced by several factors, among which include mesh refinements, the initial stress state and the modelling scheme.

4. The capacity of the tiang tongkat foundation derived by Terzaghi, Meyerhof and Hansen showed their average solutions to overestimate field load test results. This analytical solution was also higher than both SSCM and Edit et al analyses.
5. Significant increases in the *Ab*/*Ap* ratio increased the capacity of the tiang tongkat foundation. However, these increases were not as significant in contributing in increased foundation capacity when compared to increasing pile length, *L*. For both vertical and inclination loads, the most significant increase occured up to 0.2 *Ab*/*Ap* with 100 cm and then slight increase with higher *Ab*/*Ap*.
6. The formation of failure surface strongly depends on the horizontal base area, which it was large with an increased base area. This is caused by the high number of particle contacts at the horizontal base.
7. Based on the laboratory and field load test results, some parameters were same for all materials, i.e. over consolidated ratio, *OCR* = 1.5; Poisson ratio, $\nu' = 0.4$; coefficient of lateral earth pressure, $K_0 = 0.667$; interface strength, $R_{inter} = 0.35$ and Skempton *B*-parameter, *B* = 0.9. Other ones parameters were different for each location such as basic stiffness parameters, empirical parameters of primary, secondary and rate of secondary compressions.

8.2. Recommendations for Further Study

1. The traditional tiang tongkat foundation is widely used for light construction in Pontianak city. This foundation had been analysed by SSCM, which its results overestimate measurements with higher load levels and higher *Ab*/*Ap* ratio. As explained in Chapter IV, that the Pontianak soft organic soils have 100 % degree of saturation, *Sr*, and excessive water content, *Wn*. The pore water pressure in the SSCM is shown to be completely incompressible. It is widely accepted that the pore water pressure strongly influences stress deformation and strength characteristics of soils with a higher water content. Hence, advanced studies of change of excess pore water pressure around foundations are suggested.
2. The modified primary compressibility parameter, "*a*", with an empiric correction value, changes Edil et. al to be in good agreement with estimates of load-settlement of tiang tongkat foundations constructed over Pontianak soft organic soils. A mathematical analysis may be required to verify the modified primary compressibility parameter, "*a*".

3. The results of this investigation have shown the behaviour load-settlement and deformation of tiang tongkat foundation constructed over Pontianak soft organic soil. However, a large part of Pontianak city is peat soil, therefore, further studies on different soil characteristics may be useful to solve the geotechnical problems encountered in construction in Pontianak city.
4. The horizontal beams which attached to the pile are buried at about 40 cm from the ground surface. An advanced study about the affect of embedment depth of horizontal beams for tiang tongkat foundation is recommended.
5. The combination of tiang tongkat foundation with geosynthetic is a good choice for stabilisation of embankment. The interaction of soil-structure near geotextile layer especially for peat and organic soils has not been fully studied.

REFERENCES

Al-Tabbaa, A., 1995, “Consolidation and Swelling of Clay with Concentric Inner and Outer Drainge”, Proceedings of the International Symposium Compression and Consolidation of Clayey Soils-IS-Hiroshima, Yoshikuni, H. and Kusakabe, O. (ed), pp.301-306.

American Society for Testing and Materials (ASTM Standard D 2487-00).

Atkinson, J.H. and Bransby, P.L., 1978, “The Mechanics of Soils. An Introduction to Critical State Soil Mechanics”, McGraw-Hill.

Banerjee, P. K. and Davies, T. G., 1978, “The Behaviour of Axially and Laterally Loaded Single Piles Embedded in Nonhomogeneous Soils”, Geotechnique, Vol. 28, No. 3, pp. 309-326.

Bickford, W.B., 1998, “Advanced Mechanics of Materials”, Addison-Wesley.

Bo, M.W., Choa, V., Hong, K.H., 2003, “Material Characterization of Singapore Marine Clay at Changi”, Quarterly Journal of Engineering Geology and Hydrogeology, 36, pp.305-319.

Boresi, A.P., Schmidt, R.J., 2003, “Advanced Mechanics of Materials”, John-Wiley & Sons.

Bowles, J.E., 1979, “Physical and Geotechnical Properties of Soils”, McGraw-Hill.

Bratasida, L., 2003, “Indonesian Peatland Management and Condition”, Workshop on Asean Peatland Management Initiative, 16-17th October 2003, Bogor, Indonesia.

Brinkgreve, R., 2001, “The Role of OCR in the SSC Model”, PLAXIS Bulletin, No.10-March, 2001, pp. 12-14.

Burland, J.B., Broms, B.B., et al, 1977, “Behavior of Foundations and Structures”, Proceeding 13th International Conference on Soil Mechanics and Foundation Engineering, Tokyo, 2:495-546.

Callisto, L. and Calabresi, G., 1995, “Yielding of a Natural Soft Clay”, Proceedings of the International Symposium Compression and Consolidation of Clayey Soils-IS-Hiroshima, Yoshikuni, H. and Kusakabe, O. (ed), pp.37-42.

Callisto, L. and Calabresi, G., 1998, “Mechanical Behaviour of Natural Soft Clay”, Geotechnique 48, No. 4, pp.495-513.

Case, J., Chilver, L. and Ross, C.T.F., 1999, “Strength of Materials and Structures”, Arnold.

Cernica, J.N., 1995, “Geotechnical Engineering-Foundation Design”, John Wiley & Sons.

Coelho, P.A.L.F. and Lemos, L.J.L., 2001, “Compressibility Characteristics of a Portuguese Soft deposit”, Soft Soil Engineering, Lee et al (ed), pp.663-668.

Cornforth, D. H., 1964, “Some Experiments on the Influence of Strain Conditions on the Strength of Sand”, Geotechnique, Vol. 14, No. 2, pp. 143-167.

Das, B.M., 1983, “Advanced Soil Mechanics”, McGraw-Hill.

Davis, E.H. and Poulos, H.G., 1972, “The Analysis of Piled Raft Systems”, Australia Geotechnique Journal, 2:21-7.

Edil, T. B., 2003, “Recent Advances in Geotechnical Characterization and Construction over Peats and Organic Soils”, Proceedings of the Second Conference on Advance in Soft Soil Engineering and Technology, Putrajaya, Malaysia, pp.3-26.

Edil, T. B. and Dhowian, A. W., 1979, “Analysis of Long-Term Compression of Peats”, Geotechnical Engineering, Southeast Asian Society of Soil Engineering, 10(2), p. 159-178.

Edil, T. B. and Mochtar, N. E., 1984, “Prediction of Peat Settlement”, Proceeding of Symposium: Sedimentation Consolidation Models, ASCE/October, San Francisco, CA.

El-Mossallamy, Y., 2004, “The Interactive Process between Field Monitoring and Numerical Analyses by the Development of Piled Raft Foundation”, Geotechnical innovation, International symposium, University of Stuttgart, Germany, 25 June 2004, pp. 455-474.

Fellenius, B. H., 1984, “Negative skin friction and settlement of piles”, Second International Seminar, Pile Foundations, Nanyang Technology Institute, Singapore, November 28 – 30, 12 p.

Garlanger, J.E., 1972, “The Consolidation of Soils Exhibiting Creep under Constant Effective Stress”. Geotechnique 22: 71-78.

Gere, J.M., 2001, “Mechanics of Materials”, 5th edition, Bill Stenquist.

Gibson, R. E. and Lo, K.Y., 1961, “A Theory of Soils Exhibiting Secondary Compression”, Acta Polytechnica Scandinavica, C110296, p. 1-15.

Greenfield, S.J., Shen, C.K., 1992, “Foundations in Problem Soils”, Prentice-Hall.

Head, K.H., 1998, “Manual of Soil Laboratory Testing. Volume 3: Effective Stress Tests”, 2nd edition, John Wiley & Sons.

Hillis, C.F., and Brawner, C.O., 1961, “The Compressibility of Peat with Reference to Major Highway Construction in British Columbia. Proceedings. Seventh muskeg Res. Conf., NRC, ACSSM Tech. Memo. 71, pp. 204-227.

Hutchison, C.S., 1996. In: Hall, R. and Blundell, D.J., Eds., “Tectonic Evolution of SE Asia”, Geol. Soc. London Spec. Publ., 247-261.

Hobbs, N.B., 1986, “Mire Morphology and the Properties and Behaviour of some British and Foreign peats”. Quarterly Journal of Engineering Geology, London, Vol. 19, pp.7-80.

Holtz, R.D. and Kovacs, W.D., 1981, “An Introduction to Geotechnical Engineering”, Prentice-Hall.

Ishida, T. and Nakagawa, Y., 1995, “Concolidation Apparatus with Permeability Test”, Proceedings of the International Symposium Compression and Consolidation of Clayey Soils-IS-Hiroshima, Yoshikuni, H. and Kusakabe, O. (ed), pp.69-74.

Irsyam, M., 1991, “The Mechanical Interaction Between Cohesionless Soil and Ribbed Inclusions, Ph.D Dissertation, University of Michigan.

Katagiri, M., 1995, “Effect of Clay Water Content on the Consolidation of a Sediment Layer of Reclaimed Clay”, Proceedings of the International Symposium Compression and Consolidation of Clayey Soils-IS-Hiroshima, Yoshikuni, H. and Kusakabe, O. (ed), pp.261-266.

Kempfert, H.G. and Raithel, M., 2005, “Soil Improvement and Foundation Systems with Encased Columns and Reinforced Bearing Layers”, Elsevier Geo-Engineering Book Series, Volume 3, p.923-946.

Khamehchiyan, M. and Iwao, Y., 1995, “Development of Regression Equations for Soil Compressibility”, Proceedings of the International Symposium Compression and Consolidation of Clayey Soils-IS-Hiroshima, Yoshikuni, H. and Kusakabe, O. (ed), pp.93-98.

Lambe, T. W., 1951, “Soil Testing for Engineers”, Wiley Eastern Limited

Leong, E.C. and Chin, C.Y., 1997, ”Geotechnical Characteristics of Peaty Soils in SouthEast Asia.

Liang, F.Y., Chen, L.Z. and Shi, X.G., 2003, “ Numerical Analysis of Composite Piled Raft with Cushion Subjected to Vertical Load”, Computer and Geotechnics 30, 443-453.

Liu, C. and Evett, J.B., 2000, “Soil Properties-Testing, Measurement, and Evaluation”, 4th Edition, Prentice-Hall.

Maharaj, D. K., 2003, “Load-Deflection Response of Laterally Loaded Single Pile by Nonlinear Finite Element Analysis”, EJGE Paper.

Matsumoto, T. and Michi, Y., 1995, “Pore Pressure Phenomena Around a Driven Steel Pipe Pile”, Proceedings of the International Symposium Compression and Consolidation of Clayey Soils-IS-Hiroshima, Yoshikuni, H. and Kusakabe, O. (ed), pp.701-708.

Metcalfe, I., 1996. In: Hall, R. and Blundell, D.J., Eds., “Tectonic Evolution of SE Asia, Geol, Soc, London Spec. Publ., 97-122.

Muni Budhu, 2000, “Soil Mechanics and Foundations”, John Wiley & Sons.

Muskeg Engineering Handbook (1969) Ed. I. C. Mac Farlane, University of Toronto Press.

Noviarty, T., 2002, “Studi Daya Dukung Pondasi Tiang Tongkat Laci Ganda Tunggal dengan Alas Pasir pada Tanah Lempung”. Undergraduate thesis, Tanjungpura University-Indonesia.

Parry, R.H.G., 1995, “Mohr Circles, Stress Paths and Geotechnics”, E & FN SPON.

PLAXIS, 2006, “Reference Manual”, PLAXIS B.V., The Nederlands

Poulos, H. G., 1971, “Behaviour of Laterally Loaded Piles I-Single Piles”, Journal of Soil Mechanics and Foundation Division, ASCE, Vol. 97, No. 5, pp. 711-732.

Priadi, E., 1995, “Studi Transfer Beban antara Tanah Berbutir Kasar dengan Inklusi pada Kondisi Axisymmetric”. Graduate thesis, Bandung Institute of Technology.

Rahardjo, P.P., 2005, “The use of Bamboo and Bakau Piles for Soil Improvements and Application of Pile Raft System for the Construction of Embankment on Peat and Soft Soils”, Elsevier-Geo Engineering Book Series, Volume 3, p.899-921.

Raithel, M., Küster, V. & Lindmark, A., 2004, “Geotextile encased Column-a Foundation System for Earth Structures”, Illustrated by a Dyke Project for a Works Extension in Hamburg, Nordic Geotechnical Meeting, Sweden.

Raithel, M., Kirchner, A., Schade, C. & Leusink, E., 2005, “Foundation of Constructions on Very Soft Soils with Geotextile Encased Columns-State of the Art”, ASCE-Conference Geo-Frontiers, Austin, USA.

Ravaska, O. and Aalto, A., 1995, “Modelling Permeability in Consolidation”, Proceedings XIII ECSMGE, Vaniček et al. (eds), Prague, pp.211-216.

Sentanu, W. D. R., 2002, “Studi Daya Dukung Tiang Tongkat tanpa Laci dan Tiang Tongkat dengan Laci pada Tanah Lempung dalam Skala Penuh”, Undergraduate thesis, Tanjungpura University-Indonesia.

Skempton, A. W., 1954, “The Pore Pressure Coefficients A and B”, Geotechnique, vol. 4, pp. 143-147.

Song, L., Fujiwara, T. and Karube, D., 1995, “Lateral Stress and Pore Pressure Behaviour in Oedometer Test”, Proceedings of the International Symposium Compression and Consolidation of Clayey Soils-IS-Hiroshima, Yoshikuni, H. and Kusakabe, O. (ed), pp.177-182.

Sugie, S., Iizuka, A. and Ohta, H., 1995, “Pore Water Migration During Plane Strain Triaxial Test”, Proceedings of the International Symposium Compression and Consolidation of Clayey Soils-IS-Hiroshima, Yoshikuni, H. and Kusakabe, O. (ed), pp.189-194.

Suhendra, T., 2002, “Studi Daya Dukung Pondasi Tiang Tongkat Laci Ganda Rangkap dengan Alas Pasir pada Tanah Lempung”, Undergraduate thesis, Tanjungpura University-Indonesia.

Sumioka, N., Fukuhara, K., Matsukata, K., Moriwaki, T., and Kusakabe, O., 1995, “An Evaluation Method for Consolidation Parameters of Sandy Clay based on Sand Fraction”, Proceedings of the International Symposium Compression and Consolidation of Clayey Soils-IS-Hiroshima, Yoshikuni, H. and Kusakabe, O. (ed), pp.581-586.

Tan, J.L., Leong, E.C. and Rahardjo, H., 2001, “Compressibility Characteristics of Peaty Soils”, Soft Soil Engineering, Leet at al (ed), pp.689-694.

Uesugi, M., Kishida, H. and Tsubakihara, Y., 1988, “Behavior of Sand Particles in Sand-Steel Friction”, Soils and Foundations, Japanese Society of Soil Mechanics and Foundation Engineering, Vol. 28, No. 1, pp. 107-118.

Vermeer, P. A. and Neher, H. P., 1999, “A soft soil model that account for creep”, 10 Years of Plaxis International, Balkema.

Vermeer, P. A., 2000, PLAXIS Bulletin, No.9-July, 2000, pp. 1-3.

Wijaya, T., 2006, “Inventarisasi Gambut dan Waterpass Daerah Padang Tikar dan Sekitarnya Kabupaten Pontianak Propinsi Kalimantan Barat”, Proceeding Pemaparan Hasil-hasil Kegiatan Lapangan dan Non-Lapangan, Pusat Sumber Daya Geologi.

William, A.G., Lambiase, J.J., Back. S. and Jamiran, M.K., 2003, “Geol. Soc. Malaysia”, Bulletin, 47, 63-75.

Wilson, M.E.J. and Moss, S.J., 1999, “Palaegeography Palaeoclimatology, Paleoecology”, 145(4), 303-337.

Wood, D.M., 1990, “Soil Behaviour and Critical State Soil Mechanics”, Cambridge University Press.

Yagi, N., Yatabe, R. and Mukaitani, M., 1995, “Compressive Characteristics of Cohesive Soils”, Proceedings of the International Symposium Compression and Consolidation of Clayey Soils-IS-Hiroshima, Yoshikuni, H. and Kusakabe, O. (ed), pp.221-226.

Yeung, A. T., 2001, “Geotechnical Engineering Properties of Hongkong Marine Clays”, Soft Soil Engineering, Lee at al (ed), pp.695-700.

Yoshimi, Y. and Kishida, H., 1981, “Friction between Sand and Metal Surface”, Proceedings, Tenth International Conference on Soil Mechanics and Foundation Engineering, Vol. 1, pp. 831-834.